FUNCTIONAL ROLE OF RECEPTOR-INTERACTING PROTEIN 140 (RIP140) IN ADIPOCYTE DYSFUNCTIONS AND INFLAMMATORY RESPONSE IN MACROPHAGES

A THEIS SUBMITTED TO THE FACULTY OF THE GRADUATE SCHOLL OF THE UNIVERSITY OF MINNESOTA BY

PING-CHIH HO

IN PARTIAL FULFILLMENT OF THE REQUIRMENTS FOR THE DEGREE OF DOCTOR OF PHILOSOPHY

LI-NA WEI, ADVISOR

March 2012

© Ping-Chih Ho 2012

ACKNOWLEDGEMENTS

I would like to thank my advisor, Dr. Li-Na Wei, for her guidance, advice and support both scientifically and personally in my Ph. D. study. Without her support, it is impossible for me to get any success in scientific filed. I also feel fortunate and grateful to work with excellent members in Dr. Wei's lab. They inspire me in many aspects and improve my scope for life and science. This work would not be accomplished without their support. I also thank my committee members, Dr. Timothy Walseth, Dr. W. Gibson Wood and Dr. Yoji Shimizu for their discussion, technical support and advice for career plan.

Dr. Wei's laboratory members are friendly, inspiring and collaborative. I would like to thank all the past members and current members of Dr. Wei laboratory. It has been a terrific experience to work with them. It has also been a great experience to discuss science, play basketball and share my happiness with them.

I would like to thank my parents and my wife for their love and support. Foremost, I would not be able to achieve any accomplishment in my Ph. D. study without my wife's support.

ABSTRACT

The prevalence of metabolic diseases in modern society, including Type II diabetes mellitus (T2DM), hypertension and cardiovascular diseases, is a major burden on health care systems. Among these diseases, T2DM and its associated complications contribute to the progression of other metabolic diseases such as fatty liver diseases and atherosclerosis. Understanding the initiation and progression of T2DM is critical for developing treatments for T2DM and its associated metabolic disorders. Adipocyte dysfunctions and chronic inflammation have been shown recently to play essential roles in the progression of T2DM. Normally, adipocytes can store energy as triglycerides, fine-tune other metabolic tissues' lipid and glucose metabolism, and secreted cytokines (adipokines) to modulate immune response. In T2DM or obesity, adipocytes become dysfunctional, with increased lipolysis, an altered adipokine profile, and decreased insulin sensitivity and glucose uptake ability. These changes affect not only the adipocytes themself but also systemic glucose and lipid metabolism. In obese patients and in the high-fat diet (HFD)-fed mouse model, increased inflammatory response in macrophages also contributes to adipocyte dysfunction. The escalated inflammatory response plays pathophysiological roles in various metabolic disorders, including atherosclerosis and arthritis, and increases the incidence of septic shock. However, the underlying mechanisms for initiation of adipocyte dysfunctions and escalation of inflammatory response remain unclear.

Receptor-interacting protein 140 (RIP140) is a co-regulator for various transcription factors and nuclear receptors and is expressed mainly in macrophages and metabolic tissues, including adipocytes, hepatocytes and muscle cells. RIP140 affects the progression of T2DM through its nuclear activity as shown by the resistance of knockout mice to diet-induced diabetes and its associated metabolic disorders. In my studies, I found that when I used HFD feeding to induce T2DM, RIP140 could accumulate within the cytoplasm of adipocytes. I further demonstrated that cytoplasmic RIP140 not only interacted with AS160 to impede GLUT4 vesicle trafficking and adiponectin vesicle secretion, but also formed a complex with perilipin A to enhance lipolysis. These findings suggest that HFD feeding can alter RIP140's cellular distribution, which leads to

adipocyte dysfunctions including higher lipolysis, lower glucose uptake, and reduction in adiponectin secretion. I also showed that HFD feeding promoted cytoplasmic accumulation of RIP140 in adipocytes through a PKCϵ-dependent signaling pathway by enhancing intracellular lipid content (as an intrinsic stimulus) and circulating endothelin-1 (as an extrinsic stimulus). Most importantly, administration of a selective ET-1 receptor anatagonist, ambrisentan, reduced HFD-induced cytoplasmic accumulation of RIP140 in adipocytes and further ameliorate hepatic steatosis and insulin sensitivity in vivo. These findings reveal the novel roles of cytoplasmic RIP140 in adipocyte dysfunctions and provide evidence for cytoplasmic RIP140 as a promising target for treatment of T2DM.

Recently, RIP140 has also been shown to affect proinflammatory cytokine production by functioning as co-activator for NF-κB in macrophages. I showed that HFD feeding up-regulated RIP140 expression by promoting intracellular cholesterol level which led to increased proinflammatory potential in macrophages. In this study, intracellular cholesterol level regulates RIP140 expression by decreasing microRNA-33a, which targeted RIP140 via a conserved region in 3'-UTR of RIP140 mRNA. I further discovered that TLR ligands could trigger RIP140 degradation to resolve inflammation. This RIP140 degradation was modulated by RelA-recruited SCF E3 ligase and Syk-mediated phosphorylation on RIP140. My studies in macrophages demonstrate that RIP140 in macrophages can be modulated by a HFD to affect the systemic inflammatory response and further suggest that defects in RIP140 degradation may cause non-resolving inflammation which is involved in septic shock and various metabolic disorders.

Taken together, my studies provide evidence for the novel functions of RIP140 in adipocyte dysfunction and inflammatory response in macrophages and determine the mechanisms by which HFD affect RIP140's distribution and expression in adipcoytes and macrophages. These findings contribute to our understanding of how HFD causes adipocyte dysfunctions and increase inflammatory response.

Table of contents

List of Figures

CHAPTER I

Introduction

The Receptor-interacting Protein 140

Mouse receptor interacting protein 140 (RIP140) was identified as a ligand-dependent co-repressor of orphan receptor TR2 by yeast two-hybrid screening and human RIP140 was isolated as a interacting co-regulator of estrogen receptor α (ERα) [1-3]. DNA sequencing further concludes that RIP140 is highly conserved in all vertebrate species examined. The ubiquitous expression profile of RIP140 suggests its roles in many biological processes. Its interaction and co-regulatory role for several transcription factors and nuclear receptors have further been determined. The list includes ER, GR, AR, PPARα/γ/δ, PXR, RARα/β, RXRα/β, LXRα/β, ERRα/β /γ, RORβ, VDR, TR2, TR4, c-jun, AhR, HNF4α, SF-1, RelA, and GRIP1 [4-6]. Based on the phenotype of whole body RIP140-knockout mice, RIP140 is essential for ovulation and lipid and glucose metabolism. These effects mostly are attributable to RIP140's co-repressive activity in modulating gene transcription through its repressive domains (RDs) which mediate its interaction with CtBP, HDAC, and other chromatin remodeling complexes [1, 4, 7-9]. However, increasing evidence recently indicates that RIP140 can also act as a co-activator for transcription of several genes such as proinflammatory genes in macrophages and fatty acid synthase (FAS) in hepatocytes [10-13]. The opposing activities of RIP140 on gene transcriptional control might be transcription factor-, gene-, and/or cell context-specific. It has been known that post-translational modifications (PTMs) play critical roles in modulating proteins stability, sub-cellular distribution, and interacting proteins [4, 14-19]. For RIP140, using proteomic analysis, several PTMs of RIP140 have been identified, including acetylation, phosphorylation, methylation, PLP conjugation and sumoylation [4]. These PTMs modulate RIP140's co-regulator activity by affecting its recruiting co-regulators and also affect RIP140's sub-cellular distribution. These PTMs are described in details in the following:

Acetylation:

Using proteomic analysis, nine lysine residues of RIP140 wer found to be modified by acetylation. Acetylation at Lys482, Lys 529 and Lys607 of RIP140 enhances its nuclear export and decreases RIP140's gene repressive activity [17]; whereas acetylation at

Lys158 and Lys287 of RIP140 boosts its nuclear retention and gene repressive activity. ERK2-mediated phosphorylation of RIP140 triggers p300-mediated acetylation of RIP140 at Lys158 and Lys287 (see below) [17, 18]. Importantly, this event is elevated in the 3T3-L1 adipocyte differentiation process, suggesting that RIP140's repressive role on transcription is increasingly needed in adipocyte differentiation [18].

Phosphorylation:

RIP140 can be phosphorylated at two threonine residues and nine serine. Erk2 phosphorylates RIP140 at Thr202 and Thr207 to facilitate the recruitment of p300, which then acetylates RIP140 at Lys158 and Lys287. The coordination of these PTMs increases RIP140's gene repressive activity by increasing the interaction of RIP140 with HDAC3 [17, 18, 20]. Protein kinase C epsilon (PKCε) phosphorylates RIP140 at Ser102 and Ser1003 to promotes Protein arginine methyltransferase 1 (PRMT1)-mediated arginine methylation at Arg240, Arg650 and Arg948. The combination of PKCε-mediated phosphorylation and PRMT1-mediated methylation facilitates RIP140 nuclear export [19].

Methylation:

RIP140 contains both arginine and lysine methylation. PRMT1 promotes methylation of RIP140 at Arg240, Arg650 and Arg946, which reduces RIP140's nuclear activity on transcriptional repression and stimulates its nuclear export [14]. In contrast, methylation at Lys591, Lys653 and Lys757 of RIP140 elevates its repressive activity by unknown mechanisms [21]. Of note, demethylation at these lysine residues of RIP140 is necessary for its methylation at Arg240, Arg650 and Arg946 of RIP140. This indicates a signal crosstalk among different protein methylation enzyme machineries in order to fine-tune RIP140's sub-cellular localization, interacting partners, and biological activity.

PLP conjugation:

Lys613 of RIP140 can be conjugated with PLP (pyridoxal 5'-phosphoate), which elevates RIP140's gene repressive activity. This PTM is controlled by the status of cellular PLP

level, the bioactive form of vitamin B6 [16]. This finding reveals that RIP140 may sense the status of PLP or other nutrition through PTMs, which then regulate RIP140 biological activity.

Sumoylation:

Sumo-1 conjugation at Lys 756 and Lys 1154 of human RIP140 (Lys757 and Lys 1157 of the mouse RIP140), which can modulate RIP140's nuclear distribution and its gene represssive activity [22]. However, the enzyme for RIP140 sumoylation has not been identified.

Among them, protein kinase C epsilon (PKCε)-mediated phosphorylation, following with protein arginine methyltransferase 1 (PRMT1)-mediated methylation, promotes RIP140's nuclear export and its cytoplasmic distribution strongly indicate other roles of RIP140 outside the nucleus in the adipocytes. However, the biological functions and exact distribution of the cytoplasmic RIP140 in adipocytes remain unknown.

Physiological Role Adipose Tissue and Adipocyte Dysfunction in Type II Diabetes Mellitus and Metabolic Syndromes

There are two kinds of adipose tissue: white and brown. Adipose tissue originally was presumed to be an inert means of storing excess energy as triglyceride (TG). However, studies over the past two decades showed that adipose tissues exert other functions to maintain systemic homeostasis. In cold environments, brown adipose tissue uses TG to produce heat and maintain body temperature, whereas white adipose tissue is the main site of energy storage and use during food intake or fasting states [23]. In fasting states, the TG in white adipose tissue is hydrolyzed through a series of signaling pathways to form free fatty acids [24]. That can serve as an energy source for other organs and for ketone body production in the liver. In addition to lipid metabolism, adipose tissues also serve as an endocrine organ by secreting cytokines (i.e., adipokines) such as adiponectin and leptin to modulate other organs' functions as well as brain behavior [23, 25, 26]. Adiponectin, for example, improves endothelial function and has beneficial anti-inflammatory effects in cardiovascular diseases (e.g., ischemic heart

disease, cardiac hypertrophy, heart failure) [27, 28]. In obese and T2DM patients, although adipose tissue mass increases, adiponectin secretion declines and this reduction of adiponectin secretion has been implicated in obesity-caused metabolic disorders as well as cardiovascular disorders [27, 28]. Lastly, insulin can stimulate glucose uptake in adipocytes by enhancing glucose transporter 4 (GLUT4) trafficking from cytoplasm to plasma membrane. Using adipocyte-specific GLUT4-knockout mice, the importance of glucose uptake in adipocyte in insulin resistance and Type 2 diabetes mellitus (T2DM) has been demonstrated. Loss of GLUT4 expression or defects in GLUT4 trafficking in adipocytes can induce systemic insulin resistance in liver and muscle and result in diabetes [23, 29].

Studies in rodents and humans showed that a high caloric intake changes the balance of adipose tissue metabolism, reducing glucose uptake, increasing the release of free fatty acids, and decreasing secretion of adiponectin and leptin. These changes are known as adipocyte dysfunctions and have been shown to be involved in metabolic disorders [23, 30]. For example, imbalances in glucose uptake, lipid storage, and lipolysis in adipocytes contribute to systemic insulin resistance and promote lipotoxicity in muscle and liver [30, 31]. Moreover, such imbalances also play key roles in reduced cardiac function in obese patients or those with Type 2 diabetes mellitus (T2DM). Ectopic lipid deposition promotes fatty heart and eventually causes lipotoxic cardiomyopathy, important metabolic disorders with high mortality rates [30, 32, 33]. Fatty heart and lipotoxic cardiomyopathy cause increased left ventricular mass, impaired left ventricular systolic function and diastolic filling, and cardiac fibrosis [33]. It has been proposed that obesity, which reduces lipotoxicity by increasing adipocyte size might be a protective response to overnutrition [30, 34, 35]. In this model, adipose tissue in obese subjects protects against ectopic lipid deposition. However, after prolonged morbid obesity, adipocytes lose their ability to store TG and increase. On the other hand, the changes in adipokine secretion profile are also involved in systemic insulin resistance and chronic inflammation which leads to high incidence of septic shock and autoimmune diseases [34, 35].

Toll-like Receptors and the Role of Macrophage in Inflammation

Toll-like receptors (TLRs) contain at least 12 proteins that initiate the innate immune response by activating various signaling cascades, including the nuclear factor κB (NF-κB) and interferon regulatory factor (IRF) pathways [36]. Activation of inflammatory signaling cascades boosts the production of inflammatory cytokines, such as IL-1β, TNFα, and IL-6. The TLR-family members are pattern-recognition receptors (PRRs), which can recognize pathogen-associated molecular patterns (PAMPs), including peptides, carbohydrates, nucleic-acid structures, and lipids that are expressed by various microorganisms [36, 37]. This recognition is critical for eliciting inflammatory responses to eliminate the infection of pathogens by direct and indirect mechanisms modulated by inflammatory cytokines. However, recent studies show that TLRs, as well as other members of PRRs, can also recognize damage-associated molecular patterns (DAMPs), which include endogenous molecules and antigens released from damaged cells [36-38]. It has been suggested that this recognition of DAMPs is used to eliminate tissue damage and to elevate local and systemic immune response potential by inflammatory cytokines.

Macrophages are among the most critical players in the innate immune system. They can produce massive amounts of inflammatory cytokines upon recognition of infected pathogens through PRRs and also act as phagocytes to eliminate pathogens and infected cells [38, 39]. Ligation of TLR ligands to TLRs boosts macrophages' inflammatory response by activating inflammatory signaling cascades; this activation is called classical activation (M1 activation) [39]. The human body is host to resident macrophages and non-resident macrophages. Resident macrophages, such as osteoclasts in bone and microglia in the brain, are responsible for maintaining homeostasis in local tissues and for sensing infection [40]. Non-resident macrophages are derived from stimulation of circulating monocytes by chemokines and cytokines elicited by local infection and damage. Macrophages are also activated by IL-4 and IL-13 through a STAT6-dependent pathway in a process called alternative activation (M2 activation) [40]. These alternatively activated macrophages can express various negative regulators that are anti-inflammatory. They also exhibit high wound-healing activity [40]. Moreover,

macrophages can switch between M1 and M2 phenotypes [41, 42]. These findings reveal the plasticity of macrophage activation. In addition, the opposing functions of M1 and M2 macrophages suggest that the functional properties of macrophages are critical for modulating immune response and the homeostasis of surrounding tissues in response to cytokines, infection, and tissue damage [43, 44].

Non-resolving Inflammation and Its Pathophysiological Role

Although inflammation is important for eliminating pathogens, sustained inflammation can damage tissues and disrupt cellular homeostasis [43, 45, 46]. An increasing number of studies show that perpetuation of inflammation contributes to metabolic disorders and many autoimmune diseases such as inflammatory bowel disease and Alzheimer's disease [38, 46]. Importantly, the failure to resolve inflammation after infection leads to excessive production of inflammatory cytokines, including IL-1β and TNFα. The massive amount of circulating inflammatory cytokines can damage cells and cause multiple organ failure, which are typical features of septic shock. In contrast, the expression of negative regulators of inflammation causes macrophages to become insensitive to subsequent exposure to TLR ligands such as lipopolysaccharide (LPS). In patients and animals, this condition is known as endotoxin tolerance and patients with endotoxin tolerance are immunocompromised [43, 47, 48]. These features suggest that the control of timing and amplitude of inflammation are critical for health. In addition to the viewpoint that chronic low-grade inflammation causes T2DM and other metabolic disorders, many epidemiological studies suggest that over-nutrition and obesity can boost inflammatory potential [46]. However, how immune cells sense nutrition status and the underlying mechanisms for modulating the potential of immune response remain largely unknown.

Preface

This chapter has been published:

Ping-Chih Ho, Yi-Wei Lin, Yao-Chen Tsui, Pawan Gupta[#], and Li-Na Wei (2009) A negative regulatory pathway of GLUT4 trafficking in adipocyte: new function of RIP140 in the cytoplasm via AS160. Cell Metabolism 10, 516-523

CHAPTER II

A negative regulatory pathway of GLUT4 trafficking in adipocyte: new function of RIP140 in the cytoplasm via AS160

Introduction

Insulin sensitivity is key to the maintenance of systemic energy homeostasis, ensuring that metabolically healthy individuals can adapt to various fuel conditions by sensing blood glucose load and triggering its disposal [49]. The inability of an individual to respond to insulin signals to remove glucose, i.e., insulin resistance (IR), is the hallmark of Type II diabetes and can be caused by a variety of factors [49-51]. Once IR is detected clinically, reversing the progression of the disease is often difficult. Early markers for IR, especially those involved in the regulation of insulin signaling and glucose disposal, are therefore important to further understand disease progression and develop therapeutic agents.

The principal mechanism for glucose disposal, insulin-stimulated glucose uptake, mainly involves glucose transporter 4 (GLUT4) [52]. Insulin activates a cascade of intracellular signaling events, including the mitogen-activated protein kinase pathway for growth and the phosphoinositide 3-kinase (PI3K)–Akt pathway for glycogen and protein synthesis and glucose uptake via GLUT4 [49, 53]. IR is mainly attributed to defects in insulin signaling pathways [23, 51, 53-55], as well as GLUT4 synthesis, translocation, trafficking and down-regulation [23, 49, 52]. To this end, insulin stimulates the translocation of GLUT4 storage vesicles (GSVs) from intracellular compartments to the plasma membrane (PM), a key step regulating GLUT4 traffic.

Among the thirteen GLUTs, GLUT4 is the only isoform that is insulin-responsive, and it is expressed predominantly in muscle and adipose tissues [52]. Insulin-stimulated GLUT4 partitioning to the PM is mediated primarily by PI3K-activated Akt which

phosphorylates AS160, a Rab-GTPase-activating protein (Rab-GAP) [56, 57]. Phosphorylated AS160 (pAS160) is thought to become inactive, allowing more Rab-GTP to accumulate, which facilitates GSV trafficking to the PM [56, 58-60].

Receptor interacting protein 140 (RIP140), a widely known transcription corepressor [61, 62], can be modified extensively by posttranslational modifications (PTMs) [4]. Certain PTMs augment its nuclear activity [16, 19-21, 63], whereas a specific cascade of sequential PTMs, initiated by nuclear PKCε phosphorylation of RIP140's Ser-102 and Ser-1003, triggers its export to the cytoplasm in adipocytes [14, 19]. This report uncovers a new functional role for RIP140 in the adipocyte cytoplasm — to negatively regulate insulin-stimulated GLUT4 trafficking — and determines the mechanism of this action.

Materials and Methods

Cell culture

COS-1 cells, 3T3-L1 fibroblasts, and RIP140$^{-/-}$ mouse embryonic fibroblasts (MEF) were maintained and differentiated as described [19]. G7 fibroblasts were maintained and differentiated as described ([64]. Transfection was conducted with Lipofectamine 2000 (Invitrogen) as described [19] or Lipofectamine LTX according to the manufacturer's instructions. siRNA (QIAGEN) was introduced using a DeliverX Plus siRNA transfection kit (Panomics).

Myc-GLUT4-EGFP staining and GLUT4 internalization

G7 adipocytes were starved (3 hrs) in serum-free medium and treated with 100 nM insulin (20 min), cells were fixed and incubated with anti-myc (2 hrs, 4°C). After

washing, cells were stained with Cy3-conjugated secondary antibody. Images were acquired on an Olympus FluoView1000 IX2 inverted confocal microscope. GLUT4 recycling was performed as described [60].

In vitro competition assays for protein interaction

In vitro protein interaction assay was performed as described [19] to examine competition between RIP140 and AS160. Flag-RIP140 was synthesized in a transcription–translation system (Promega) and incubated with GST-AS160 and an equal amount of Akt2 (Upstate) in coimmunoprecipitation buffer overnight at 4°C. Detail was described in the supplement. After washing, immunocomplexes and supernatants were analyzed with indicated antibodies on blots.

PKCε kinase activity assay

Nuclear PKCε activity was assayed using 200 μg of immunoprecipitated nuclear extract with a radiometric kit (Upstate) according to the manufacturer's instructions.

Statistical analysis

Experiments were performed at least twice and that results were the same. Results are presented as means ± SD. Comparisons between groups were made by unpaired two-tailed Student's *t*-tests. *P* values < 0.05 were considered to be statistically significant.

Results

Increased cytoplasmic RIP140 reduces GLUT4 trafficking in 3T3-L1 adipocytes.

We first found cytoplasmic RIP140 readily detectable in four-day differentiated cells, and robustly detected in eight-day differentiated cells (Figure 1A). Interestingly, 4-day cells were more responsive to insulin stimulation in glucose uptake than the 8-day cells (Figure 1B). Consistently, insulin dramatically stimulated GLUT4 partitioning into the

PM of 4-day cells. The 8-day cells had higher basal glucose uptake and PM-associated GLUT4 levels, which could be stimulated by insulin (Figure 1C). Insulin-stimulated glucose uptake in these 3T3-L1 adipocytes seems lower than that of some reported studies, which might be due to difference in experimental procedures such as the differentiation cocktail [65].

Cytoplasmic RIP140 was evident in 4-day cells, and its levels increased by day 8; similarly, PKCε levels also increased during differentiation (Figure 1C). When RIP140 and PKCε were knocked down individually, both basal and insulin-stimulated PM-associated GLUT4 levels in 8-day cells increased significantly (Figure 1D), and basal and insulin-stimulated glucose uptake was also enhanced significantly (Figure 1E). While GLUT4 mRNA level was not altered by RIP140 or PKCε silencing (Figure 1D), total GLUT4 protein level was up-regulated (~2.5 folds) by RIP140 silencing (Figure S1), indicating additional functions, beyond affecting GLUT4 protein level, of RIP140 to modulate glucose uptake.

GLUT4 trafficking was assessed using G7 adipocytes which stably express myc-GLUT4-EGFP [64]. Silencing RIP140 or PKCε increased, by approximately twofold, the number of cells exhibiting surface-stained myc-GLUT4 (i.e., an intact myc rim stained with anti-myc) (Figure 1F); this was confirmed by immunoblotting (Figure S2). Myc-GLUT4 recycling was monitored by incubating G7 adipocytes with anti-myc for 60 min in the presence or absence of insulin, followed by fixation and permeabilization to stain internalized myc-GLUT4 with a secondary antibody. The internalized myc-GLUT4 signal was stronger in both RIP140- and PKCε-silenced cells (Figure 1G). Overall, these results suggest a functional role for both RIP140 and PKCε in negatively regulating GLUT4 trafficking to the PM.

We previously identified nuclear PKCε activation as an initial trigger to stimulate the export of nuclear RIP140. Two RIP140 mutants, CP (a phosphor-mimetic export enhancer) and CN (a phosphor-deficient mutant with reduced export), were used to rescue RIP140$^{-/-}$ adipocytes (Figure 2A). Re-expressing the wild type, or CP, but not CN,

RIP140 reduced both basal and insulin-stimulated GLUT4 partitioning to the PM. Likewise, glucose uptake of the RIP140-null cells was significantly reduced by expressing Wt or CP RIP140, but unaffected by the CN mutant (Figure 2B). Taken together, these results indicate that cytoplasmic RIP140 negatively regulates basal and insulin-stimulated GLUT4 trafficking to the cell surface in these adipocytes. Furthermore, this effect can be initiated by PKCε-mediated phosphorylation of RIP140 in the nucleus.

Regulation of AS160 phosphorylation by RIP140

Several regulatory points of GLUT4 trafficking where RIP140 might play a role were examined. We found that RIP140 directly affected the phosphorylation of AS160 on Thr-642 by Akt (Figure 2C). Neither RIP140- nor PKCε-silencing affected the basal or insulin-activated Akt or ERK1/2 activation profiles, but both manipulations enhanced pAS160 levels (Figure 2D). AS160 protein, but not its mRNA, level was decreased slightly by silencing RIP140 or PKCε. Therefore, RIP140 silencing slightly decreases AS160 protein expression, but profoundly increases its phosphorylation. Treatment with PKC effectors indicated that PKC activation increased RIP140/AS160 complex formation (Figure 2E), suggesting that such complex formation might inhibit the phosphorylation of AS160.

RIP140 directly interacts with AS160 to impede Akt phosphorylation of AS160.

The direct interaction and *in vivo* complex formation of RIP140 with AS160 was confirmed using glutathione *S*-transferase (GST) pulldown (Figure 3A) and coimmunoprecipitation (Figure 3B). The AS160-interaction domain of RIP140 was mapped to its amino (peptides 1–350) and carboxyl (peptides 717–end) termini. The interaction of RIP140 with AS160 interfered with the ability of AS160 to interact with Akt (Figure 3C). *In vitro* kinase assays confirmed that RIP140 reduced AS160 phosphorylation by approximately 50% (Figure 3D). Thus, RIP140 interacts directly with AS160, impeding its phosphorylation by Akt, and presumably maintaining the GAP activity of AS160. This would inactivate downstream targets such as Rab-GTPases, thereby reducing GSV trafficking.

High-fat diet activates nuclear PKCε and promotes cytoplasmic RIP140 accumulation.

To determine if this signaling pathway could be recapitulated in animals under physiological or pathophysiological conditions, mice were fed a normal diet (ND) or a high-fat diet (HFD) for 5 weeks. Primary adipocytes from these mice were compared with respect to RIP140 subcellular distribution, nuclear PKCε activation and glucose uptake. Cytoplasmic RIP140 was clearly detected in the white adipocytes from epididymides of HFD-fed mice, but not in the ND controls (Figure 4A, upper). Indeed, the number of adipocytes expressing cytoplasmic RIP140 was nearly threefold higher in HFD mice than ND mice (Figure 4A, lower). (The specificity of anti-RIP140 was validated by immunohistochemistry and immunoblotting [Figures S3 and S4]). Likewise, the response of glucose uptake to insulin decreased from a nearly six-fold stimulation in ND mice to only about a 1.5-fold increase in HFD adipocytes (Figure 4B), although basal glucose uptake in primary adipocytes was comparable between HFD and ND groups. This is different from the apparent elevation of basal glucose uptake levels in later (day 8) *in vitro* differentiated adipocytes (Figure 1), which might be due to factors varied between *in vivo* and *in vitro* conditions. RIP140 was located predominantly in the nuclei of ND adipocytes but appeared abundantly in the cytoplasm of HFD adipocytes (Figure 4C). Total RIP140 levels also increased in HFD adipocytes, which appeared to partially result from increased mRNA levels (Figure 4C, bottom). Finally, nuclear PKCε activity was also significantly (~fourfold) higher in HFD adipocytes (Figure 4D). Previous studies showed that long-term (>12 weeks) exposure to a HFD decreases insulin-stimulated signaling pathways, including phosphorylation of Akt, by regulating insulin receptor substrate's modifications [51, 55]. In the present study, feeding a HFD for only 5 weeks profoundly decreased insulin-stimulated AS160 phosphorylation, but not Akt activation (Figure 4E and Figure S5).

Discussion

RIP140 knockout animals exhibit a phenotype mostly opposite to that of metabolic syndromes [61, 66]. At least one study has shown that silencing RIP140 improves insulin-stimulated glucose uptake in adipocytes [67]. These effects have been attributed to the nuclear actions of RIP140, largely because of its widely recognized function as a nuclear receptor coregulator [4, 61, 68]. Here we report, for the first time, a new functional role for the cytoplasmic form of RIP140 as a negative regulator of GLUT4 trafficking. Cytoplasmic RIP140 interacts directly with AS160, preventing its phosphorylation by Akt, and thus, its inactivation. Maintaining AS160 in its active state preserves its ability to inactivate Rab-GTPase, thus reducing GLUT4 trafficking. The fact, that in mice exposure to a high-fat diet for 5 weeks readily elevates the level of RIP140 (particularly cytoplasmic RIP140) in epididymal adipose tissues, suggests a role for RIP140 in the progression of IR in diet-induced obesity. Interestingly, the mechanism of action appears to involve, at least in part, the activation of nuclear PKCε, which phosphorylates nuclear RIP140 and facilitates its subsequent export to the cytoplasm.

Most studies of IR focus on membrane-elicited insulin signal transduction pathways that stimulate GLUT4 trafficking. The nuclear-initiated signaling pathway identified here negatively regulates GLUT4 trafficking by increasing the export of RIP140. This conclusion is supported by the apparently effective rescue of RIP140-null cells by the CP, but not the CN, RIP140 mutant (Figure 2A, B). However, we have not completely ruled out contributions from the nuclear-localized RIP140. Rescuing RIP140 null adipocytes with RIP140 wild type or its cytoplasm-localized form (CP) slightly decreases GLUT4 protein level (Figure 2A), indicating certain unknown activity of cytoplasmic RIP140 that could modulate total GLUT4 protein level. Since manipulating the RIP140 level (or altering its PTMs) in 3T3-L1 adipocytes did not change GLUT4 mRNA levels (Figure 1D), the negative regulatory effect of RIP140 on GLUT4 trafficking does not involve its traditional function as a transcriptional corepressor. A recent study has reported that RIP140 is a key regulator in muscle metabolism [69]. It would be interesting to determine if the mechanism described here for RIP140 function in adipocytes functions similarly in muscle cells.

Inflammation and ER stress in adipose tissue are critical events in diet-induced IR and subsequent diabetes [23, 51, 55]. However, whether inflammation and ER stress represent early contributing events to IR has been debated [51, 55]. In fact, several studies showed that diet-induced inflammation and ER stress in adipose tissues are relatively late events [70, 71]. In this study, feeding mice a HFD for 5 weeks readily stimulated cytoplasmic RIP140 levels and reduced insulin stimulation of glucose uptake, without impairing Akt activation. This suggests that HFD-induced accumulation of cytoplasmic RIP140 could be an early event that dampens insulin sensitivity in adipocytes. Whether and how cytoplasmic RIP140 is related to inflammation or ER stress under prolonged feeding with a HFD needs to be evaluated.

PKCε activation in liver and muscle is an important factor for impaired insulin-stimulated glucose disposal [72, 73]. Targeting PKCε in β-cells elevates insulin secretion, whereas PKCε deletion augments whole-body glucose disposal [74, 75]. This study shows that nuclear PKCε activity could also indicate a pathophysiological condition, at least with respect to the control of GLUT4 trafficking in adipocytes.

AS160 is a newly identified GAP that functions as a negative regulator of several Rab-GTPases involved in vesicular transport, docking and fusion [56, 57, 59]. Our results show that RIP140 markedly down-regulates AS160 phosphorylation, with only a slight effect on AS160 protein expression and no effect on its mRNA levels. Thus, cytoplasmic RIP140 could also regulate AS160 protein levels via other, as yet unknown, posttranscriptional mechanisms. Whether RIP140 regulates trafficking of other vesicles remains to be determined.

Figures

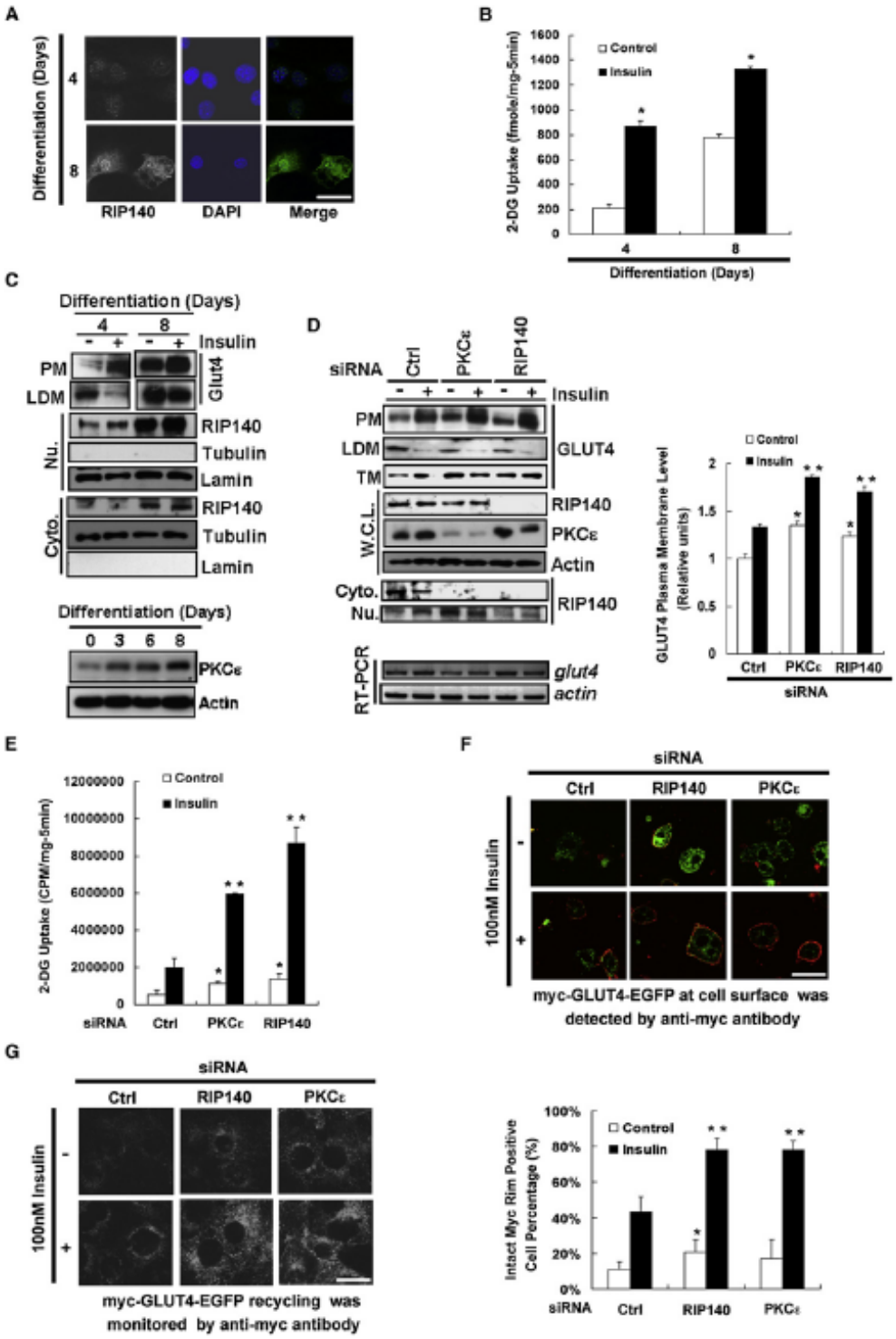
A
Differentiation (Days)
4
8
RIP140
DAPI
Merge
B
2-DG Uptake (fmole/mg-5min)
Control
Insulin
Differentiation (Days)
C
Differentiation (Days)
Insulin
PM
LDM
Glut4
Nu.
RIP140
Tubulin
Lamin
Cyto.
RIP140
Tubulin
Lamin
Differentiation (Days)
PKCε
Actin
D
siRNA
Ctrl
PKCε
RIP140
Insulin
PM
LDM
TM
GLUT4
W.C.L.
RIP140
PKCε
Actin
Cyto.
Nu.
RIP140
RT-PCR
glut4
actin
GLUT4 Plasma Membrane Level (Relative units)
Control
Insulin
siRNA
E
2-DG Uptake (CPM/mg-5min)
Control
Insulin
siRNA
F
siRNA
100nM Insulin
myc-GLUT4-EGFP at cell surface was detected by anti-myc antibody
G
siRNA
100nM Insulin
myc-GLUT4-EGFP recycling was monitored by anti-myc antibody
Intact Myc Rim Positive Cell Percentage (%)
Control
Insulin
siRNA

Figure 2-1 Increase of basal and insulin-stimulated GLUT4 trafficking and glucose uptake in adipocytes by knockdown of RIP140 or PKCε. (A) Cytoplasmic RIP140 in 3T3-L1 adipocytes (on day 4 and day 8 of differentiation). Scale bar = 40μM. (B) Glucose uptake in 3T3-L1 adipocytes which were serum starved (3 hr) and stimulated with or without insulin (100nM) for 20 min. (C) Membrane partitioning of GLUT4; distribution and expression of RIP140 in differentiated 3T3-L1 adipocytes in the absence or presence of 170nM insulin for 20 min. Levels of PKCε and other marker proteins were also monitored. PM: plasma membrane; LDM: low-density membrane; Nu: nuclear fraction; Cyto: cytoplasmic fraction. (D) Basal and insulin-stimulated GLUT4 partitioning in 3T3-L1 adipocytes. Knockdowns were conducted on day 5 of differentiation; insulin (170nM) stimulation for 20 min was performed on day 8. Left: Distributions of GLUT4, RIP140, and marker proteins. GLUT4 mRNA levels were monitored by RT-PCR. TM: total membrane fraction; W.C.L.: whole-cell lysate. Right: Relative GLUT4 levels in PM, normalized to the non-insulin-treated control. *: $p < 0.05$ vs. control; **: $p < 0.05$ vs. insulin treatment (n = 3). (E) Glucose uptake in differentiated 3T3-L1 adipocytes (Day 8). (F) Myc-GLUT4-GFP labeling in G7 adipocytes. Upper: Membrane-localized GLUT4 was detected with anti-myc. Bar = 30 μM. Lower: Quantification by scoring the percentage of cells with an intact myc rim on the surface. *: $p < 0.05$ vs. control; **: $p < 0.05$ vs. insulin treatment (n = 3). (G) Immunohistochemical staining of recycled myc-GLUT4 in G7 adipocytes. Bar = 40 μM. Data are presented as means ± SD.

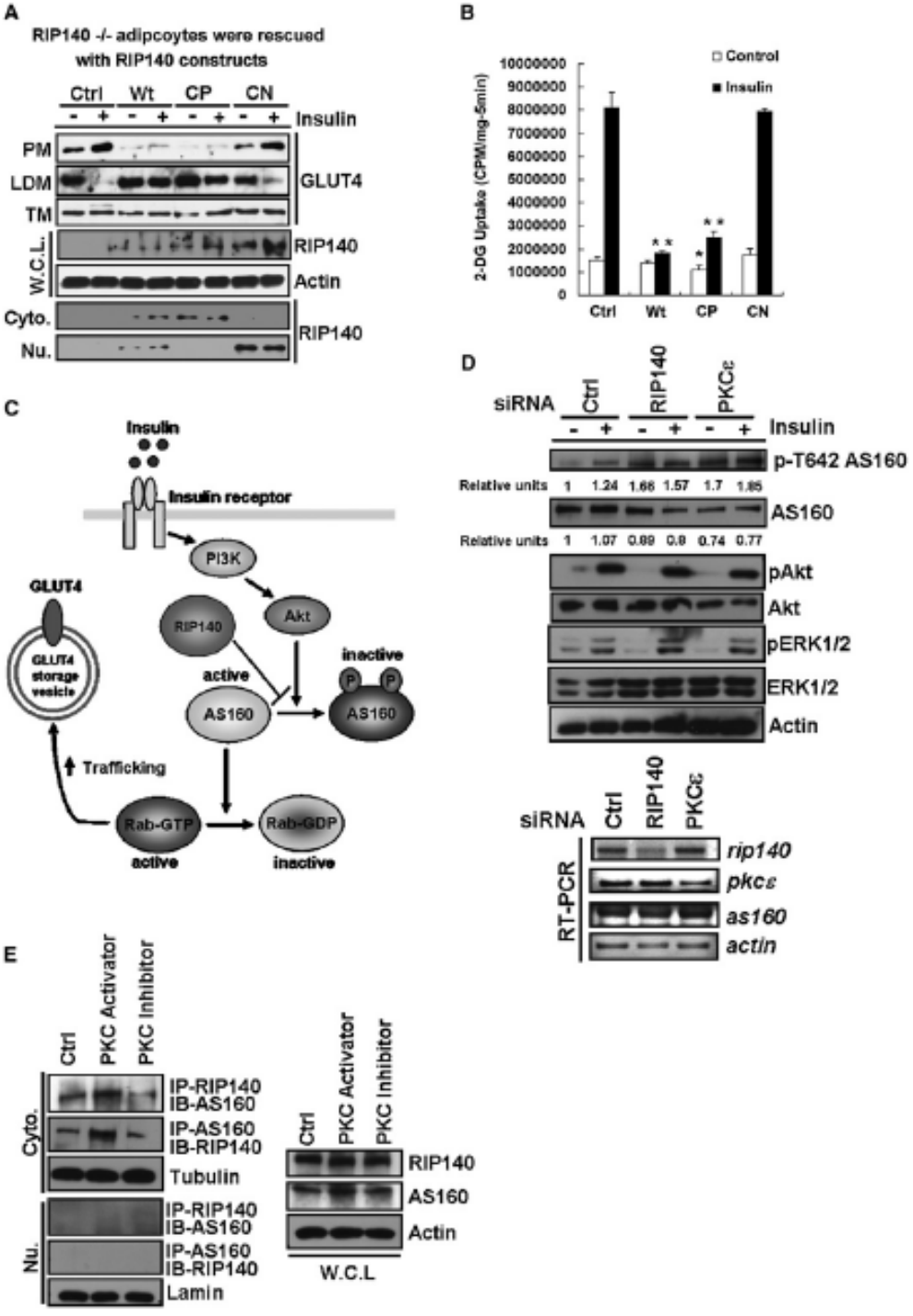
A
RIP140 -/- adipcoytes were rescued with RIP140 constructs
Ctrl
Wt
CP
CN
Insulin
PM
LDM
TM
GLUT4
W.C.L.
RIP140
Actin
Cyto.
Nu.
RIP140
B
Control
Insulin
2-DG Uptake (CPM/mg-5min)
Ctrl
Wt
CP
CN
C
Insulin
Insulin receptor
PI3K
Akt
RIP140
GLUT4
GLUT4 storage vesicle
active
inactive
AS160
Trafficking
Rab-GTP
Rab-GDP
active
inactive
D
siRNA
Ctrl
RIP140
PKCε
Insulin
p-T642 AS160
Relative units 1 1.24 1.66 1.57 1.7 1.85
AS160
Relative units 1 1.07 0.89 0.8 0.74 0.77
pAkt
Akt
pERK1/2
ERK1/2
Actin
siRNA
Ctrl
RIP140
PKCε
RT-PCR
rip140
pkcε
as160
actin
E
Ctrl
PKC Activator
PKC Inhibitor
Cyto.
IP-RIP140
IB-AS160
IP-AS160
IB-RIP140
Tubulin
Nu.
IP-RIP140
IB-AS160
IP-AS160
IB-RIP140
Lamin
RIP140
AS160
Actin
W.C.L

Figure 2-2. Cytoplasmic RIP140 modulates AS160 phosphorylation and negatively regulates GLUT4 trafficking. (A) GLUT4 trafficking. RIP140-null adipocytes were differentiated and transfected with wild type (Wt) RIP140, a PKCε phosphormimetic mutant (CP), or a constitutive negative mutant (CN) on day 5. Cells were starved for 3 hr and then treated with or without insulin for 20 min and lysates were prepared on day 8. (B) Glucose uptake in RIP140-null and rescued adipocytes. Data are presented as means ± SD. *: $p < 0.05$ vs. control treatment; **: $p < 0.05$ vs. insulin treatment in control vector-transfected cells (n = 3). (C) Summary of GLUT4 trafficking regulated by AS160, with the potential point of RIP140 intervention indicated. (D) Upper: Phosphorylation of AS160 and related kinases in G7 adipocytes, with and without insulin (170nM) stimulation for 20 min. Lower: mRNA levels monitored by RT-PCR. (E) RIP140/AS160 complex formation in 3T3-L1 adipocytes. Day-8 differentiated cells were treated with control vehicle (Ctrl), 4 μM of phorbol 12-myristate 13-acetate (PKC activator) or 50 μM of calphastin (PKC inhibitor) for 3 hrs. Left: Nuclear and cytoplasmic fractions were subjected to reciprocal immunoprecipitation (IP) and immunoblotting (IB) as indicated. Right: Total protein levels.

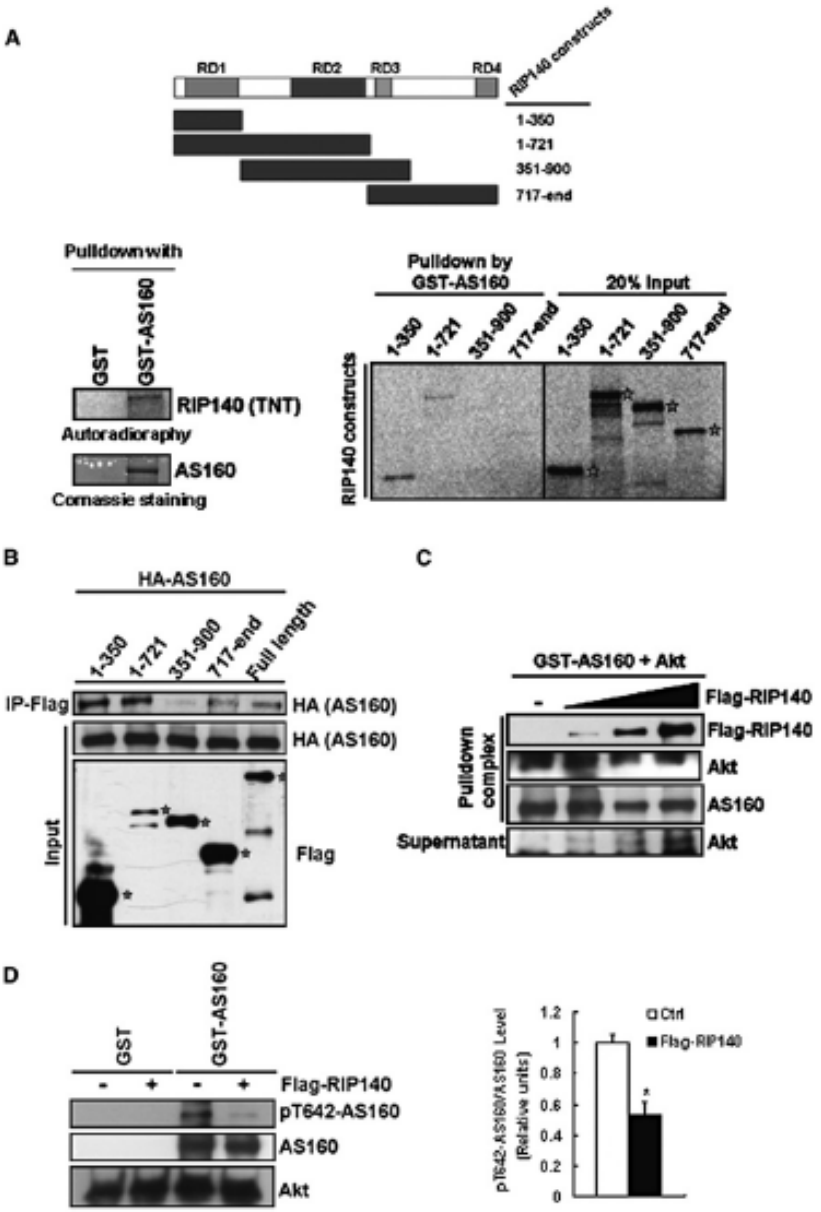
A
RD1
RD2
RD3
RD4
RIP140 constructs
1-350
1-721
351-900
717-end
Pulldown with
GST
GST-AS160
RIP140 (TNT)
Autoradiography
AS160
Comassie staining
Pulldown by GST-AS160
20% Input
1-350
1-721
351-900
717-end
RIP140 constructs
B
HA-AS160
1-350
1-721
351-900
717-end
Full length
IP-Flag
HA (AS160)
HA (AS160)
Input
Flag
C
GST-AS160 + Akt
-
Flag-RIP140
Flag-RIP140
Pulldown complex
Akt
AS160
Supernatant
Akt
D
GST
GST-AS160
-
+
-
+
Flag-RIP140
pT642-AS160
AS160
Akt
pT642-AS160/AS160 Level (Relative units)
1.2
1
0.8
0.6
0.4
0.2
0
Ctrl
Flag-RIP140
*

Figure 2-3. Direct interaction of AS160 with RIP140 maintains AS160 activity by impeding Akt-mediated phosphorylation. (A) GST pulldown assay. Upper: Map of RIP140 constructs. Lower left: Interaction of isotope-labeled full-length RIP140 with full-length GST-AS160. Lower right: Interaction of AS160 with various RIP140 segments. (B) *In vivo* complex formation of RIP140 with AS160 in COS-1 cells: immunoprecipitation with anti-Flag (for Flag-RIP140) antibodies and immunoblotting with anti-HA (for HA-AS160). Specific Flag-RIP140 fragments are indicated (*). (C) Competition between RIP140 and Akt to form complexes with AS160. GST-AS160 (~5μg) was incubated overnight with 0.25 μg active Akt2 and increasing amounts of Flag-RIP140 in a 0.5ml Co-IP buffer. Pulldown complexes and supernatants were immunoblotted as indicated. (D) Akt-mediated AS160 phosphorylation *in vitro*. GST or GST-AS160 (~5μg) were incubated overnight with or without *in vitro*-synthesized Flag-RIP140 (i.e., the highest amount used in panel C). After washing, 0.5 μg active Akt was added to the pulldown complexes in Akt kinase buffer for kinase reaction. pAS160 (pT642-AS160), total AS160 and Akt were determined by immunoblotting. Right: quantitative result of kinase assay for AS160 from two independent experiments. Data are presented as means ± SD. *: $p < 0.05$ vs. control.

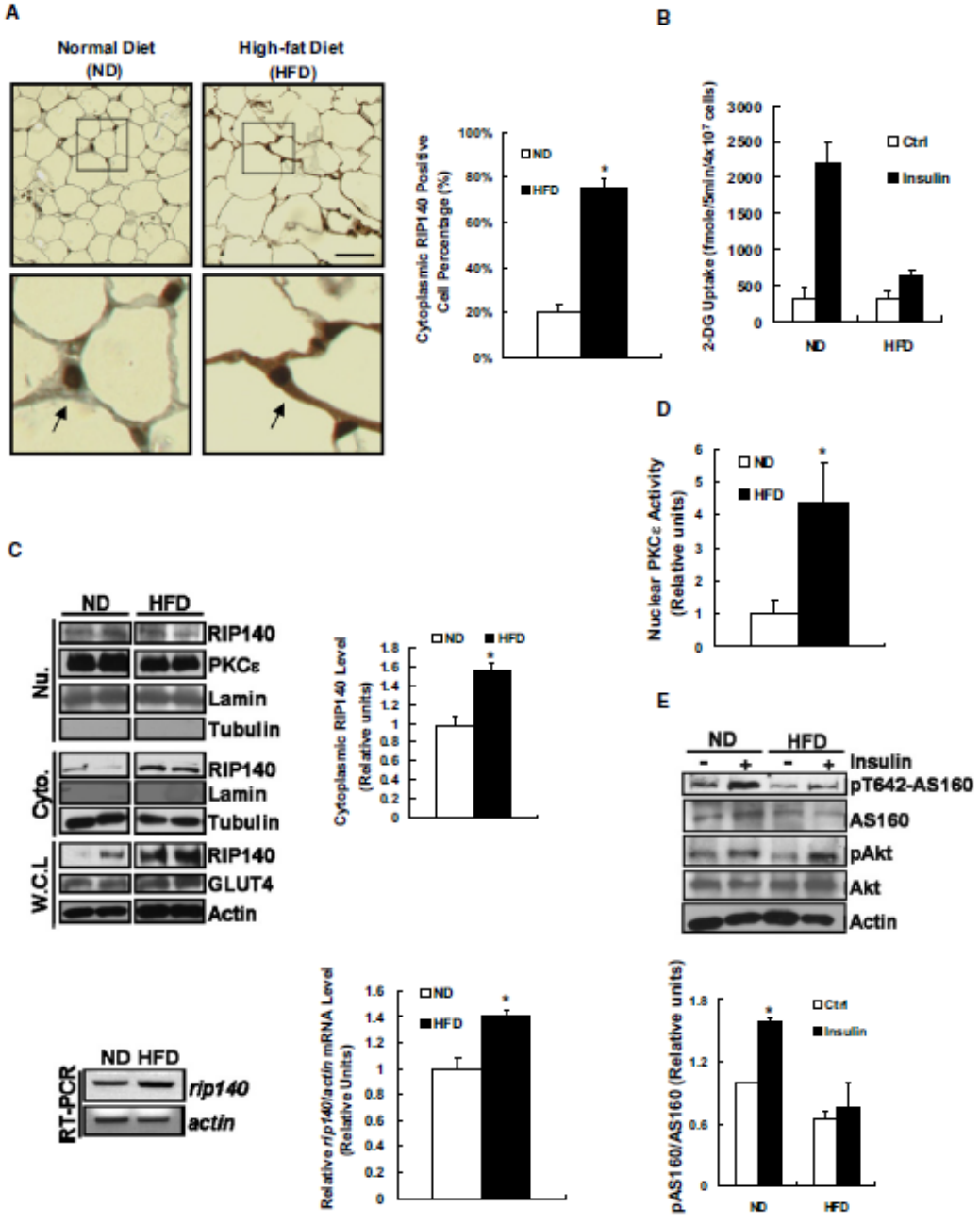
A
Normal Diet (ND)
High-fat Diet (HFD)
Cytoplasmic RIP140 Positive Cell Percentage (%)
ND
HFD
B
2-DG Uptake (fmole/5ml/4x10^7 cells)
Ctrl
Insulin
ND
HFD
C
ND HFD
Nu.
RIP140
PKCε
Lamin
Tubulin
Cyto.
RIP140
Lamin
Tubulin
W.C.L.
RIP140
GLUT4
Actin
Cytoplasmic RIP140 Level (Relative units)
RT-PCR
rip140
actin
Relative rip140/actin mRNA Level (Relative Units)
D
Nuclear PKCε Activity (Relative units)
E
Insulin
pT642-AS160
AS160
pAkt
Akt
Actin
pAS160/AS160 (Relative units)

Figure 2-4. Increases in cytoplasmic RIP140 and nuclear PKCε activity in epididymal white adipose tissues from obese mice. (A) Endogenous RIP140 in epididymal adipose tissues from mice fed ND or HFD for 5 weeks. Arrows in enlarged images (lower) point to the cytoplasmic signals of RIP140. Scale bar = 25μM. Right: Effect of HFD on the percentage of cytoplasmic RIP140-positive cells. (B) Glucose uptake in epididymal adipocytes (ND: 24 mice; HFD: 16 mice). (C) Upper left: Immunoblots of nuclear, cytoplasmic, and whole-cell RIP140 in epididymal adipocytes; each lane shows samples pooled from five mice. Relevant protein markers were monitored. Upper right: Quantification of cytoplasmic RIP140, normalized against that in ND-fed mice. Lower left: The mRNA levels determined by RT-PCR. Lower right: Quantification of RIP140 mRNA, normalized against actin. (D) Nuclear PKCε activity (ND: 18 mice; HFD: 12 mice). The average PKCε activity in ND group was set as 1. *: $p < 0.05$ vs. normal diet. (E) Phosphorylation of AS160 and relevant kinases in adipocytes, with or without insulin treatment (170nM, 20 min). Lower panel: ratio of pT642-AS160/total AS160. Data are presented as means ± SD. *: $p < 0.05$ vs. control set.

Preface

This chapter has been published:

Ping-Chih Ho, Ya-Shan Chuang, Chen-Hsiang Hung and Li-Na Wei (2011) Cytoplasmic Receptor-Interacting Protein 140 (RIP140) interacts with perilipin to regulate lipolysis. Cellular Signalling 23, 1396-1403

CHAPTER III

Cytoplasmic Receptor-Interacting Protein 140 (RIP140) interacts with perilipin to regulate lipolysis

Introduction

Adipocytes store energy as triglyceride (TG) in lipid droplets (LDs) under a nutrient-excess condition, and triglyceride can be used as the energy source through lipolysis in a nutrient-deprived state [76]. In healthy individuals, adipocytes alter their lipid storage, lipolysis, and glucose uptake according to the nutritional status and hormonal fluctuations. Defects in homeostasis of the adipose tissue (e.g., glucose uptake, proper lipid storage, adiponectin secretion) can contribute to the initiation and progression of metabolic disorders, including type 2 diabetes mellitus (T2DM) [23, 26, 28]. Increased lipolysis following a high fat diet (HFD) can also contribute to T2DM as a result of lipotoxicity, which can manifest in the liver, muscle and heart and cause insulin resistance and cardiomyopathy [23, 30, 31, 34, 35]. Free fatty acids (FFA) released by increased lipolysis can also enhance low-grade chronic inflammation by activating adipocyte tissue macrophages (ATMs), which further suppresses insulin sensitivity and adipocyte function [30, 77]. However, the exact mechanism contributing to the dysregulation of lipolysis remains elusive [23, 78].

During fasting, or in time of energy demand, TG is hydrolyzed into fatty acids and glycerol to provide a source of energy [23]. Lipolysis is a tightly regulated process, modulated by catecholamine, insulin and natriuretic peptides [76, 79]. Perilipin, a structural protein associated with LDs and involved in their formation, is the major regulator of lipolysis and can modulate the basal and stimulated lipolytic rates. In resting adipocytes, perilipin reduces lipolysis and increases lipid storage, partly by sequestering comparative gene identification-58 (CGI-58), an activator of adipose triglyceride lipase (ATGL). Normally, the cytoplasmic hormone-sensitive lipase (HSL) cannot access its substrates within the LDs, but is catecholamine-stimulated adipocytes, activated protein kinase A (PKA) phosphorylates both perilipin and HSL. Phosphorylation of perilipin frees CGI-58 to stimulate ATGL activity, whereas phosphorylation of HSL increases its association with the phosphorylated perilipin on LDs, thereby enhancing its access to substrate [80, 81]. Both mechanisms are promoted by perilipin phosphorylation, but it is less clear if the actions of perilipin can be modulated by other mechanisms.

Receptor-interacting protein 140 (RIP140) is well known as a co-regulator for numerous transcription factors and nuclear receptors. It is abundantly expressed in various tissues including ovary, uterus, and testis, as well as in metabolic tissues/organs such as adipose tissue, liver and muscle [4, 61]. Studies of RIP140 knockout mice demonstrated that RIP140 plays roles in numerous biological processes such as ovulation and metabolism [61, 82, 83]. In the nucleus, it recruits additional cofactors such as histone deacetylases (HDACs) and C-terminal binding protein (CtBP) for transcriptional regulation [1, 4]. Depleting RIP140 from adipocytes leads to decreased TG accumulation and a higher rate of fatty acid oxidation [67, 84]. Conversely, RIP140 expression is elevated during adipogenesis. Following a series of post-translational modifications (PTMs), RIP140 is increasingly exported to the cytoplasm [4, 14, 19]. In animals, HFD can induce cytoplasmic accumulation of RIP140 in adipocytes, but the signal triggering cytoplasmic accumulation of RIP140 is unclear [85]. Mechanistically, the export of RIP140 to the cytoplasm is stimulated by nuclear protein kinase C epsilon (PKCε)-elicited serine phosphorylation, followed by protein arginine methyltransferase 1 (PRMT1)-stimulated arginine methylation of RIP140 [19]. Predictably, cytoplasmic RIP140 performs functions different from those involved in gene regulation [19, 67, 84]. For example, cytoplasmic RIP140 can negatively regulate glucose transporter type 4 (GLUT4) trafficking by interacting with the 160-KDa Akt substrate (AS160), thereby reducing glucose uptake [85]. Questions remain to be answered concern the possible roles of cytoplasmic RIP140 in lipid-loaded adipocytes, especially with regards to their lipid metabolism, and the identity of specific mediators that might transmit lipid signals to promote aberrant accumulation of RIP140 in the cytoplasm of fully differentiated, lipid-loaded adipocytes after a HFD feeding.

This study shows that the adipocyte fat content can trigger cytoplasmic accumulation of RIP140, and demonstrates a new functional role for cytoplasmic RIP140 in adipocyte; specifically, it positively modulates lipolysis through its direct interaction with perilipin. The physiological relevance of this pathway is validated by examining the pro-inflammatory potential of conditioned media collected from adipocyte cultures with altered cytoplasmic RIP140 accumulation. Our findings provide new insights into the

roles of cytoplasmic RIP140 in HFD-induced adipocyte dysfunction and support the notion that targeting cytoplasmic RIP140 could be a therapeutic strategy in managing T2DM or other metabolic syndromes.

Materials and Methods

Cell Culture and Treatment

3T3-L1 cells were maintained and differentiated as described [18]. For DAGK inhibitor, mature 3T3-L1 adipocytes were treated with R59022 for 24 h and cell lysates were collected. For lipolysis, mature 3T3-L1 adipocytes were starved in serum-free medium for 3 h and then incubated with serum-free medium with or without 10 μM isoproterenol for another 2 h.

Reagents and Transfection

Antibodies for actin, lamin, CGI-58 and PKCε were from Santa Cruz Biotechnology. Anti-flag, anti-alpha tubulin, anti-calnexin and anti-perilipin A were from Sigma Aldrich. Anti-Oxophos complex IV antibody was from Upstate. Anti-HSL, anti-ATGL and anti-Phospho-PKA substrate antibodies were from Cell signaling. Anti-perilipin A, anti-giantin and anti-calreticulin antibodies were from Abcam. Anti-RIP140 (ab42126) was from Abcam and its specificities in immunofluoresence and immunoblotting were determined in previous report [85]. Anti-cyclophilin A antibody was from calbiochem. siRNAs were from Qiagen. Insulin was from Sigma Aldrich. Isoproterenol was from Cayman. BODIPY 493/503 was from Molecular Probes (Invitrogen). siRNA transfect ion was conducted by DeliverX Plus siRNA transfection kit (Panomics) as manufacturer's instruction. Plasmid of full length and different fragments of Flag-RIP140 constructs

were as described [85]. Plasmid of full length and different fragment of perilipin were cloned from cDNA of 3T3-L1 adipocyte and then cloned into pCMV-PL vector-containing 3xFlag tags.

Western Blotting, Immunoprecipitation and Immunofluoresence

Western blotting was conducted as described previously [18]. For immunoprecipitation, 500 μg whole cell lysates were incubated with 5 μg indicated antibodies for 2~3 h in 500 μl Co-IP buffer (50mM Tris-HCl pH 8.0, 10% glycerol, 100mM NaCl, 1mM EDTA and 0.1% NP-40) and then incubated with protein G beads (Upstate) overnight. After centrifugation, beads were washed using a Co-IP buffer three times, and the precipitates were subjected into SDS-PAGE for western blotting. Immunofluorescence assay was conducted as a previous report [85]. For co-staining with lipid droplet, BODIPY 493/503 and fluorescence-conjugated secondary antibodies were co-incubated with cells for 1~3 h. Images were acquired by Olympus FluoView1000 IX2 inverted confocal microscope. Colocalization analysis was performed by Manders Coefficients in Image J as previous described [86].

Cell fractionation

Nuclear and cytoplasmic fractionation, cells were collected and fractions were collected as in a previous report [85]. Forty 10-cm plates with mature 3T3-L1 adipocytes were collected for isolating organelles as reported (31). 80 μg proteins from indicated organelles were subjected into western blotting. Organelles isolation was performed as previous report [87].

TG Content Measurement and Lipolysis Assay

TG content was assayed as described previously [18]. For lipolysis assay, cells were starved in serum-free medium and then stimulated with or without isoproterenol for 2 h. Media were collected and glycerol levels within the media were determined by adipolysis

assay kit (Cayman) as manufacture's instruction. The glycerol levels were normalized to the protein amounts of the cell lysates.

In Vitro GST Pull-down Assay

GST-RIP140 and GST-perilipin were produced by BL-21 strain. Expression was induced by IPTG at 20^{o}C overnight. Bacteria pellets were lysed in PBS. For GST-perilipin, lysate was collected and incubated with GST beads to purify GST-perilipin. For GST-RIP140, after centrifugation, insoluble pellet was lysed by Inclusion Body Solubilization Reagent (Thermo Scientific) and lysate was dialyzed as instruction. Dialyzed lysate was incubated with GST beads to purify refolded GST-RIP140. For pull-down assay, it was conducted as a previous report with modifications [85]. In GST-RIP140 set, the washing condition was 50mM Tris-HCl pH 8.0, 10% glycerol, 100mM NaCl, 1mM EDTA and 2% NP-40. Peptide fragments were synthesized in vitro by TNT assay kit as previous report [85].

Mice

Male mice (C56BL/6J) (Jackson Laboratory) were housed in a temperature-controlled environment with 12-hr light/dark photocycle and fed with a normal diet (5% fat) (#2018, Harlan Teklad) or a high-fat diet (HFD) (60% fat) (#F3282, Bio-Serv). Animal experiments were conducted in procedures approved by University of Minnesota Institutional Animal Care and Use Committee.

Tissue Collection and Immunohistochemical Staining

Epididymal adipose tissues were fixed, embedded and sectioned by the Histology & Microscopy Core Facility (University of Minnesota). Immunohistochemical staining of RIP140 and perilipin was performed as previously described [19]. The nuclei of sections were stained with DAPI then mounted (Vector Laboratories) for microscopic analysis (Olympus FluoView1000 IX2 inverted confocal microscope).

Results

Fat content modulates sub-cellular distribution of RIP140 in adipocytes. Previously, we reported that, in adipocyte, RIP140 could be exported to the cytoplasm by PKCε- and PRMT1-mediated post-translational modifications [15, 21, 22]. In mature adipocyte, nuclear export of RIP140 is profound, and a HFD feeding dramatically increases cytoplasmic RIP140 levels in the animals' adipose tissues [19, 85]. These observations suggest that fat content within adipocytes may be involved in cytoplasmic accumulation of RIP140. To investigate the relationship between fat content and RIP140 sub-cellular localization, we monitored RIP140 localization and the size of LDs in 3T3-L1 adipocytes. Those differentiated 3T3-L1 adipocytes containing larger LDs exhibited stronger cytoplasmic RIP140 staining (Fig. 1A). Approximately 80% of adipocytes containing large LDs displayed cytoplasmic RIP140, whereas only ~15 % of the adipocytes containing small LDs had RIP140 in the cytoplasm, suggesting that an increase in fat content stimulates cytoplasmic accumulation of RIP140. It has been shown that the DAG level is elevated when adipocytes extensively accumulate lipid [75, 78]; further, DAG is an important activator for PKCε activation which is involved in nuclear export of RIP140 [4]. We then hypothesized that, in adipocyte, an increase in DAG levels may promote cytoplasmic accumulation of RIP140. To investigate this possibility, we treated fully differentiated 3T3-L1 adipocytes with a non-selective DAG kinase inhibitor (R59022) to block DAG metabolism (thus increasing DAG levels). This treatment reduced nuclear RIP140 levels and increased cytoplasmic RIP140 levels (Fig. 1B). DAG kinase alpha (DGKα) is the most common form in the DAG kinase family and is mainly expressed in the cytoplasm. In contrast, DAG zeta (DGKζ) is a nuclear form of the DAG kinase family and is involved in ET-1-induced cardiomyote hypertrophy [88, 89]. To confirm the functional role for DAG kinases in the accumulation of cytoplasmic RIP140, we used siRNAs to knock down these two DAG kinases (Fig. 1C). The data show that knocking down either DGKα or DGKζ substantially increased the accumulation cytoplasmic RIP140 but reduced nuclear RIP140 level. Together, these results suggest that changes in DAG levels can modulate RIP140's sub-cellular localization. Therefore, in adipocytes, an

increase in fat content, or more specifically an increase in intracellular DAG levels, can promote cytoplasmic accumulation of RIP140.

RIP140 localizes to lipid droplet surfaces and interacts directly with perilipin. Although it was clear that RIP140 could be exported into the cytoplasm in adipocytes, the specific cytoplasmic localization of RIP140 was unknown. We then performed sub-cellular fractionation, by ultracentrifugation, of mature 3T3-L1 adipocytes. RIP140 was then detected by immunoblotting of these sub-cellular fractions. The result shows that RIP140 is detected in cytosol, endoplasmic reticulum, and LD (Fig. 1D), but not in mitochondria, or Golgi (Fig. S1). Interestingly, the LD fraction had particularly abundant RIP140. We then examined if RIP140 could associate with perilipin, a LD-associated protein and an important regulator of the formation and maintenance of LDs. Intriguingly, RIP140 can be colocalized with perilipin around LDs and formed immuno-complexes with perilipin *in vivo,* and knocking down either component reduced the formation of these complexes (Fig. 1E and F). The quality and specificity of RIP140 antibody in these experiments have been described previously [23]. Note that in the cytoplasm, RIP140 is wide distributed; therefore it is only partially co-localized with perilipin that is much more enriched in LDs. We have shown that RIP140 accumulated in the cytoplasm of adipose tissue in animals after a HFD feeding [85], we then evaluated if RIP140 could colocalize with perilipin in the primary adipocytes of animals fed a HFD. Indeed, RIP140 also partially colocalized with perilipin in epididymal adipose tissue from mice fed with a HFD (Fig. 1G, the lower boxed area showing prominent yellow signal indicative of co-localization), whereas no such colocalization was seen in adipocytes from mice fed a normal diet (Fig. 1G, the upper boxed area showing little yellow signal). The degree of colocalization in ND versus HFD animals was examined and indicated with Pearson's coefficient (Fig. 1G, right panel). All together, the results show that cytoplasmic RIP140 can associate with perilipin around LDs in adipocyte, which can be enhanced by a HFD feeding in animals.

In vitro reciprocal protein interaction assays further confirmed that RIP140 interacted directly with perilipin (Fig. 2A). We then examined the perilipin-interacting

domain of RIP140 by GST pull-down assay, and found that the perilipin-interacting domain of RIP140 was located in the amino terminus (amino acids 1-350) of RIP140, which contains the repressive domain 1 (RD1) (Fig. 2B). As shown in the reciprocal GST pull-down assay, the amino terminus (1-160) of perilipin could not, but all the remaining fragments of perilipin could, interact with GST-RIP140 (Fig. 2C). Interestingly, the amino terminal portion (amino acids 1-405) that extends to the hydrophobic regions of perilipin interacted weakly with RIP140 as compared to fragments of 1-250 residues and 251-the end. It is possible that these hydrophobic regions could form structural barriers, reducing perilipin's interaction with RIP140 in the *in vitro* assay [90]. This result suggests that the central portion (amino acids 161-300) of perilipin is the major RIP140-interacting domain and the hydrophobic region of perilipin may be involved in the regulation of this interaction. Importantly, although the amino terminus of perilipin (amino acids 17-121) is the most highly conserved domain in this protein family [91], this region failed to interact with RIP140, suggesting that interaction between perilipin and RIP140 is highly specific, but not a general phenomenon common to the perilipin protein family.

Silencing RIP140 expression or inhibiting its export reduces lipolysis. Perilipin contributes to LD formation and controls lipolytic rates [76, 81, 91]. Nuclear RIP140 can promote lipid accumulation in adipocytes through its gene regulatory activities, thus nuclear export of RIP140 would reduce the lipid content in adipocytes [4, 14, 82]. However, it was elusive whether other mechanisms could also be contributed by cytoplasmic RIP140 to regulate lipid metabolism in adipocyte. The association of RIP140 with perilipin around LDs suggests that RIP140 may modulate lipolysis by regulating the activity of perilipin, or its associated lipases. To test this hypothesis, we manipulated adipocyte's RIP140 level or its nuclear export (stimulated by PKCε) and monitored lipolysis, indicated by the reduction in TG content under isoproterenol treatment. This assay monitors changes in the percentage of TG content under a 2h isoproterenol treatment, reflecting, primarily, the effects via lipolysis. We found that reducing cytoplasmic RIP140 levels, by direct silencing or blocking its nuclear export (through silencing PKCε), significantly reduced isoproterenol-stimulated lipolysis (Fig. 3A). But

the basal TG content (reflecting, primarily, lipid synthesis) was reduced only in RIP140-silenced, but not in PKCε-silenced (only blocking RIP140 export) adipocytes (Fig. S2). The nuclear RIP140 is known to regulate genes that modulate lipogenic capacity in adipocytes [5, 19, 67], which is blocked only when its expression, rather than its export, is reduced. Furthermore, direct assessment of lipolysis by measuring the amount of glycerol released to the culture medium showed that silencing RIP140 or PKCε significantly reduced both the basal and stimulated glycerol release relative to the control silencing (Fig. 3B). Interestingly, silencing RIP140 or PKCε did not affect the expression of key lipolytic enzymes/regulators (HSL, ATGL, cofactor CGI-58, and perilipin) (Fig. 3C). Of note, isoproterenol effectively induced glycerol release in either RIP140- or PKCε-silencing adipocytes, although PKCε-silencing seemed to cause a more profound effect. However, basal glycerol release was significantly reduced by silencing either RIP140 or PKCε. These results suggest that cytoplasmic RIP140 might regulate the basal lipolytic machinery but not isoproterenol-stimulated signaling pathways. Altogether, these results indicate that cytoplasmic RIP140 positively modulates the lipolytic machinery, but does not seem to affect the expression of lipolytic proteins.

Effects of cytoplasmic RIP140 on the formation of lipolytic enzyme complexes. Lipolysis is controlled, primarily, by the formation of perilipin-HSL and CGI-58-ATGL enzyme complexes [76, 91]. In resting adipocytes, inactive HSL is dispersed throughout the cytoplasm whereas ATGL is localized on LDs and remains inactive because it is segregated from its perilipin-associated activator CGI-58. In catecholamine-stimulated adipocytes, perilipin on LDs recruits HSL to access its substrates, and CGI-58 dissociates from perilipin to activate ATGL [76, 80, 81]. We first asked if cytoplasmic RIP140 can affect the interaction of perilipin with HSL. It appears that silencing RIP140 or PKCε markedly reduced the formation of HSL-perilipin complexes in co-immunoprecipitation assay (Fig. 4A). Importantly, silencing RIP140, or PKCε, had no effect on perilipin phosphorylation (Fig. 4B) or HSL phosphorylation (Fig. 4C). These results further support that cytoplasmic RIP140 does not alter PKA signaling which is in agreement with the observation shown in Fig. 3B that cytoplasmic RIP140 does not affect

isoproterenol-stimulated signaling pathways. Instead, cytoplasmic RIP140 appears to promote lipolysis by facilitating the formation of perilipin-HSL complexes. Finally, silencing RIP140 or PKCε enhanced complex formation between CGI-58 and perilipin (Fig. 4D), thus reducing ATGL activation. Taken together, the data show that cytoplasmic RIP140 elevates lipolysis by promoting the formation of HSL/perilipin and ATGL-CGI-58 complexes, which increases the accessibility of HSL with its substrate, and enhance ATGL activity, respectively.

Conditioned medium from cytoplasmic RIP140-deficient adipocyte cultures is less effective in eliciting a pro-inflammatory response in macrophages. Free fatty acids released by adipocytes can be proinflammatory for macrophages, i.e., they trigger M1 activation of macrophages via a TLR4- NF-κB-dependent mechanism, thus contributing to diabetic progression [77]. Based on the role of cytoplasmic RIP140 in regulating lipolysis, we then examined the effect of cytoplasmic RIP140 in modulating the proinflammatory potential of adipocyte-conditioned media, assessed by M1 activation of macrophages. As predicted, the conditioned media from isoproterenol-treated control cultures (increased lipolysis renders free fatty acid release) more effectively induced NF-κB activity in macrophage cultures than did the medium from the unstimulated controls (Fig. 5A). In contrast, the conditioned media from RIP140- or PKCε-silenced adipocyte cultures (blocking cytoplasmic RIP140 to reduce lipolysis, resulting in less free fatty acid release) exerted much weaker effects on NF-κB activation in macrophages. Furthermore, the conditioned media from RIP140- or PKCε-silenced adipocyte cultures were less effective than the controls in elevating the expression of endogenous proinflammatory genes IL-1β and IL-6 in macrophages (Fig. 5B). Together, these data show that the conditioned media of adipocyte cultures with reduced cytoplasmic RIP140 accumulation is less proinflammatory.

Discussion

HFD feeding promotes nuclear export of RIP140 in adipocytes [85]. Although RIP140, as a nuclear coregulator, has been known for its role in lipid accumulation in the adipose tissue, its functional role in the cytoplasm of adipocyte, with regards to lipid metabolism, was unclear. This study aimed to determine the signals promoting cytoplasmic RIP140 accumulation, and to determine the role of cytoplasmic RIP140 in lipid metabolism of adipocytes. Here, we demonstrate that fat content, especially an elevation in DAG levels (such as those triggered by a high fat content), facilitated RIP140 nuclear export and its localization on LDs. Cytoplasmic RIP140 facilitated lipolysis neither by affecting the expression nor the phosphorylation of key lipolytic enzymes, but rather via its direct interaction with perilipin that ultimately activates HSL and ATGL, two key lipolytic enzymes (Fig. 5C). Thus, RIP140's cytoplasmic functions appear to rely primarily on its ability to interact with various proteins: In glucose uptake, RIP140 interferes with GLUT4 trafficking via its direct interaction with AS160 [85], whereas in lipolysis it interacts with perilipin associated with LDs.

The underlying mechanisms by which RIP140 alters its molecular interactions with perilipin remain to be determined. The dissection of key interacting domains, with respect to each interacting partner, would be needed to address this question. To this end, it is known that perilipin interacts with CGI-58 through its C-terminal region (amino acids 382-429) and with HSL through both its N- (amino acids 141-200) and C-terminal (amino acids 406-480) regions [90, 91]. This study identified the putative TAG protection regions of perilipin – a region that partially overlaps with the HSL- and CGI-58-interacting domains- as its major RIP140-interaction domain. Upon recruitment of RIP140, conformational changes could occur on perilipin, promoting its interaction with HSL while reducing its ability to associate with CGI-58. Importantly, the regulation of perilipin interaction with HSL and CGI-58, by RIP140, does not involve perilipin phosporylation. Further studies are required to determine the molecular details of such conformational changes, and to evaluate whether other PTMs of RIP140 might regulate its interactions with these cytoplasmic factors.

Studies in transgenic mice identified DAG as an important regulator that promotes insulin resistance and T2DM. An over abundance of nutrition, especially by HFD feeding, dramatically increases DAG levels in adipose tissue, muscle cells and liver, which in turn activates several members of the PKC family to reduce insulin sensitivity [31, 75]. Among these, PKCε is a novel member that can be activated solely by DAG [75]. The exact mechanisms responsible for elevated DAG levels in fully differentiated adipocytes and in HFD-fed mice remain to be determined [75, 78]. Nevertheless, activation of PKCε by elevated DAG levels presents a likely mechanism by which HFD could stimulate the nuclear export of RIP140. Activated PKCε phosphorylates two specific serine residues on nuclear RIP140, which then stimulates arginine methylation of three arginine residues; this in turn increases RIP140's interaction with exportin for nuclear export [4, 14]. Conversely, blocking PKCε activation might retard RIP140 nuclear export and reduce its cytoplasmic activity. Consistent with this mechanism, promoting fatty acid oxidation by the mitochondrial uncoupler or inhibiting acetyl-CoA carboxylase-1 and -2 to reduce intracellular DAG levels prevents PKCε activation and enhances glucose uptake in adipose tissue [92, 93]. Thus, regulating RIP140 nuclear export could be an effective strategy to modulate glucose uptake and lipolysis in adipose tissue.

Other studies in transgenic mice suggest that the increased adipogenic capacity in adipose tissue is an anti-diabetes response [30, 34, 35]. Adipocytes normally expand in a healthy process, and reduced necrosis and lipolysis can be protective for liver, muscle and heart under over-nutrition [23, 30]. The increase in the lipolytic rate in both obese mice and patients contributes to the initiation and progression of several metabolic disorders. However, the mechanisms that regulate healthy adipocyte expansion and reduce unwanted lipolysis remain elusive. The adipose tissues of RIP140 knockout mice have reduced fat and increased β-oxidation. Some of these effects can be partially attributable to the transcriptional regulatory activity of nuclear RIP140 [5, 67]. In the nucleus, RIP140 regulates the expression of genes that are important for lipid accumulation and fatty acid oxidation [5, 84]. However, the discovery that RIP140 also modulates important biological processes in the cytoplasm justifies a re-evaluation of its

possible contributions to the overall regulation of metabolic processes in whole animals and under diseased conditions. For example, increasing cytoplasm RIP140 could decrease glucose uptake (thus reducing the availability of acetyl-CoA) [23] and escalate lipolysis (enhancing TG degradation) (this study); this would presumably provide a counteracting mechanism to maintain the overall lipid homeostasis in adipocytes when they mature and begin to accumulate lipid. Interestingly, over-expression of RIP140 in mice results in impairment of cardiac functions and cardiac hypertrophy [6]. To this end, RIP140 might contribute to these cardiac defects by promoting lipotoxicity.

Overall, these studies support the hypothesis that RIP140 responds to changes in the nutritional status of an individual by altering its activity and sub-cellular distribution. The cytoplasmic RIP140 can retard glucose uptake by interacting with AS160 [23], which would reduce the availability of acetyl-CoA for lipid synthesis. This study further shows that the cytoplasmic RIP140 can promote lipolysis to reduce lipid load. Accordingly, it may be a vital strategy to target cytoplasmic RIP140, such as by preventing its nuclear export, to provide beneficial effects under certain pathological conditions, such as by enhancing glucose uptake and reducing lipolysis.

Figures

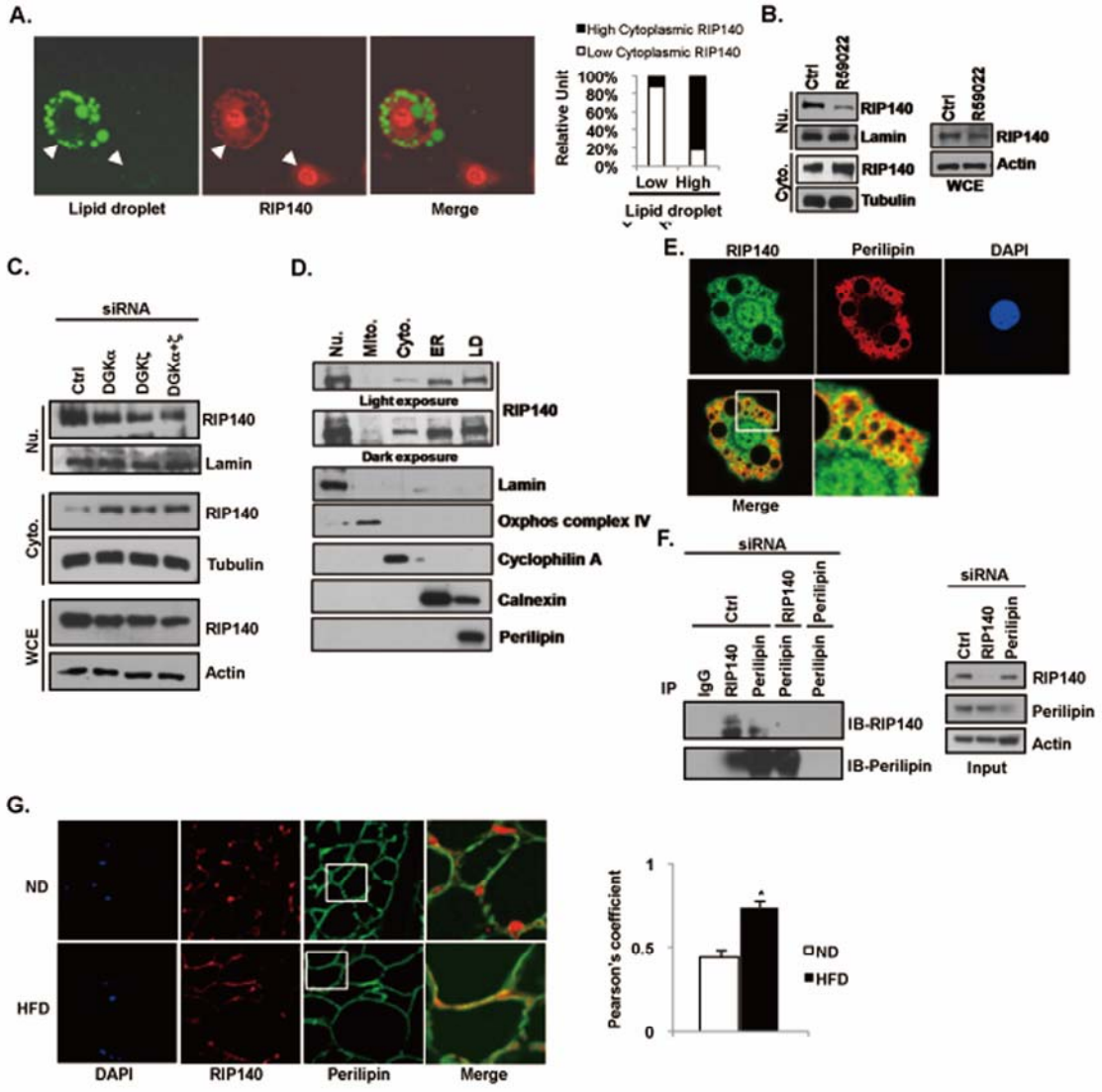
A.
Lipid droplet
RIP140
Merge
High Cytoplasmic RIP140
Low Cytoplasmic RIP140
Relative Unit
100%
80%
60%
40%
20%
0%
Low High
Lipid droplet
B.
Ctrl
R59022
Nu.
RIP140
Lamin
Cyto.
RIP140
Tubulin
WCE
RIP140
Actin
C.
siRNA
Ctrl
DGKα
DGKζ
DGKα+ζ
Nu.
RIP140
Lamin
Cyto.
RIP140
Tubulin
WCE
RIP140
Actin
D.
Nu.
Mito.
Cyto.
ER
LD
Light exposure
RIP140
Dark exposure
Lamin
Oxphos complex IV
Cyclophilin A
Calnexin
Perilipin
E.
RIP140
Perilipin
DAPI
Merge
F.
siRNA
Ctrl
RIP140
Perilipin
IP
IgG
RIP140
Perilipin
Perilipin
Perilipin
IB-RIP140
IB-Perilipin
siRNA
Ctrl
RIP140
Perilipin
RIP140
Perilipin
Actin
Input
G.
ND
HFD
DAPI
RIP140
Perilipin
Merge
Pearson's coefficient
1
0.5
0
*
ND
HFD

Figure 3-1 Fat content in adipocytes affects RIP140 localization. (A) Immunofluorescence analysis of RIP140 distribution in mature 3T3-L1 adipocytes. Left: Green: lipid droplet staining; red: RIP140 staining. Right: Quantitative analysis of RIP140 distribution and lipid droplet size. Data are the percentage of cell in each category. (B) The DAG kinase inhibitor R59022 enhances cytoplasmic RIP140 distribution but reduces nuclear RIP140 in mature 3T3-L1 adipocytes *(left)*, whereas total RIP140 levels remain unchanged (right). (C) Knocking down DGKa and DGKz increases the cytoplasmic RIP140 level, but decreases the nuclear RIP140 level in mature 3T3-L1 adipocytes. (D) Immunoblot analysis of the sub-cellular distribution of RIP140. Fractions were identified by probing with the indicated organelle-specific markers. Nu: nuclei; Mito: mitochondria; Cyto: cytosol; ER: endoplasmic reticulum; LD: lipid droplets. (E) RIP140 colocalizes with perilipin in adipocytes. The yellow indicates complete colocalization of RIP140 with perilipin. (F) RIP140 and perilipin form immunocomplexes *in vivo*. Knocking down either RIP140 or perilipin reduces immunocomplex formation. (G) Short-term HFD feeding promotes the colocalization of RIP140 with perilipin in mouse epididymal adipose tissue. ND: normal diet; HFD: high-fat diet. Right: the quantification of co-localization. Data show the averages of Pearson's coefficient for the indicated group. *: p value < 0.05 compared to the ND group.

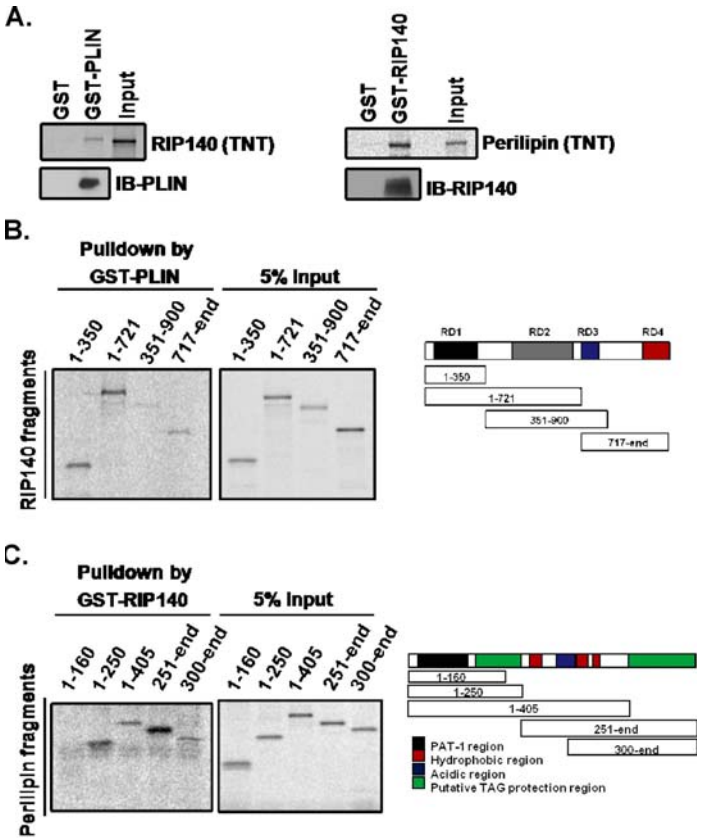

Figure 3-2. Interacting domains of RIP140 and perilipin, as determined by glutathione *S*-transferase (GST) pull-down assays. (A) RIP140 directly interacts with GST-perilipin (left) and perilipin (PLIN) directly interacts with GST-RIP140 (right). (B) Interacting domains of RIP140. Right: Schematic of the *in vitro*-produced RIP140 peptide fragments. RD: repressive domain. (C) Interacting domains of perilipin. Right: Schematic of the *in vitro*-produced perilipin peptide fragments.

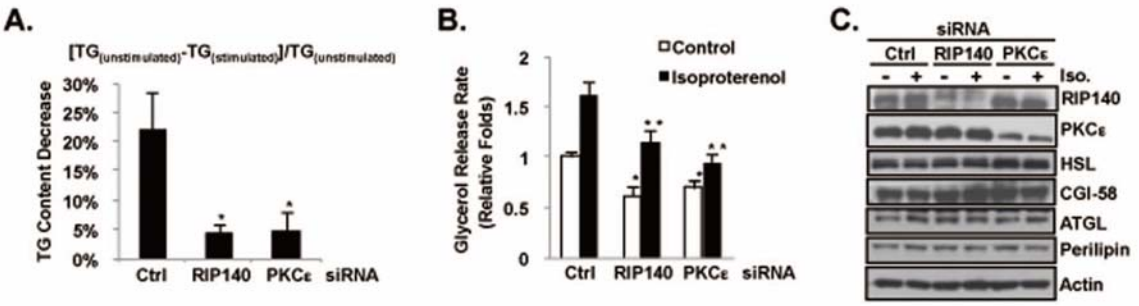

Figure 3-3. Cytoplasmic RIP140 facilitates lipolysis. (A) Silencing RIP140 or PKCε reduces the isoproterenol-triggered decrease of triglyceride (TG) content in adipocytes. Bars indicate the means ± SD of the ratios of reduced TG : total TG content from untreated cells (as calculated by the equation above the figure). *: p value < 0.05 compared to the control (Ctrl) group. (B) Silencing RIP140 or PKCε decreases basal and isoproterenol-stimulated glycerol release from cultured adipocyte. Bars indicate the means ± SD of the relative amounts of released glycerol. *: p value < 0.05 compared to the control siRNA in the control group. **: p value < 0.05 compared to the control siRNA in the isoproterenol group. (C) Targeting RIP140 or PKCε did not change the expression profile of lipolysis-related proteins. Expression levels of indicated proteins in whole cell lystaes were determined by immunoblotting.

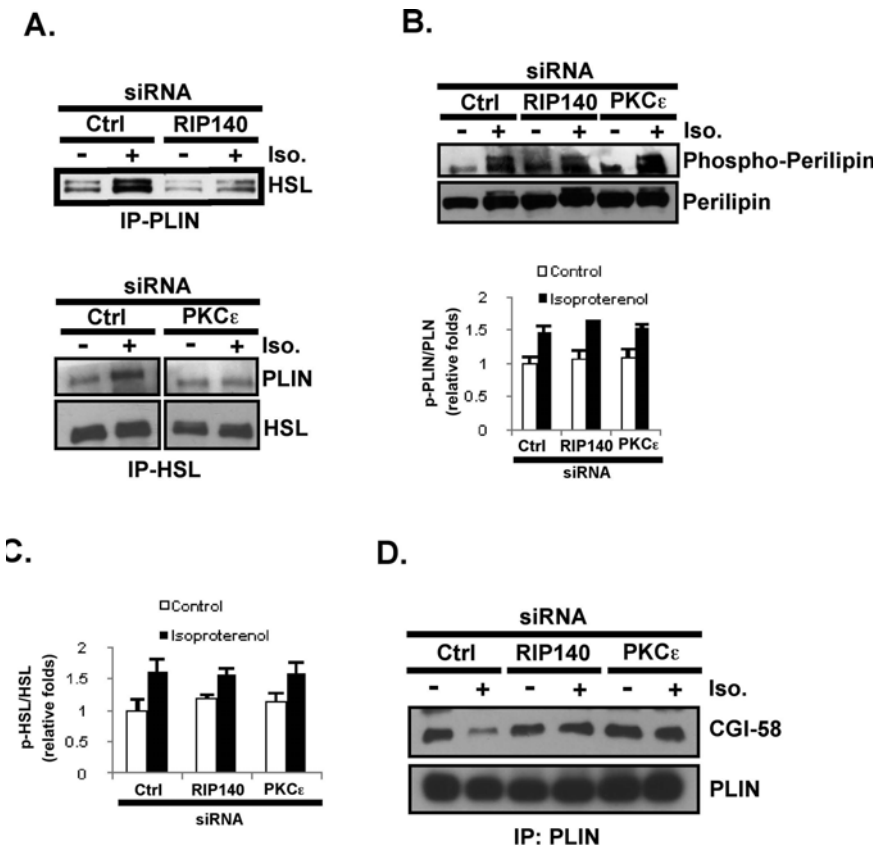

Figure 3-4. Silencing cytoplasmic RIP140 reduces isoproterenol-stimulated HSL-perilipin colocalization and complex formation, as well as CGI-58 association with ATGL. (A) Isoproterenol-stimulated HSL-perilipin complex formation, *in vivo,* is reduced by silencing RIP140 (left) or PKCε (right). (B) Upper: Basal and stimulated phosphorylation status of perilipin under RIP140 or PKCε silencing. Lower: Quantified result is presented as mean ± SD of phosphor-perilipin/perilipin ratios. (C) Neither RIP140- or PKCε-silencing can alter the basal or stimulated phosphorylation status of HSL. Quantified result is presented as mean ± SD of phosphor-HSL/HSL ratios. (D) silencing RIP140 or PKCε blocks the isoproterenol-stimulated dissociation of CGI-58 from perilipin.

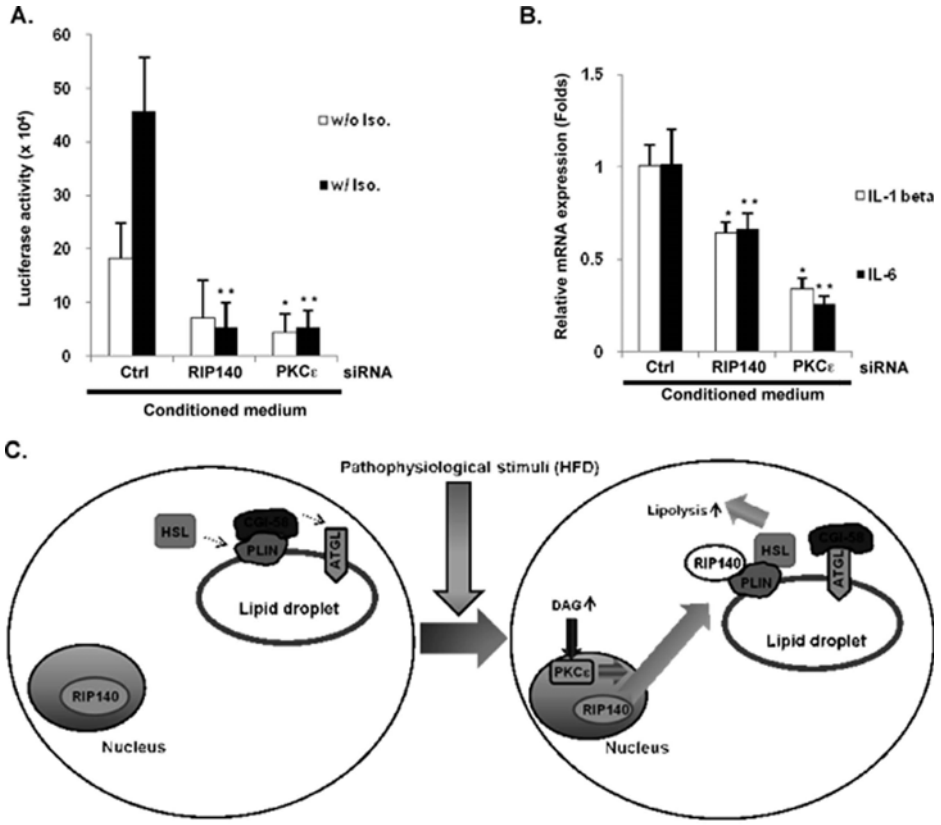

Figure 3-5. Reducing cytoplasmic RIP140 in adipocytes suppresses the inflammatory properties of their conditioned media. (A) Silencing RIP140 or PKCε in adipocytes reduces the ability of the conditioned media to activate NF-κB activity in cultured Raw264.7 macrophages. *: p value < 0.05 compared to the control siRNA in the control group. **: p value < 0.05 compared to the control siRNA in the isoproterenol group. (B) Silencing RIP140 or PKCε in 3T3-L1 adipocytes reduces the ability of their conditioned media to activate expression of endogenous proinflammatory genes in Raw264.7. *: p value < 0.05 compared to the control group of IL-1 beta. **: p value < 0.05 compared to the control group of IL-6. (C) Schematic presentation of the role of cytoplasmic RIP140 in modulating lipolysis in adipocytes. After HFD feeding, the DAG-PKCε signaling cascade promotes nuclear export of RIP140. Cytoplasmic RIP140 then interacts with perilipin to enhance lipolysis by promoting the formation of perilipin-HSL and ATGL/CGI-58 complexes.

Preface

This chapter has been published:

Ping-Chih Ho, and Li-Na Wei (2012) Negative regulation of adiponectin secretion by receptor interacting protein 140 (RIP140). Cellular Signalling 24, 71-76

CHAPTER IV

Negative regulation of adiponectin secretion by receptor interacting protein 140 (RIP140)

Introduction

In recent years obesity has become a worldwide epidemic. A major complication of obesity is type 2 diabetes mellitus (T2DM). The hallmark of this condition is the development of insulin resistance in adipose, muscle and liver [49]. In healthy individuals, adipocytes store lipid and secretes adipokines, and these adipokines are important in the regulation of metabolism. But in diabetic subjects, there is adipocyte dysfunction with changes in the profile of secreted adipokines, increase of lipolysis and reduction in glucose uptake. These changes may worsen the disease state leading to such complications as hypertension, atherosclerosis and cardiomyopathy [23, 49]. Although inflammation and endoplasmic reticulum (ER) stress could cause adipocyte dysfunction, the exact etiology of many of these pathophysiological processes is unclear [23, 51, 55].

RIP140 is a co-regulator for various nuclear receptors and transcription factors. It plays important roles in many biological activities and several disease conditions including the metabolic syndrome, especially T2DM [4, 67, 84, 85]. In adipogenesis, both the expressions of RIP140 mRNA and protein are elevated. In this process, RIP140 acquires extensive post-translational modifications (PTMs) such as phosphorylation, acetylation, methylation and vitamin B6 conjugation. These PTMs can modulate RIP140's gene-regulatory activity and alter its sub-cellular distribution [4, 14, 16, 84]. Recently, we found that activated nuclear PKCε phosphorylates RIP140 in adipocytes and the phosphorylated RIP140 is subsequently methylated at three arginine residues by protein arginine methyltransferase 1 (PRMT1). These modifications enhance the interaction of exportin 1 with RIP140 to promote RIP140's nuclear export [4, 14]. We also demonstrated that the cytoplasmic RIP140 can blunt both basal and insulin-stimulated glucose uptake by interacting with AS160 to retard GLUT4 vesicle trafficking in adipocytes [85]. We found that interaction of RIP140 with AS160 maintains AS160's activity by preventing Akt-mediated inactivation. In another study, we reported cytoplasmic RIP140 can reduce lipolysis through interacting with

perilipin [11]. However, the full spectrum of functions of cytoplasmic RIP140 in adipocytes is not clear. The understanding of these functions and the regulatory mechanisms may reveal novel targets to treat adipocyte dysfunctions frequently observed in metabolic disorders.

Adiponectin is one of the most abundant adipokines and is known for its insulin-sensitizing effect. It also regulates systemic glucose and fatty acid metabolism and may also reduce inflammation [25, 94, 95]. Adiponectin's targets include muscle, liver, macrophages, and the central nervous system [94]. There are three major oligomeric forms of adiponectin: trimer (low molecular weight: LMW), hexamer (medium molecular weight) and the high molecular weight form (HMW) which consists of 12- to 18-mer of adiponectin. These three oligomers of adiponectin have different affinities for adiponectin receptors in different cell types and they also show different biological activities [94]. Although disulfide bond formation in ER has been shown to control the oligomerization of adiponectin, the regulation of the secretion of adiponectin vesicle is not fully understood. In adipocytes of obese and diabetic patients and animals, secretion of adiponectin, as well as the translocation of GLUT4 vesicle, is reduced. It has been proposed that a reduction in circulating adiponectin levels in these subjects may lead to the development of cardiovascular diseases and other metabolic complications [27, 28, 96]. In adipocytes, insulin can stimulate both adiponectin and GLUT4 vesicles trafficking but they are two different secretory vesicles [97]. When adipocytes are dysfunctional, the trafficking of both GLUT4 and adiponectin vesicles is retarded, implying that these two vesicles may share some common mechanisms to regulate their transport.

Other studies have also suggested that receptor interacting protein 140 (RIP140) may be involved in the regulation of adipocyte function [10, 85]. In our preliminary screening for RIP140-related adipocyte dysfunctions, we found that cytoplasmic RIP140 can regulate adiponectin secretion. This current study presents evidence for this new functional role of cytoplasmic RIP140. We also determine the underlying mechanism, and provide a proof-of-concept that targeting RIP140 itself or PKCε to prevent RIP140's nuclear export can

promote the secretion of functional adiponectin. This can be beneficial for several adiponectin's target cells, such as improving glucose uptake in C2C12 muscle cells and reducing glucose production in HepG2 hepatocytes.

Materials and Methods

Cell culture, reagents and transfection

3T3-L1 cells and RIP140-null mouse embryonic fibroblasts were maintained and differentiated as described [18]. C2C12 cells were maintained in DMEM with 10% FBS, and differentiated in DMEM with 2% horse serum for six days. HepG2 was maintained in DMEM with 10%FBS. 293TN (System Biosciences) were maintained in low glucose DMEM with 10%FBS. siRNAs in this study were from Qiagen. Adiponectin ELISA kit was from Invitrogen. DeliverX Plus siRNA transfection kit (Panomics) was used for siRNA transfection. Plasmid transfection in 3T3-L1 adipocytes was done by electroporation with GenePluser (Bio-Rad). Lentivirus transduction was conducted for RIP140-null adipocytes.

Plasmid and reagents

The wild type and phosphor-deficient form (CN) of Flag-RIP140 fragments were amplified by PCR from Flag-RIP140 vectors [85] and cloned into pCDH-CMV-EF1 (System Biosciences). The wild type and non-phosphorylatable form (4P) of AS160 were amplified from AS160 vectors (gifts of Gustav Lienhard) and cloned into pCMV-PL1 containing HA-tag. Adiponectin ELISA kit was from Invitrogen. Endothelin-1 ELISA kit was from Assay Designs. Mouse/Rat insulin ELISA kit was from Millipore.

Lentivirus production and transduction

Lentivirus was produced in 293TN cells using lentivirus packing system (System Biosciences) and concentrated with lenti-X concentrator (Clontech). For transduction, RIP140-null adipocytes were differentiated with concentrated lentivirus for 4 days, and

changed to a polybrene-containing medium (8 μg/ml) on day 5. After 24 h, medium was refreshed using a normal medium with the differentiation cocktail.

Treatment and protein precipitation

Differentiated 3T3-L1 adipocyte cultures were washed with PBS twice and incubated with DMEM without serum for another 6 hr. Secreted proteins in the medium were precipitated by TCA. Medium and cell lysate were both collected for Western blotting and ELISA. To quantify adiponectin complex, media were collected and subjected into SDS-PAGE in a non-reducing loading buffer. Immunoblots were quantified by Image J.

Antibodies, Western blotting and cellular fractionation

Anti-actin, anti-HA and anti-lamin antibodies were from Santa Cruz. Anti-RIP140 antibody and anti-alpha-tubulin antibody were purchased from Abcam and Sigma-Aldrich, respectively. Isolation of nuclear and cytoplasmic fractions was conducted as described [85]. Briefly, cells were gently lysed by hypotonic buffer and then, after centrifugation for 10 min at 1,000g, supernatants (cytosolic fraction) were collected. Pellets were further lysed in RIPA buffer by sonication. Lysates were centrifuged and supernatants were nuclear fraction.

Glucose uptake and glucose production assays

Conditioned media were collected from mature adipocytes cultured in DMEM with 10% FBS for 48 hr. Glucose uptake assay was conducted as described [98] with modification. Differentiated C2C12 was serum-starved for 3 hrs and then treated, in the presence or absence of 100 nM insulin, with conditioned medium. After 30 min, cultures were refreshed with KRPH buffer containing 25 μM 2-deoxy-glucose for 5 min. To determine glucose production, HepG2 was serum-starved for 3 hr and then treated with conditioned media for another 1 hr. Cells were washed with PBS and then incubated in a glucose production medium in the absence or presence of 100 nM insulin for 4 hr. Glucose levels were determined using a glucose assay kit (Sigma Aldrich) and normalized to the protein concentrations of cell lysates. To neutralize the activity of adiponectin, 200 μg anti-

mouse adiponectin antibody (AF1119, R&D Systems) was added to a 5 ml conditioned medium for 2 hr at 4^{o}C [99]. The neutralized conditioned media were used in glucose uptake and glucose production assays.

Statistical analyses

Results were presented in the means ± SD. *P* values were examined using student t test in the two-tail condition. $P < 0.05$ is considered as statistically significant.

Results

Reducing RIP140 or its nuclear export stimulus, PKCε, enhances adiponectin secretion

We previously found that RIP140 can be exported into the cytoplasm of adipocytes both in vitro and in vivo [4, 85]. In 3T3-L1 adipocytes, silencing RIP140, or more specifically knocking down its nuclear export stimulator PKCε to decrease cytoplasmic RIP140, enhanced basal adiponectin secretion without altering adiponectin mRNA levels (Fig. 1A). But we found no change in other adipokines such as leptin, resistin, IL-6 and TNFα (data not shown). To rule out potential effects on adiponectin translation or its protein stability, we performed metabolic labeling in the presence of a proteosome inhibitor, MG132, and a post-Golgi trafficking inhibitor, Brefeldin A to block protein degradation and post-Golgi secretion [100]. Neither general translation nor specific adiponectin translation was altered, which ruled out the possibility that these treatments might affect adiponectin production (Fig. 1B). Adiponectin secretion is mainly controlled by post-translational modifications in ER and vesicle transport in trans-Golgi networks (TGN) [94, 101-103]. Disulfide bond formation of adiponectin molecules is also critical to their secretion. We performed Western blotting in a non-reducing condition to detect various forms of secreted adiponectin obtained from adipocyte cultures under RIP140- or PKCε–silencing. It appeared that silencing of RIP140 or PKCε enhanced the secretion of all forms of adiponectin (Fig. 1C), suggesting that RIP140 regulated adiponectin secretion in an unbiased manner.

We then assessed the functional role of RIP140 in modulating adiponectin secretion using RIP140-null adipocytes. As shown in Fig. 2, RIP140-null adipocytes rescued with a wild type (Wt) RIP140 secreted less adiponectin as compared to the control vector (GFP). On the contrary, adiponectin secretion from RIP40-null adipocytes rescued with a mutant RIP140-GFP defected in its nuclear export (CN, a phospho-deficient form that loses cytoplasmic activity) was not affected as compared to the control group. Taken together, these results show that cytoplasmic RIP140 dampens adiponectin secretion in an unbiased manner, and targeting the nuclear export or RIP140 itself can elevate the secretion of adiponectin.

Adiponectin secretion is regulated by AS160 activity

AS160 is a Rab GTPase-activating protein (GAP) whose activity can be diminished by Akt-mediated phosphorylation upon insulin binding with insulin receptor [56]. Rab GTPases are important in vesicle secretion in many steps including recycling, trafficking, tethering and membrane docking. The increased activity of AS160 reduces GLUT4 vesicle secretion by decreasing GTP-bound form of Rab proteins [56]. In addition, insulin also promotes the secretion of adiponectin vesicle, but the mechanism is unclear [104]. Recently, we found that, in adipocytes, AS160 activity can be maintained by interacting with RIP140 in the cytoplasm [85]. A recent study demonstrated that Rab11 regulates adiponectin vesicle trafficking and suspected that AS160 might modulate Rab11 activity by interacting with Rab11-interacting protein, Rip11 (also see Discussion) [104]. We then determined the functional role for AS160 in adiponectin secretion using a gain-of-function approach. Figs. 3A and 3B show that over-expression of the wild type (Wt) AS160, or its constitutively active form (4P) [56], dramatically reduced basal and insulin-stimulated adiponectin secretion. Of note, constitutively active AS160 (4P) almost blocked the secretion of adiponectin completely. Besides, both over-expressions of the wild type (Wt) AS160 and constitutively active form (4P) blunted insulin's effect on promoting adiponectin secretion. Altogether, the data support the notion of negative regulation of adiponectin secretion by AS160**.**

Blocking RIP140-AS160 interaction enhances adiponectin secretion

RIP140 interacts with AS160 through its amino terminal domain to prevent AKT-mediated inactivation [85]. The results described above suggest that AS160 can negatively regulate adiponectin vesicle secretion and cytoplasmic RIP140 may retard adiponectin secretion through interacting with AS160. Because RD1 is the main interacting domain for RIP140 to interact with AS160 [85], over-expression of this domain might compete the interaction between AS160 and the full length RIP140. We then examined if over-expressing RIP140's RD1 (repressive domain 1) can enhance adiponectin secretion. Interestingly, expressing RD1 in 3T3-L1 adipocytes substantially elevated adiponetin secretion (Fig. 4). This result further supports the hypothesis that cytoplasmic RIP140 might dampen adiponectin secretion via interacting with AS160 and targeting the interaction of RIP140 with AS160 might elevate adiponectin vesicle trafficking .

Targeting cytoplasmic RIP140 is beneficial for glucose metabolism in C2C12 muscle cells and hepatocytes in an adiponectin-dependent manner

Adiponectin is an important insulin sensitizer to promote glucose uptake in muscle cells and to reduce glucose production in hepatocytes through an AMPK-dependent signaling cascade. The net effect of elevation of circulating adiponectin is better glucose tolerance [94]. To further examine if targeting RIP140 or its nuclear export trigger, PKCε, can be beneficial for glucose metabolism in muscle cells, we determined the effect of conditioned media collected from RIP140- or PKCε-silencing 3T3-L1 adipocytes on glucose uptake ability of C2C12 muscle cells. Indeed, the conditioned media from both RIP140- and PKCε-knocked down adipocytes increased both basal and insulin-stimulated glucose uptake (Fig. 5A). Besides, the phosphorylation status of AMP-activated protein kinase (AMPK) in C2C12 cells was also elevated by conditioned media from both RIP140- and PKCε-knocked down adipocytes (Fig. 5B). Finally, the anti-adiponectin antibody substantially blocked the effect of conditioned media from both RIP140- and PKCε-knocked down adipocytes on elevation of glucose uptake ability (Fig. 5C), supporting that the beneficial effect on glucose uptake ability in C2C12 muscle cells was likely due to the secreted adiponectin in the conditioned media.

In addition to the effect on C2C12 muscle cells, we further investigated the effect of adipocyte-conditioned media from RIP140- or PKCε-silencing adipocytes on gluconeogenesis ability in hepatocytes. As shown in Fig. 6A, conditioned media from both RIP140- and PKCε-knocked down adipocytes significantly reduced glucose production in HepG2 hepatocytes. In the presence of insulin, there is no further reduction of glucose production in HepG2 cells. As same as the effects on C2C12 muscle cells, these conditioned media promoted the level of phosphorylated AMPK in HepG2 cells. Most importantly, the anti-adiponectin antibody effectively neutralized the effect of conditioned media on glucose production in the absence of insulin (Fig 6C).

All together, the data demonstrate that cytoplasmic RIP140 may play a role in regulating adiponectin secretion in adipocytes, and the elevated secretion of adiponectin is functional in promoting glucose uptake in muscle cells and reducing glucose production in hepatocytes.

Discussion

We have previously shown that HFD increases the levels of RIP140 in the cytoplasm of epididymal adipocytes, and proposed that the cytoplasmic accumulation of RIP140 may provide a disease marker [85]. The cytoplasmic RIP140 interacts with AS160 to retard GLUT4 vesicle trafficking, and with perilipin A on lipid droplets to promote lipolysis [10, 85]. The current study reports a new function of cytoplasmic RIP140 in adipocytes, that is to negatively regulate adiponectin secretion. Because adiponectin can target multiple cell/tissue types for different functions, its role in maintaining metabolic homeostasis on a systemic level has been intensively studied; but regulation of its secretion is poorly understood. The regulatory role of cytoplasmic RIP140 in adiponectin secretion significantly expands the scope of the biological activity of cytoplasmic RIP140, and suggests that targeting the functions of cytoplasmic RIP140 may provide a potential therapeutic strategy in managing metabolic diseases.

Although both adiponectin release and GLUT4 trafficking can be stimulated by insulin, the two proteins are localized in two different types of vesicles [97]. But both adiponectin and GLUT4 vesicles reside in the trans-Golgi network (TGN) and the recycling endosomes [103]. Secretion of these vesicles is regulated by Rab GTPases in multiple steps such as trafficking, docking, tethering and fusion of the vesicles [56, 105]. AS160 is a RIP140 interacting GAP that can inactivate several Rab GTPases [56]. RIP140 can maintain AS160 activity through a direct interaction and preventing its Akt-mediated inactivation. This would presumably affect the trafficking of multiple types of vesicles. This would also suggest a possible mechanism for the action of insulin in enhancing both adiponectin release and GLUT4 trafficking, and substantiates the significance of the molecular interaction between RIP140 and AS160. Rab5 and Rab11 are the only two Rab GTPases shown to be involved in adiponectin vesicles trafficking to modulate adiponectin release [103, 104]. However, neither Rab5 nor Rab11 activities can be directly modulated by AS160 *in vitro* [56]. Therefore, the detailed mechanism by which AS160 regulates adiponectin vesicles, such as via regulating Rab5 or Rab11, or other unknown factors, remains to be examined. To this end, a previous study has suggested that AS160 may modulate Rab11 by interacting with its interacting proteins such as Rip11 [56, 106], which would be a potential topic of future studies**.**

Figures

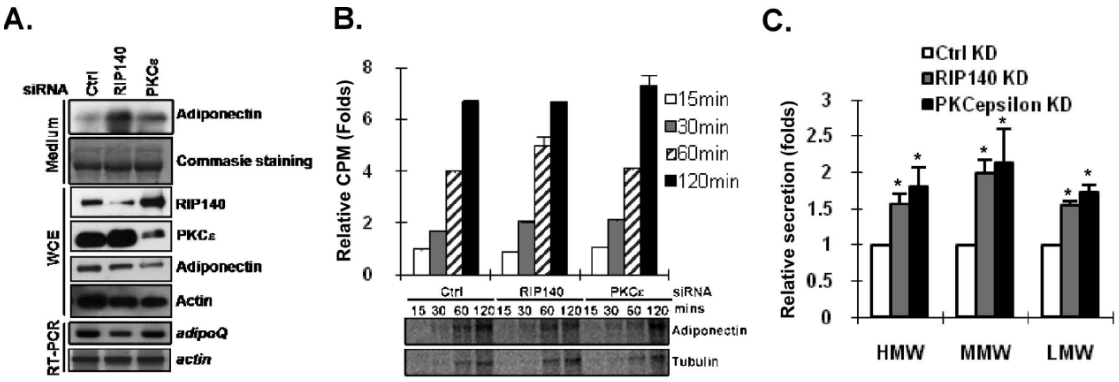

Figure 4-1 Targeting RIP140 or PKCε increases adiponectin secretion. (A) Adiponectin secretion pattern in ctrl-, RIP140- or PKCε-silenced 3T3-L1 adipocytes. Commasie staining shows loading control. WCE: whole cell extract. (B) Production of adiponectin and its mRNA. Differentiating adipocytes were transfected with indicated siRNA on day 5. On day 8, mature adipocytes were treated with MG132 and Brefeldin A in the presence of ^{35}S-labeled methionine for indicated time. General (total cpm counts) and specific (determined by antibody against adiponectin and actin, respectively) translation was each examined. The general translation rate, per 100 μg whole cell lysate, in each experimental condition was represented as the relative fold of CPM using the CPM of control at 15 minutes as the value of 1. The differences of same time points among indicated knockdown are not statistically significant. (C) Secreted adiponectin profiles. Differentiating adipocytes were transfected with indicated siRNA on day 5. On day 8, mature adipocytes were cultured in serum-free medium for 6 h. Adiponectin profile was determined by western blotting in non-reducing condition. HMW: high molecular weight complex; MMW: medium molecular weight complex; LMW: low molecular weight complex. *: $P < 0.05$, compared to ctrl knockdown group (CtrlKD).

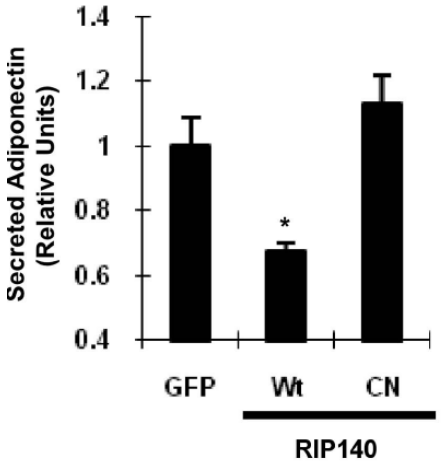

Figure 4-2. Cytoplasmic RIP140 reduces adiponectin secretion in RIP140-null adipocytes. The effect of various forms of RIP140 on adiponectin secretion in RIP140-null adipocytes rescued with RIP140 expression vectors. Wt: wild type RIP140; CN: phosphor-defective mutant RIP140. All values represent the means ± SD., n=3; *: $P < 0.05$, compared to ctrl group.

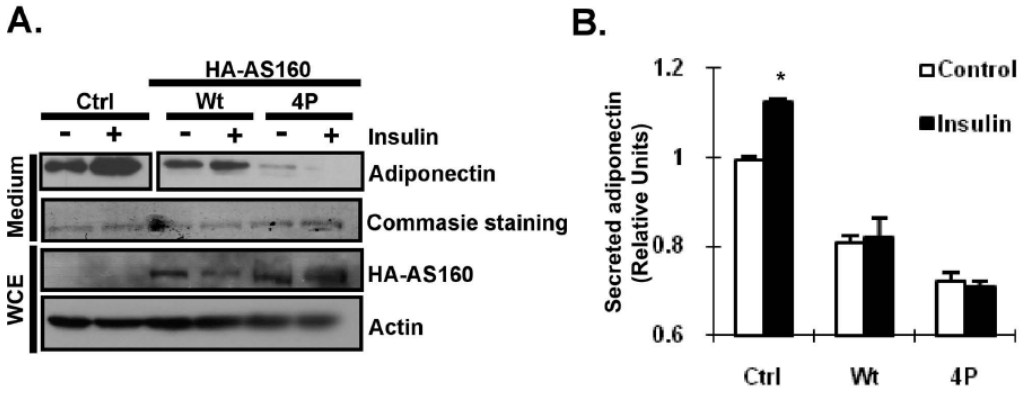

Figure 4-3. AS160 modulates adiponectin secretion. (A) Western blot detection of adiponectin secretion from adipocytes transfected with control vector (Ctrl) or indicated AS160 vectors. Differentiating 3T3-L1 adipocytes were electroporated with indicated vector on day 6. After two days, mature adipocytes were cultured in serum-free medium with or without 100nM Insulin for 6 h. Adiponectin profile was determined by western blotting in non-reducing condition. Wt: wild type; 4P: constitutive active form of AS160. Commasie staining shows loading control. (B) ELISA detection of secreted adiponectin from transfected adipocytes was examined by ELISA. All values represent the means ± SD., n=3; *: $P < 0.05$ compared to control treatment.

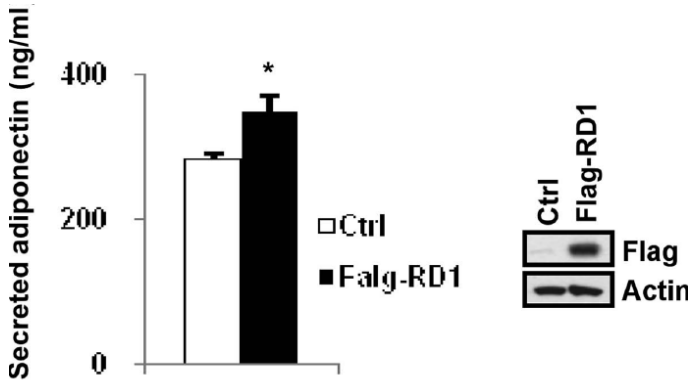

Figure 4-4. Over-expression of the amino terminus (RD-1) of RIP140 elevates adiponectin secretion. Left: Secreted adiponectin from transfected adipocytes was examined by ELISA. Control vector or flag-RD1 vector was electroporated into day 6 differentiating 3T3-L1 adipocytes. After two days, adipocytes were cultured in serum-free medium for 6 h. The adiponectin levels of culture supernatants were measured by ELISA. All values represent the means ± SD., n=3; *: $P < 0.05$ compared to control group. Right: immunoblotting of whole cell lysates for indicated antibodies to determine the efficiency of over-expression.

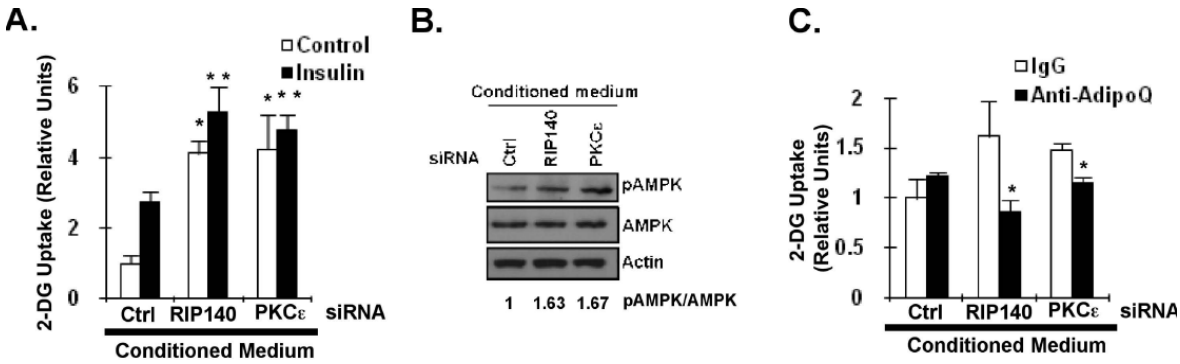

Figure 4-5. Targeting RIP140 or PKCε in adipocytes enhances functional adiponectin secretion to promote glucose uptake in muscle cells. (A) The effect of conditioned media from ctrl-, RIP140- or PKCε-silenced adipocytes on glucose uptake in C2C12 cells in the absence (control) or presence of insulin. All values represent the means ± SD., n=3; *: $P < 0.05$ compared to control group in Ctrl conditioned medium. **: $P < 0.05$ compared to insulin group in Ctrl conditioned medium. (B) The effect of conditioned media in (A) on AMPK activation in C2C12 cells. The ratio of pAMPK/AMPK was quantified. (C) Anti-adiponectin antibody (anti-adipoQ) neutralized the effect of conditioned media on C2C12 glucose uptake in the presence of insulin

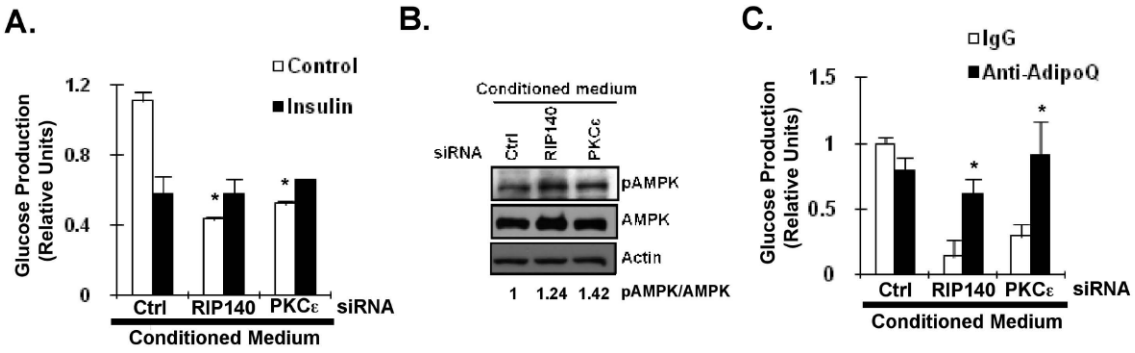

Figure 4-6. Targeting RIP140 or PKCε in adipocytes enhances functional adiponectin secretion to reduce gluconeogenesis in hepatocytes. (A) The effect of conditioned media from ctrl-, RIP140- or PKCε-silenced adipocytes on gluconeogenesis in HepG2 cells in the absence (control) or presence of insulin. All values represent the means ± SD., n=3; *: $P < 0.05$ compared to control group in Ctrl conditioned medium. (B) The effect of conditioned media on AMPK activation in HepG2 cells. The ratio of pAMPK/AMPK was quantified. (C) Anti-adiponectin antibody (anti-adipoQ) neutralized the effect of conditioned media on glucose production ability of HepG2 in the absence of insulin. *: $P < 0.05$ compared to IgG group in conditioned medium from indicated silencing group.

Preface

This chapter has been published:

Ping-Chih Ho, Yao-Chen Tsui, Yi-Wei Lin, Shawna D. Persaud, and Li-Na Wei (2012) Endothelin-1 promotes cytoplasmic accumulation of RIP140 through a ET_A-PLCβ-PKCε pathway. Molecular and Cellular Endocrinology 351, 176-183

CHAPTER V

Endothelin-1 promotes cytoplasmic accumulation of RIP140 through a ET_A-PLCβ-PKCε pathway

Introduction

In recent years obesity has become a worldwide epidemic. A major complication of obesity is type 2 diabetes mellitus (T2DM). The hallmark of this condition is the development of insulin resistance in adipose, muscle and liver [49]. In healthy individuals, adipocytes take up glucose, store lipid and secretes adipokines, and these adipokines are important in the regulation of metabolism. But in diabetics, adipocytes may become dysfunctional, as shown in the reduction of their glucose uptake ability, change in the profile of secreted adipokines, and increase in lipolysis. These changes may worsen the disease state leading to such complications as hypertension, atherosclerosis and cardiomyopathy [23, 49]. Reports have shown that inflammation and endoplasmic reticulum (ER) stress could cause adipocyte dysfunction, but the exact etiology of many of these pathophysiological processes remains to be determined [23, 51, 55].

RIP140 is a nuclear co-regulator for many transcription factors. It plays important roles in various biological processes and affects many disease conditions including the metabolic syndrome [4, 67, 84, 85]. Both its mRNA and protein expression are significantly elevated in fully differentiated, fat-accumulating adipocytes. As adipocytes mature, RIP140 undergoes extensive post-translational modifications (PTMs). These changes can modulate its gene-regulatory activity and facilitate its export to the cytoplasm [4, 14, 16, 84]. Recently, we have reported that in 3T3-L1 adipocytes, activated nuclear PKCε phosphorylates RIP140, and the phosphorylated RIP140 is subsequently modified by protein arginine methylation, which enhances the recruitment of exportin 1 to RIP140 for its nuclear export [4, 14]. We have also found that in the primary adipocytes isolated from mice fed a high-fat diet (HFD), RIP140 is increasingly accumulated in their cytoplasm, and that the cytoplasmic RIP140 can negatively regulate basal and insulin-stimulated glucose uptake by decreasing GLUT4 vesicle trafficking [85]. However, it remains to be determined as to the physiological trigger and/or the extracellular signal for RIP140's nuclear export in adipocytes.

According to the dissected intracellular signaling pathway that stimulates RIP140's nuclear export in 3T3-L1 adipocytes, i.e. activated nuclear PKCε that initiates

specific phosphorylation on RIP140 to enhance its subsequent arginine methylation for recruiting exportin 1, we investigated several extracellular factors associated with nuclear PKCε activation, and uncovered that endothelin-1 (ET-1) could be such an extracellular trigger. ET-1 is a vasoconstrictor secreted primarily by endothelial cells. It regulates airway and blood vessel tone and wound healing [107-109], and is the major therapeutic target in managing chronic thromboembolic pulmonary hypertension, pulmonary arterial hypertension, and pulmonary fibrosis [110-112]. Clinical studies have shown that obese and T2DM patients have higher levels of circulating ET-1. As a result, several investigators have proposed that high levels of ET-1 might be an important factor in the observed adipocyte dysfunction [100, 109, 113-115]. However, the underlying mechanism through which ET-1 modulates adipocyte functions is unclear.

In the current study, we examine the relationship between high levels of ET-1 and cytoplasmic accumulation of RIP140 in 3T3-L1 adipocytes. We find that chronic ET-1 exposure can promote the accumulation of RIP140 in the cytoplasm of adipocytes by activating the ET_A-PLCβ-nuclear PKCε pathway. Further, we show that targeting this signaling pathway in 3T3-L1 adipocytes by antagonizing ET-1 receptor, inhibiting PLCβ, or silencing PKCε can inhibit cytoplasmic accumulation of RIP140. Importantly, using a selective antagonist of ET_A, the principal ET-1 receptor expressed in adipocytes, we demonstrate that blocking ET-1 signal input to adipocytes in animals indeed can reduce cytoplasmic accumulation of RIP140 in adipoyctes. This treatment also reduces adipocyte dysfunctions, improve blood glucose control and ameliorates hepatic steatosis in HFD-fed mice.

Materials and Methods

Cell culture, reagents and transfection

3T3-L1 cells and RIP140-null cells were maintained and differentiated as described [18]. siRNAs were purchased from Qiagen. ET-1 was from MP Biomedicals. Mouse adiponectin ELISA kit was from Invitrogen. siRNA transfection was conducted using a

DeliverX Plus siRNA transfection kit (Panomics). Plasmid transfection was by electroporation with GenePluser (Bio-Rad) using 960 μF and 200 Ω.

Endothelin-1 Treatment

For ET-1 treatment, mature 3T3-L1 adipocyte cultures were treated with 50 nM ET-1 for 24 hr and cell lysates were collected for Western blotting.

Antibodies, Western blotting and cellular fractionation

Anti-RIP140 antibody was from Abcam. Anti-PKCε and anti-lamin antibodies were from Santa Cruz. Anti-alpha-tubulin antibody was from Sigma-Aldrich. Cell lysate was collected as described [18] and protein concentration was determined by Bradford method. Immunoblots were quantified by Image J. For nuclear and cytoplasmic isolation, cells were broken by hypotonic buffer (10mM HEPES, pH7.9, 1.5 mM $MgCl_2$, 10mM KCl with protease inhibitors). Then after centrifugation for 10 min at 1,000g, supernatants (cytosolic fraction) were collected and pellets were lysed in RIPA buffer. Lysates were centrifuged at 14,000 rpm for 15 min. Supernatants were nuclear fraction.

Adipocyte isolation and glucose uptake assays

Primary adipocyte isolation was conducted as described [85]. Glucose uptake assay in primary adipocytes was also performed as describe [85] and glucose uptake was normalized to the same number of cells.

PKCε kinase activity and PLCβ activity assays

Nuclear PKCε activity was determined using a radiometric kit (Upstate) as described [85]. PLCβ activity assay was conducted as described [116] with some modification. A 100-μg lysate was incubated with 300 nmole PLP Thio-PIP_2 (Cayman Chemical) in the reaction buffer at room temperature for1 hr, supplemented with a 20μl DTNB solution (25mM DTNB and 475mM EGTA in 0.5M Tris-HCL) for another 5 min at room temperature, and OD_{405} was determined.

Mice

Five-week-old male C57BL/6J mice (Jackson Laboratory) were maintained on a 12-hr light/dark photocycle and fed a normal diet containing 5% fat (#2018, Harlan Teklad) or a HFD (60% fat) (#F3282, Bio-Serv). After feeding for 2 weeks, mice were randomly divided into groups for different treatments. Treatments were given daily by oral gavage for another 3 weeks. All the animal experiments were conducted according to procedures approved by University of Minnesota Institutional Animal Care and Use Committee.

Tissue collection and immunohistochemical staining

Liver and epididymal white adipose tissues and livers were fixed in 10% neutral formalin, embedded in paraffin and sectioned by the Histology & Microscopy Core Facility (University of Minnesota). RIP140 immunohistochemical staining was performed (with antigen retrieval) using Vector® Elite ABC kit (Vector Laboratories). The sections were counterstained with hematoxylin then mounted (Vector Laboratories) for microscopic analysis (Zeiss Axioplan 2).

Blood sample and glucose tolerance test

Blood samples were collected from mice and then analyzed for insulin, adiponectin and endothelin-1 using ELISA kits. For glucose tolerance test, following overnight fasting, blood sugar levels were determined using a glucometer, with a 2-gram/kg-bodyweight D-glucose injection. The blood glucose levels were then monitored at 30, 60 and 120 min after injection.

Statistical analyses

All immunoblottings were done at least twice, and representative results were shown. All results were presented as the means ± SD. *P* values were calculated using student t test in the two-sided condition. *P* value < 0.05 is considered as statistically significant.

Results

ET-1 promotes cytoplasmic accumulation of RIP140. We found that RIP140 was progressively exported to the cytoplasm in primary adipocytes of HFD animals accompanied by elevated nuclear PKCε activity, but the physiological trigger and/or extracellular signal to activate this pathway in adipocytes were unclear [85]. Since PKCε is one of the signal mediators of PLCβ, which can be activated by numerous extracellular factors including ET-1, we examined if chronic ET-1 treatment could alter the sub-cellular distribution of RIP140 in 3T3-L1 adipocytes. As shown in Fig. 1A, in 3T3-L1 adipocytes, with or without insulin stimulation, ET-1 indeed reduced the nuclear level, and elevated the cytoplasmic level, of RIP140. In adipocytes, endothelin receptor type A (ET_A) is the major form of ET-1 receptor [100]. We therefore examined RIP140's sub-cellular distribution in adipocytes under a chronic ET-1 treatment in the absence or presence of an ET_A receptor-selective antagonist, BQ-610 (Fig. 1B). The ET_A antagonist effectively dampened the accumulation of RIP140 in the cytoplasm of ET-1 treated adipocytes. In the absence of ET-1 treatment, BQ-610 had no effect on the accumulation of RIP140 in the cytoplasm. Using immunofluorescence analysis, we further confirmed that ET-1 promoted RIP140 cytoplasmic accumulation in an ET_A receptor-dependent manner (Fig. 1C). These results show that for 3T3-L1 adipocytes, ET-1 can be such an extracellular factor triggering the accumulation of RIP140 in the cytoplasm, which occurs in an ET_A-dependent manner.

ET-1 increases nuclear PKCε level and promotes nuclear PKCε activity. ET-1 signals, primarily, through G-protein coupled receptor-mediated activation of phospholipase Cβ (PLCβ) [117]. The activated PLCβ converts phosphatidylinositol 4,5-biphosphate (PIP_2) into inositol 1,4,5-triphosphate (IP_3) and diacyglycerol (DAG), which can activate a spectrum of signal mediators. Among the downstream signal mediators, PKCε is most relevant to RIP140's activity because it can promote nuclear export of RIP140 and insulin resistance in adipocytes [4, 85]. In addition to canonical activation of PLCβ, which is activated on the plasma membrane, a nuclear membrane form of PLCβ has recently been identified to regulate adipocyte differentiation [116]. To determine if ET-1 regulates cytoplasmic or nuclear PLCβ to elicit the nuclear PKCε activity in our

experimental condition, we first monitored the PLCβ activity of the nuclear and cytoplasmic fractions of 3T3-L1 adipocytes treated with ET-1 for various durations. The result shows that ET-1 robustly up-regulated the cytoplasmic, but not the nuclear, PLCβ activity (Fig. 2A). We further found that ET-1 indeed enhanced the nuclear PKCε activity (Fig. 2B) and substantially increased the nuclear PKCε level (Fig. 2C). Interestingly, the kinetics of ET-1-promoted accumulation of cytoplasmic RIP140 paralleled that of nuclear PKCε activation (Fig. 2B, right panel). This result suggests that ET-1 stimulates cytoplasmic accumulation of RIP140 through activating nuclear PKCε. Taken together, these data show that ET-1 elevates cytoplasmic PLCβ activity and promotes nuclear accumulation of PKCε, accompanied by elevated nuclear PKCε activity in 3T3-L1 adipocytes.

ET-1 modulates RIP140's sub-cellular distribution through the PLCβ-nuclear PKCε signaling pathway. To determine the functional roles for the major signaling players in the PLCβ-nuclear PKCε pathway, we used inhibitor and siRNA to manipulate the players of this signaling pathway in adipocytes. We treated mature 3T3-L1 adipocytes with ET-1 in the absence or presence of a PLCβ inhibitor, U73122 [100]. Indeed, PLCβ inhibitor effectively reduced nuclear PKCε activity as compared to the control treatment (Fig. 3A). This result supports that ET-1 promotes nuclear PKCε activity via a PLCβ-dependent manner. This was further confirmed by the finding that ET-1 failed to increase the cytoplasmic accumulation of RIP140 as well as nuclear PKCε level in the presence of the PLCβ inhibitor (Fig. 3B). To investigate if PKCε is required for ET-1-stimulated cytoplasmic accumulation of RIP140, we knocked down PKCε in ET-1-treated cells and monitored the distribution of RIP140 (Fig. 3C). Indeed, there was a decrease in the cytoplasmic accumulation of RIP140 and an increase in the nuclear RIP140 in PKCε-silenced adipocytes as compared to the control group. Our previous study identified that cytoplasmic RIP140 can interact with AS160 to diminish glucose uptake [85]. We then further examined the functional role for RIP140, particularly its cytoplasmic form, in modulating ET-1 stimulated glucose uptake by rescuing RIP140 null adipocytes. We treated three groups of RIP140 null adipocytes with ET-1: i) RIP140-null adipocytes

rescued with control vector (Ctrl), ii) RIP140 null adipocytes rescued with wild type RIP140 (Wt), and iii) RIP140 null adipocytes rescued with mutant RIP140 (CN, a phosphor-deficient mutant that loses cytoplasmic localization and activity), and monitored their insulin-stimulated glucose uptake. In agreement with previous reports showing that chronic ET-1 could decrease glucose uptake in adipocytes by dampening insulin-stimulated Akt signaling [115], we also detected a reduction in glucose uptake following ET-1 treatment in all three groups (Fig. 3D). However, comparing to the group rescued with the control vector, the group rescued with wild type RIP140 showed a significantly greater reduction in glucose uptake, whereas the group rescued with the CN mutant (that lost its cytoplasmic activity) had their glucose uptake reduced to a level comparable to that in the control rescue group. This result not only supports our conclusion that RIP140 plays a role in modulating ET-1's effect, but also validates that it is the cytoplasmic accumulation of RIP140 that plays such a role in dampening glucose uptake. Taken together, the data show that ET-1 modulates RIP140's sub-cellular localization by activating PLCβ-PKCε pathway, and targeting this pathway can effectively block ET-1-promoted accumulation of cytoplasmic RIP140.

Ambrisentan, ET_A Antagonist, blocks HFD-triggered cytoplasmic RIP140 accumulation in epididymal adipose tissues. Our data of 3T3-L1 adipocytes suggest that the ET-1-triggered signaling pathway could elevate the level of cytoplasmic RIP140 in adipocytes. We next examined whether this signaling pathway is active in the context of whole animals. Previously, we showed that RIP140 accumulated in the epididymal adipose tissue in mice after feeding with HFD for 5 weeks (Ho et al. 2009). We treated HFD-fed mice with a selective ET_A antagonist that has been approved for animal and clinical uses, ambrisentan (10 mg/kg or 30 mg/kg), for three weeks. Since ambrisentan is a potent vasodilator, we therefore included hydralazine (10 mg/kg) as a control treatment to rule out the potential effects of vasodilation [117-120]. HFD indeed elevated plasma ET-1 levels in mice (Fig. 4A). Of note, ambrisentan treatment enhanced the circulating ET-1 level in ND-fed mice, which could be caused by certain feedback mechanism to maintain the ET-1 affected vascular tone. Further, both hydralazine and a high dose of ambrisentan decreased the body weights of those mice fed with HFD, which might be

due to side effects caused by vasodilation, such as a reduction in appetite (Fig. 4B) [117]. Because sub-cellular fractionation of primary adipose tissues is not as reliable for examining a protein's sub-cellular localization, we then used an established immunohistochemical method for detecting RIP140 (Ho et al. 2009) to examine the sub-cellular distribution of endogenous RIP140 in the epididymal tissue collected from these animals. As expected, the epididymal adipocytes significantly accumulated RIP140 in their cytoplasm under a HFD as compared to the control (Fig. 4C, HFD-Ctrl versus ND-Ctrl). Interestingly, ambrisentan treatment, in either a high or low dose, significantly reduced cytoplasmic accumulation of RIP140 in the epididymal adipose tissue of HFD-fed mice (Fig. 4C, HFD-Am10 and HFD-Am30). In contrast, hydralazine could not reduce cytoplasmic accumulation of RIP140 (Fig. 4C, HFD-Hydra). Moreover, these treatments did not affect the total RIP140 level in the epididymal adipose tissue (Fig. 4D). Since cytoplasmic RIP140 can retard GLUT4 vesicle trafficking to reduce glucose uptake in adipocytes (Ho et al. 2009), we then examined if glucose uptake in primary adipocytes was also increased in the ambrisentan-treated mice. As shown in Fig. 4E, HFD animals had a defect in insulin stimulated glucose uptake into their primary adipocytes (comparing HFD Ctrl to the ND Ctrl). Interestingly, a low dose ambrisentan readily rescued this defect and increased glucose uptake in the primary adipocytes of treated animals (comparing HFD Am-10 to HFD Ctrl). Of note, a high dose of ambrisentan also increased the basal level of glucose uptake; this may be due to the effect of ET-1 on the expression of GLUT1 [121]. A low dose of ambrisentan did not affect body weight but significantly reduced the cytoplasmic RIP140 level and improved glucose uptake. These results support the notion that the ET_A antagonist, ambrisentan, can prevent certain pathological conditions caused by HFD, including increased cytoplasmic accumulation of RIP140 and reduced glucose uptake in epididymal adipocytes. These animal data also support our prediction based on the studies of cell cultures, that ET-1 can promote the accumulation of RIP140 in the cytoplasm of adipocytes through an ET_A-mediated pathway.

Ambrisentan, ET_A Antagonist, increases circulating adiponectin levels, improves blood glucose control and ameliorates hepatic steatosis in HFD-fed mice. Recently,

we have shown that cytoplasmic RIP140 also contributed to adipocyte dysfunctions such as an increase in lipolysis and a decrease in GLUT4 vesicle trafficking and adiponectin secretion [85, 122, 123]. We therefore also monitored the circulating adiponectin levels and crown-like structure (CLS), a proinflammatory sign, in the epididymal adipose tissue of ND- or HFD-fed mice treated with ambrisentan. We found that HFD indeed lowered the circulating adiponectin levels. Feeding with ambrisentan, but not hydralazine, for three weeks, enhanced the circulating adiponectin levels, which suggests that ambrisentan promotes adiponectin secretion, but this is not caused by its vasodilating effect (Fig. 5A). Additionally, ambrisentan decreased the number of CLS in the adipose tissue, indicating that ambrisentan also improves chronic inflammation [77] (Fig. 5B and 5C). Taken together, these animal studies show that the ET_A antagonist, ambrisentan, can prevent certain pathological conditions caused by HFD, such as reduction in adiponectin secretion and the accumulation of inflammatory macrophages in the adipose tissue.

We then examined the effect of ambrisentan on the fasting blood glucose level. It appears that none of these treatments altered the fasting blood glucose levels in the ND group, but ambrisentan effectively reduced the fasting blood glucose levels in HFD animals (Fig. 5D) without significantly changing their plasma insulin levels (Fig. 5E), ruling out the effect through altering the circulating insulin levels. In glucose tolerance test (GTT), ambrisentan improved the glucose clearance rate of HFD-fed mice to a level similar to that of the ND group (Fig. 5F and 5G). Furthermore, ambrisentan administration to HFD animals also decreased their hepatic steatosis (Fig. 5H), accompanied by a dose-dependent reduction in liver TG content (Fig. 5I). Together, these results show that ET_A antagonist, ambrisentan, is beneficial for the maintenance of systemic glucose homeostasis, and can be protective against liver steatosis induced by HFD.

Discussion

We have previously shown that a HFD increases the levels of RIP140 in the cytoplasm of epididymal adipocytes [85], but the physiological trigger, or extracellular signal, for this

phenomenon in adipocytes was unclear. In the current study, we extend these findings and demonstrate that ET-1 can be such a physiological/extracellular signal, and that the effect of ET-1 to stimulate RIP140's nuclear export in adipocytes is mediated by the ET_A-PLCβ-nuclear PKCε signaling cascade (Fig. 6). Using a diet-induced obese mouse model, we further provide a proof-of-concept that, it might be useful to exploit this signaling pathway to manage adipocyte dysfunction, such as to improve their glucose uptake. This is supported by the effectiveness of using the ET_A antagonist, ambrisentan, to block cytoplasmic accumulation of RIP140 and improve glucose uptake in adipocytes. However, considering that PLCβ can affect multiple downstream PKC isoforms and cytoplasmic accumulation of RIP140 is specifically triggered by the nuclear PKCε, it could be even more specific and efficient to reduce cytoplasmic accumulation of RIP140 by targeting PKCε. Of note, ET_A antagonists are widely used for pulmonary hypertension and other vascular diseases, and it has been suggested that ET_A antagonists can provide beneficial effects to reduce diabetes-caused complications [108, 111, 117]. There are also increasing studies showing that ET-1 can modulate adipocyte function, including adipokine secretion, lipid metabolism and insulin sensitivity. It is important in future studies to examine the beneficial effects of administration of ET_A antagonists to ameliorate certain complications affected by HFD.

In recent years, our lab has revealed the importance of PTMs of RIP140 in modulating RIP140's activity and nuclear export [4, 14, 16]. Although we have identified that cytoplasmic RIP140 can block glucose uptake by impeding GLUT4 trafficking and enhance lipolysis by interacting with perilipin [85, 122], the full spectrum of cytoplasmic RIP140's activities remains to be examined. Nevertheless, these limited studies have begun to illustrate that cytoplasmic RIP140 can also be involved in regulating lipid and glucose metabolism in response to an alteration in the nutrient status or pathological conditions. Determining the interacting proteins of cytoplasmic RIP140 should be helpful to the elucidation of the full spectrum of cytoplasmic RIP140's activities [4]. On the same note, it may also be interesting to determine whether RIP140 can accumulate in the cytoplasm of other cell types and, if so, it will be important to identify the physiological or pathological stimuli for nuclear export of RIP140 in various cell types. Our limited

studies already show that that there are extrinsic (circulating ET-1) (this current study) and intrinsic (lipid content within adipocyte) (Ho et al. 2011) mechanisms to modulate RIP140's sub-cellular distribution in adipocytes.

Finally, in obese and diabetic patients, increased secretion of ET-1 from endothelial cells has been considered as an important factor contributing to vascular dysfunction. Although we show that targeting ET-1 signaling by ET_A antagonist can be beneficial, such as improving glucose control and hepatic steatosis, it remains unclear if adipose tissue is the key target through which ET_A antagonists produce these beneficial effects, because ET-1 is also the strongest vasoconstrictor and is involved in vascular tone and other physiological homeostasis [117]. In our study, a high dose ambrisentan indeed reduced body weight gain (Fig. 4B), which might be caused by ambrisentan's side effects. Understanding the essential target of ET-1 blockage that produces these beneficial effects will help to design better treatments with fewer side effects such as hypotension.

Taken together, we report that ET_A antagonist ambrisentan exerts beneficial effects in controlling the progression of diet-induced diabetes, suggesting that blockade of ET-1 signaling would attenuate the vicious crosstalk between endothelial and adipocyte dysfunctions in diabetes progression. Moreover, this study reveals a pathological signal crosstalk between the vascular system and the adipose tissue through ET-1. This signal crosstalk provides points of intervention to develop novel therapeutic/preventive strategies for obesity- and diabetes-related metabolic syndromes.

Figures

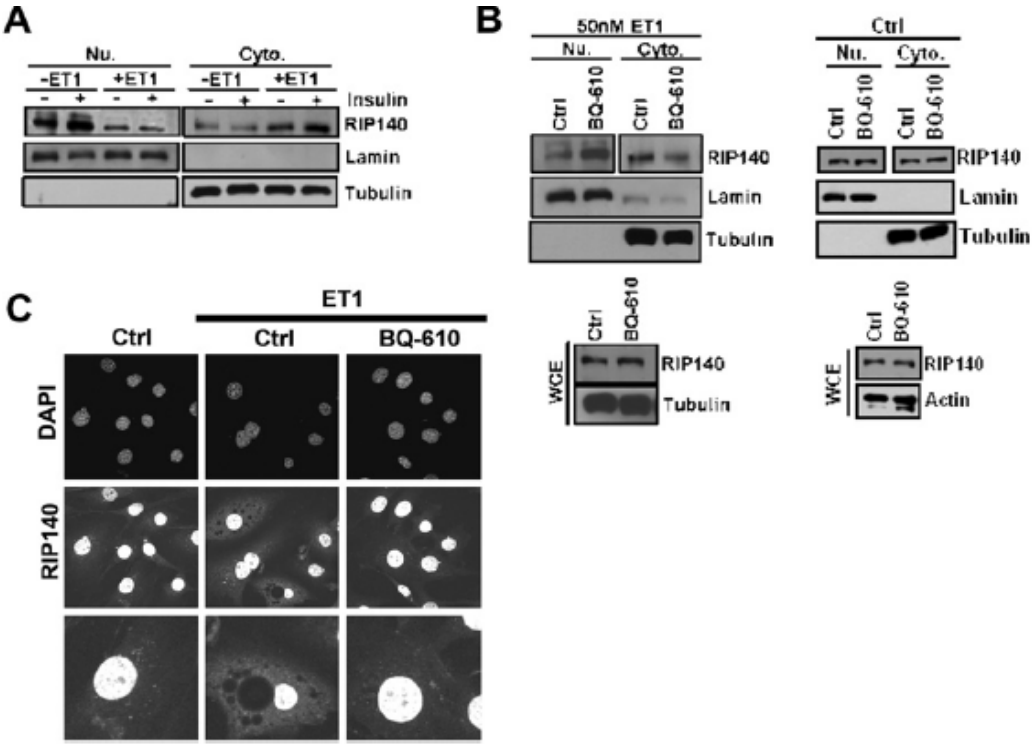

Figure 5-1 Chronic endothelin-1 treatment promotes cytoplasmic accumulation of RIP140. A, Sub-cellular distribution of RIP140 in 3T3-L1 adipocytes stimulated with or without insulin (6 hr) in the absence or presence of 50 nM ET-1 for 24 hr. Lamin and tubulin show the loading control and fractionation markers for nucleus and cytoplasm, respectively. Nu.: nuclear fraction; Cyto.: cytoplasmic fraction. B, Effect of ET_A antagonist (BQ-610) on sub-cellular distribution of RIP140 in 3T3-L1 adipocytes under chronic ET-1 treatment. Left: 3T3-L1 adipocytes were pretreated with BQ-610 for 1 h and then incubated with ET-1 for another 24 h. Right: 3T3-L1 adipocytes were treated with BQ-610 25 h. C, Representative confocal images showing RIP140 distribution in 3T3-L1 adipocytes treated as indicated. DAPI shows nucleus staining.

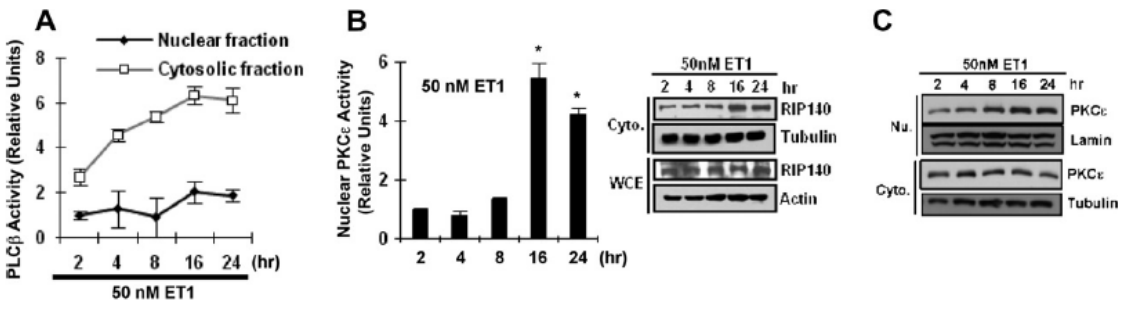

Figure 5-2. Endothelin-1 increases cytoplasmic PLCβ and nuclear PKCε activity. A, PLCβ activity of the nuclear or cytoplasmic fraction of 3T3-L1 adipocytes stimulated by ET-1 for the indicated time period. All values show the means ± SD., n=3. B, Left: Quantification of nuclear PKCε activity of 3T3-L1 adipocytes stimulated by ET-1 for the indicated time period. Right: Cytoplasmic level of RIP140 in 3T3-L1 adipocytes stimulated by ET-1. C, Sub-cellular distribution of PKCε in 3T3-L1 adipocytes stimulated by ET-1. All values show the means ± SD., n=3; *: $P < 0.05$ compared to 2 hr treatment.

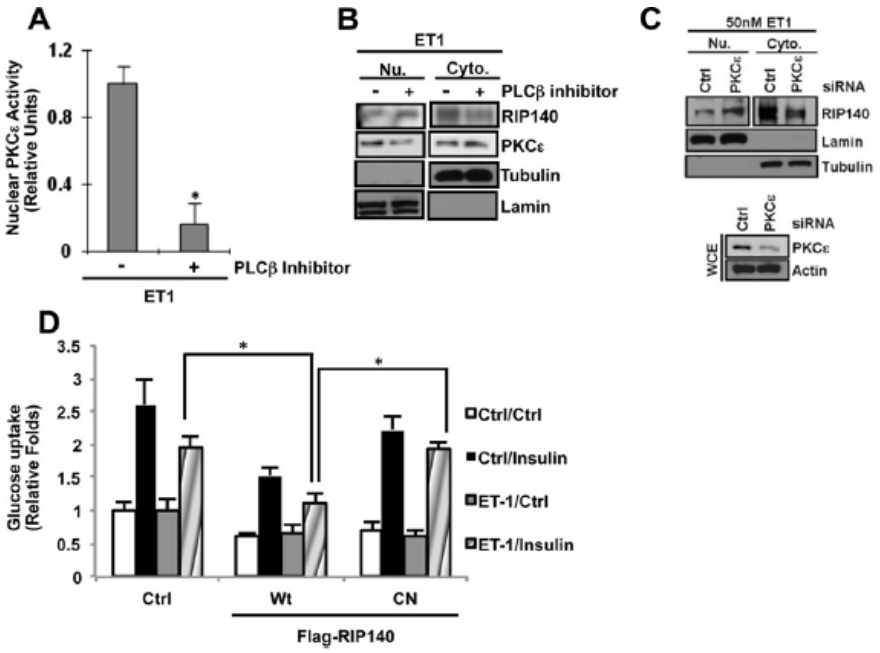

Figure 5-3. Endothelin-1 promotes cytoplasmic accumulation of RIP140 in adipocytes via the PLCβ-PKCε pathway. A, PLCβ inhibitor, U73122, blocks nuclear PKCε activity under chronic ET-1 treatment. 3T3-L1 adipocytes were pretreated with U73122 for 1 h and then incubated with ET-1 for another 24 h. The nuclear fraction was collected and subjected into PKCε activity assay. All values show the means ± SD., n=3; *: $P < 0.05$ compared to ctrl treatment. B, PLCβ inhibitor decreases ET-1-mediated cytoplasmic accumulation of RIP140 in 3T3-L1 adipocytes. Nuclear and cytoplasmic fractions were collected in the same procedure as described in Fig. 2C. C, Western blot analyses of RIP140 in the nuclear and cytoplasmic fractions from ctrl- or PKCε-silenced 3T3-L1 adipocytes after chronic ET-1 treatment. Knockdown efficiency was monitored by western blot analyses of PKCε in whole cell extract. Nu.: nuclear fraction; Cyto.: cytoplasmic fraction; WCE: whole cell extract. D, Basal and insulin-stimulated glucose uptake of RIP140-null adipocytes rescued with control vector (Ctrl), wild type RIP140 (Wt) or phosphor-deficient mutant (CN) RIP140 under a control or chronic ET-1 treatment. Glucose uptake was measured. The relative fold was determined by normalization to the control vector group under the control treatment that was arbitrarily set at the value of 1. All values represent the means ± SD., n=4; *: $P < 0.05$.

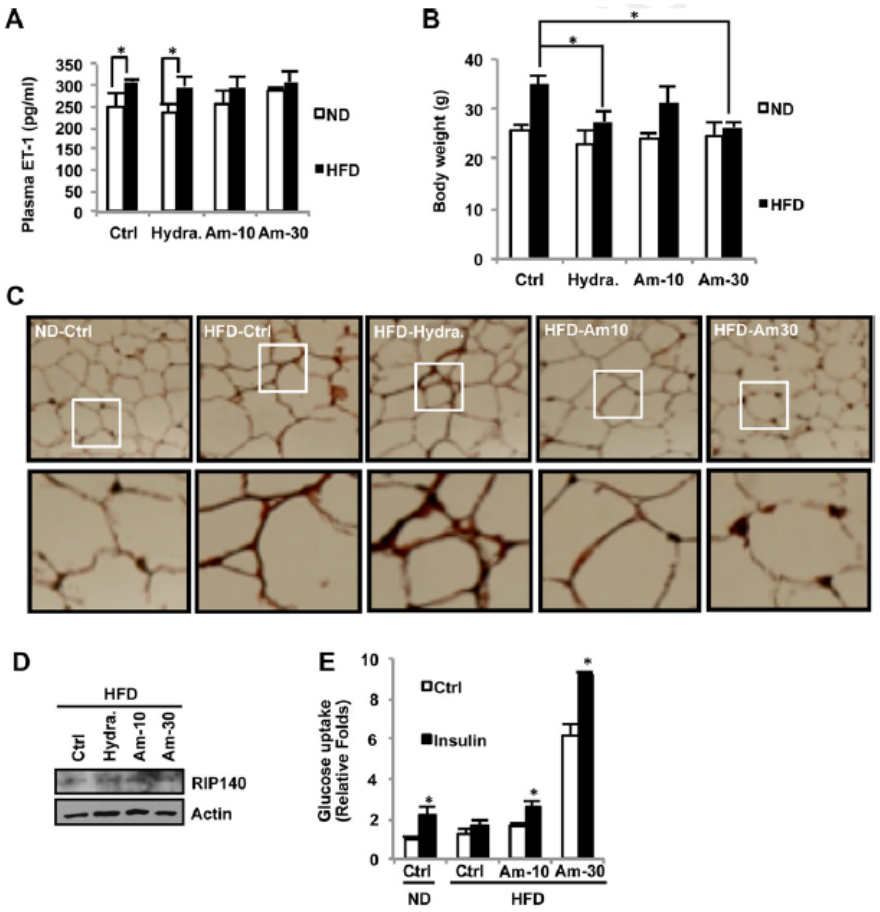

Figure 5-4. ET_A antagonist, ambrisentan, decreases cytoplasmic RIP140 accumulation in epididymal adipose tissue of HFD-fed mice. Mice were fed a normal diet (ND) or a high-fat diet (HFD) for two weeks and then treated, daily, as indicated for three more weeks. A, Plasma ET-1 levels were determined by ELISA. B, Body weight of mice from indicated group. C, Representative immunohistochemical staining of RIP140 in epididymal adipose tissue of the ND or HFD animals. D, The expression level of total RIP140 in epididymal adipose tissue of indicated group of mice. E, Basal and insulin-stimulated glucose uptake of primary adipocytes isolated from epididymal adipose tissues. Glucose uptake, per 10^6 cells, was measured. The relative fold was obtained by normalization to the control of the ND group that was arbitrarily set at the value of 1. All values represent the means ± SD., n=4-7; *: $P < 0.05$. Hydra.: hydralazine (10 mg/kg); Am-10: ambrisentan (10 mg/kg); Am-30: ambrisentan (30 mg/kg).

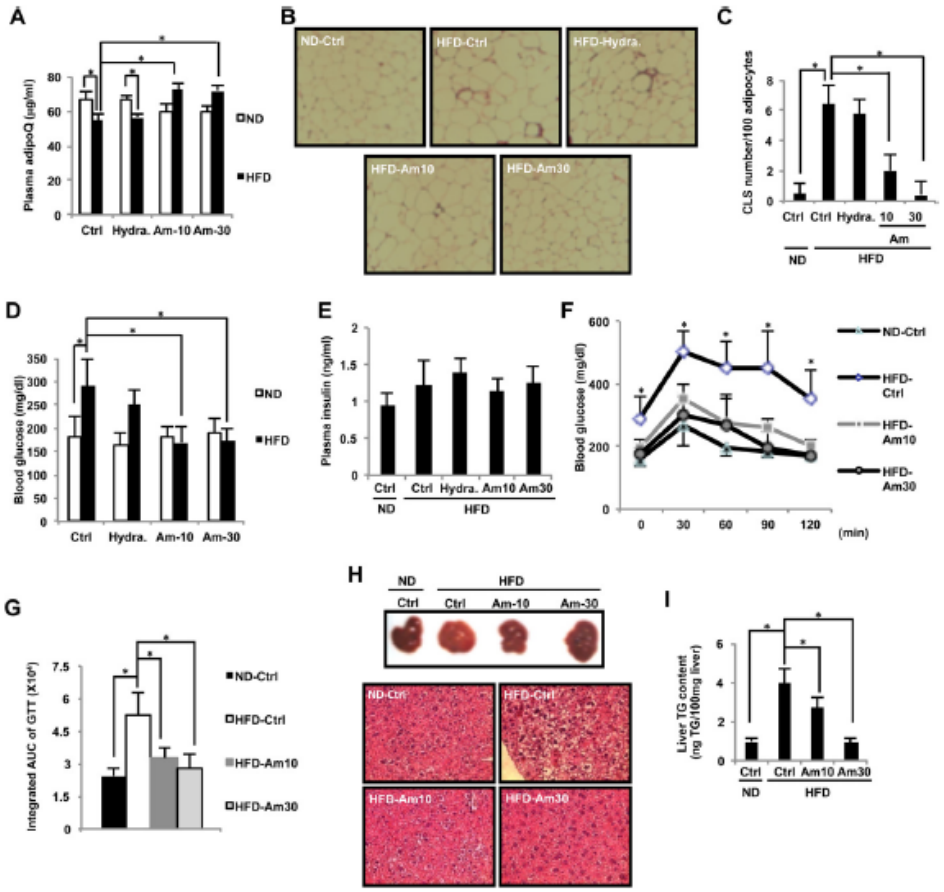

Figure 5-5 ET_A antagonist, ambrisentan, ameliorates metabolic dysfunctions in HFD-fed mice. A, Plasma adiponectin levels of mice fed a normal (ND) or high-fat diet (HFD) were determined by ELISA. All values represent the means ± SD, n=4-7; *: $P < 0.05$. B, H&E staining of epididymal adipose tissue to detect crown-like structures. C, Quantitative analysis of crown-like structures in adipose tissue. All values represent the means ± SD, n=5~7 random images from 3 different mice in the same group; *: $P < 0.05$. D, Fasting blood glucose. E, plasma insulin levels from overnight fasted mice fed with a ND or HFD. F, Glucose tolerance test. G, The area under curve (AUC) in glucose tolerance tests. H, Upper panel: Representative images of liver appearance. Lower panel: Representative images of H&E staining of liver sections. I, Triglyceride (TG) contents in animal livers. All values represent the means ± SD, n=4-7; *: $P < 0.05$. Hydra.: hydralazine (10 mg/kg); Am-10: ambrisentan (10 mg/kg); Am-30: ambrisentan (30 mg/kg).

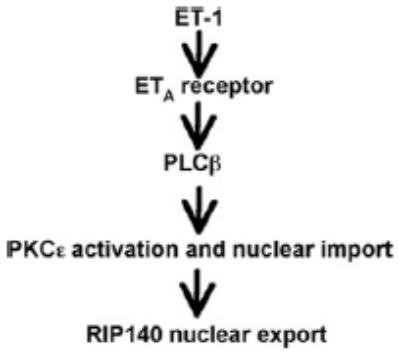

Figure 5-6. Proposed model for ET-1-mediated nuclear export of RIP140. ET-1 binds with ETA receptor on adipocytes and then activates cytoplasmic PLCβ. Activated PLCβ promotes nuclear accumulation of PKCε, that initiates the PTMs of RIP140 and its nuclear export.

Preface

This chapter has been published:

Ping-Chih Ho, Kun-Che Chang, Ya-Shan Chuang, and Li-Na Wei (2011) Cholesterol regulation of receptor-interacting protein 140 via microRNA-33 in inflammatory cytokine production. FASEB Journal 25, 51758-51766

CHAPTER VI

Cholesterol regulation of receptor-interacting protein 140 via microRNA-33 in inflammatory cytokine production

Introduction

Macrophages are central components of the innate immune system and important players in maintaining cholesterol homeostasis [124-126]. Resident and circulating macrophages can recognize invading pathogens and sense tissue damage mediated by Toll-like receptors (TLRs), and produce proinflammatory cytokines that evoke inflammation. However, massive production of TNFα and IL-1β by activated macrophages can also lead to septic shock, causing tissue damage, multiple organ failure and death. Clinically, both the susceptibility to, and mortality from, septic shock are dramatically higher in obese patients [127-129]. Studies over the past decade revealed that nutrient status (especially lipid and cholesterol) could be sensed by macrophages to modulate inflammation in metabolic diseases [130, 131].

Although free fatty acids have been shown to promote proinflammatory cytokines production via TLRs, the role of cholesterol in modulating macrophage activity remains unclear. Modified forms of low-density lipoprotein (LDL) are engulfed by macrophages, and the cholesterol is either stored in lipid droplets or transported out by cholesterol efflux. Defects in cholesterol efflux result in cholesterol accumulation in the macrophages; this has been implicated in inflammation-related diseases such as atherosclerosis [130, 132, 133]. Interestingly, the HMG-CoA reductase inhibitor statin (which is used to lower plasma cholesterol) has been shown to possess anti-inflammatory properties that act by both cholesterol-dependent and –independent mechanisms [134-136]. Although these studies suggest that cholesterol is important to the proinflammatory potential of macrophages and might play a role in related diseases, the exact mechanisms by which cholesterol modulates macrophage activity remain elusive [132, 133, 137, 138].

Receptor-interacting protein 140 (RIP140) is a master coregulator for a variety of transcription factors [2, 3, 66, 82] and affects gene expression in ovary and metabolic tissues including liver, muscle, and adipocytes. In addition to being infertile, RIP140-null mice are lean and resistant to diet-induced diabetes [5, 67, 82-85]. Recent proteomic analyses identified several post-translational modifications (PTMs) of RIP140 that play

important roles in modulating RIP140's function and cellular localization [4, 14, 15, 20, 21]. Furthermore, changes in these PTMs in response to nutrient status in adipocytes trigger different signaling pathways that modulate RIP140's functions [16, 19, 85]. In addition to its role in metabolic tissues, RIP140 can associate with NF-κB in macrophages to coactivate proinflammatory cytokines production [11]. Specifically, RIP140 is essential for TLR2-, TLR3- and TLR4-mediated production of inflammatory cytokines. However, it remains unclear if the expression of RIP140 in macrophages is altered in response to changes in cellular lipid contents, and whether this underlines the regulation of macrophages' inflammatory potential.

MicroRNAs (miRNAs) are single-stranded non-coding RNAs 21-23 nucleotides in length. These molecules regulate gene expression by recognizing targets in either the 5′- or 3′-untranslated region (UTR). Binding to 3′-UTR is the major mechanism by which miRNAs form miRNA-RNA-induced silencing complexes, thus promoting the degradation of target mRNAs and reducing protein expression [139]. Unique miRNA expression profiles have been identified in both innate and adaptive immune systems and are believed to control their development and functions. For example, several miRNAs modulate macrophage inflammatory responses by negative- or positive-feedback [139-142]. These miRNAs could play roles in the progression of inflammation-related diseases such as atherosclerosis, Alzheimer's disease and rheumatoid arthritis [139]. Recent studies have revealed that cholesterol content within macrophages can affect miRNA-33 expression, modulating cholesterol efflux [143-147].

This study examines RIP140 expression levels in macrophages in response to alterations in cholesterol content, both in vitro and in vivo. The results show that miR-33 mediates the regulation of RIP140 expression by intracellular cholesterol. Specifically, high-fat-diet (HFD)-feeding reduces miR-33, but elevates RIP140, levels in peritoneal macrophages, and promotes an inflammatory response that manifests as acute septic shock. Consistently, simvastatin treatment (to block cholesterol synthesis) reduces RIP140 expression by increasing miR-33 expression. Further investigations reveal that

miR-33 affects RIP140 by recognizing a highly conserved sequence in its 3′-UTR. These findings demonstrate the importance of the levels of the transcription coregulator RIP140 in the macrophage inflammatory response and establish that its expression in macrophages can be modulated by cholesterol content. This study also identifies miR-33 as an anti-inflammatory miRNA that acts in response to cholesterol depletion.

Materials and Methods

Materials

Male C56BL/6J mice were from Jackson labs (Bar Harbor, ME, USA). Raw264.7 murine macrophage and 293T cell lines were from ATCC (Manassas, VA, USA). Modified LDLs (Ox-LDL and Ac-LDL) were purchased from Intracel (Frederick, MD, USA). Simvastatin, mevalonate, Sandoz 58-035, LPS and D-galactomsamine were from Sigma Aldrich (St. Louis, MO, USA). Cholesterol assay kit was from Cayman Chemicals (Ann Arbor, MI, USA). ELISA kits for TNFα and IL-1β were from BD Biosciences (San Jose, CA, USA) and RayBiotech (Norcross, GA, USA), respectively. Anti-beta-actin antibody was from Santa Cruz (Santa Cruz, CA, USA). Antibodies for RIP140 and F4/80 were from Abcam (Cambridge, MA, USA). Hiperfect, miScript Reverse Transcription kit, miScript SYBR PCR kit, miR-33 PCR primer, siRNAs, miRNA-33 and miRNA-33 inhibitor were from Qiagen (Valencia, CA, USA). Lipofectamine 2000 was from Invitrogen (Carlsbad, CA, USA).

Cell culture and transfection

Raw 264.7 murine macrophages, BV2 microglia cell line and 293T cells were maintained in DMEM with 10%FBS and 1% antibiotics. For modified LDL treatment, Raw264.7 cells were treated with 50 μg/ml oxidized LDL or 50 μg/ml acetylated LDL for 8 hr. For simvastain treatment, Raw264.7 cells were treated with 5 μM simvastatin alone, 100 μM mevalonate alone or 5 μM simvastatin plus 100 μM mevalonate for 24 hr. Plasmid transfection was performed using Lipofectamine 2000 and siRNAs and miRNAs

transfection was performed using Hiperfect according to the manufacturer's instructions. For proinflammatory cytokine production, Raw264.7 macrophages or peritoneal macrophages were treated with vehicle or 20 ng/ml LPS for 4 hr. Media were collected to determine TNFα and IL-1β levels by ELISA kits.

Plasmids and luciferase reporter assays

RIP140 3'-UTR was amplified from cDNA of 3T3-L1 cell by primers as following: Forward primer: 5'-gagtcatctagaatgtgtacctgccataccac-3'; Reverse primer: 5'-gagtcatctagactggtgaagttgtgcattttaatg-3'. The amplified 3'UTR was cloned into pGL3-promoter vector (Promega, Madison, WI, USA) with the XbaI site. The mutant with point mutations in the seed sequence of miR-33 was cloned by different reverse primer with point mutations: Reverse primer: 5'-gagtcatctagactggtgaagttgtcgattttaatg-3'.

For RIP140 3'-UTR luciferase reporter assay, 293T cells were transfected with 0.03 μg reporter plasmid, 0.2 μg LacZ plasmid and 100nM microRNA by Lipofectamine 2000 according to manufacturer's instruction. After twenty-four hours, luciferase and LacZ activities were determined as described previously [18]. For reporter assay with simvastatin, BV2 microglia cells were transfected with 0.03 μg reporter plasmid and 0.2 μg LacZ plasmid using Lipofectamine 2000. Twenty-four hours after transfection, cells were treated with or without 50 μM simvastatin for another 24 hr. For NF-κB reporter assay, 293T cells were transfected with 0.6 μg NF-κB reporter [148] and 0.2 μg Flag-RIP140 containing different 3'-UTR or control vector.

Animal studies and peritoneal macrophage isolation

5-week-old male C56BL/6J mice were fed with a normal diet containing 18% calories from fat and undetectable cholesterol (#2018, Harlan Teklad, Madison, WI, USA) or a high-fat diet containing 60% calories from fat and 345 mg cholesterol per kg body weight (#F3282, Bio-Serv, West Chester, PA, USA). After 2 weeks, mice were analyzed for acute septic shock and peritoneal macrophage isolation. For primary peritoneal macrophage isolation, mice were injected intraperitoneally with 3 ml thioglycolate. After 3 days, mice were sacrificed to isolate peritoneal macrophages as described previously.

Peritoneal macrophages were plated within RPMI-1640 medium containing 0.2% fatty acid-free BSA. After 2 hours, cells were washed with same medium once and then used for indicated analysis.

Acute septic shock animal model

Acute septic shock was performed as previous report [149]. Briefly, mice were injected intraperitoneally with LPS (0.1 mg per 25 g body weight) plus D-galactosamine (0.5 mg per g body weight). Survival was monitored every hour for the next 18 hr.

Flow cytometry

Macrophages derived from mice were cultured for two hours for adhesion. Macrophage surface antigens were stained with rat-anti mouse F4/80 antibody for 30 min. in staining buffer (1% heat-inactivated FCS, 0.09% (w/v) sodium azide in DPBS) at 4°C and fixed as well as permeabilized with Fixation/Permeabilization solution (BD Bioscience) for 30 min. at 4°C. Cells were further stained with rabbit-anti RIP140 antibody for 30 min. in staining buffer. PE F(ab')2 Donkey anti-Rabbit IgG (BD Bioscience) and Goat F(ab')2 anti-rat IgG-PerCP (R&D system, Minneapolis, MN, USA) in staining buffer were incubated with cells at 4°C 30 min in the dark. The stained cells were analyzed with fluorescence-activated cell sorting (FACS) (BD Biosciences) according to the manufacturer's instructions. Fluorescence of F8/40 was collected in the FL3 detector, and fluorescence of RIP140 was collected in the FL2 detector.

Semi-quantitative real-time PCR and quantitative microRNA real-time PCR

mRNA from cells were extracted by Trizol (Invitrogen, Carlsbad, CA, USA) and then converted into cDNA by Omniscript RT kit or miScript Reverse Transcription kit (Qiagen, Valencia, CA, USA). Real-time PCR for gene expression was performed with specific primer sets by Brilliant II Fast SYBR Green QPCR reagent (Agilent, Santa Clara, CA, USA) in Mx3005P QPCR system (Agilent). Primers for QPCR are as following:

mouse RIP140 forward 5'- GGCAGCAAACCTGAATTCGGC-3';

mouse RIP140 reverse 5'-CTCACCGGGCACGGAACATC-3';

mouse TNFα forward: 5'-ATGAGCACAGAAAGCATGATCCGC-3';

mouse TNFα reverse: 5'- CCAAAGTAGACCTGCCCGGACTC-3';

mouse IL-1β forward: 5'-TCAGGCAGGCAGTATCACTCA-3';

mouse IL-1β reverse: 5'-GGAAGGTCCACGGGAAAGAC-3'.

For miR-33 expression, real-time PCR was performed by miScript SYBR PCR kit (Qiagen) with miR-33 specific primer.

Statistical analysis

Results were presented as means ± SD. Statistical analysis was performed by Student's *t* test and *P* value < 0.05 was considered as significant difference. For survival rate, result was analyzed by Kaplan-Meier analysis.

Results

High-fat diet upregulates RIP140 expression in macrophages

Hypercholesterolemia is a risk factor contributing to various inflammatory diseases, and RIP140 has been shown to be involved in inflammatory cytokine production [11]. We asked if a high-fat diet (HFD), that drastically elevates cholesterol levels in the animals, could affect RIP140 expression in macrophages through which their proinflammatory potentials might be modulated. We compared the RIP140 expression levels in peritoneal macrophages from male C56BL/6J mice fed with either a normal diet (ND) or HFD for 2 weeks. We co-stained peritoneal macrophages with anti-RIP140 and an antibody against the macrophage surface marker, F4/80, which were analyzed by flow cytometry. Approximately 30.4% of macrophages from ND mice expressed high levels of RIP140; whereas HFD dramatically expanded the population expressing high-RIP140 levels to approximately 50% (Fig. 1A). Importantly, although the profile of macrophage RIP140 levels was altered in HFD mice, there was no change in the F4/80 expression profile. We compared the histograms of RIP140 expression between the F4/80-positive macrophage

populations from ND and HFD mice, and found a substantial increase in the mean of RIP140 expression levels for the HFD mice (Fig. 1B). This was further supported by real-time qPCR analyses of RIP140 mRNA in peritoneal macrophages from ND and HFD mice, which detected approximately a 3-fold increase in RIP140 mRNA for the HFD mice (Fig. 1C). Taken together, these results show that HFD feeding can increase RIP140 mRNA and protein levels in macrophages.

Intracellular cholesterol content modulates RIP140 levels

Under a HFD, circulating LDL can be acetylated and oxidized, which can then be recognized and engulfed by macrophages. These cholesterol-loaded macrophages become foam cells [125, 132], increasing their proinflammatory potential [132, 133]. Given that a short-term HFD feeding in animals substantially increased their RIP140 expression in macrophages (Fig. 1) and intracellular cholesterol content in peritoneal macrophages (Fig. 2A), we asked if intracellular cholesterol accumulation could promote RIP140 expression in Raw264.7 mouse macrophage cell line. It appeared that both acetylated LDL and oxidized LDL significantly enhanced RIP140 mRNA levels (Fig. 2B), suggesting that intracellular cholesterol content might be an important regulator for RIP140 expression in macrophages. We then applied an HMG-CoA reductase inhibitor, simvastatin, to block cholesterol synthesis (mimicking a cholesterol-depletion state) in these macrophages [144, 150], and found that simvastatin treatment for 24 hr indeed significantly decreased RIP140 mRNA levels. Further, in the presence of mevalonate, the product of HMG-CoA reductase, simvastatin failed to reduce RIP140 mRNA levels (Fig. 2C). Consistently, the reduction in RIP140 protein level after simvastatin treatment was also abolished by mevalonate treatment (Fig. 2D). These results show that indeed, RIP140 expression in macrophages, at both mRNA and protein levels, is negatively regulated by intracellular cholesterol accumulation.

Cholesterol up-regulates RIP140 expression via repressing microRNA-33 that down-regulates RIP140 by targeting its conserved 3'-UTR

Recent studies have shown that miR-33 is produced from an intron of *SREBP-2* in response to intracellular cholesterol accumulation, which inhibits cholesterol efflux by down-regulating ABCA1 and ABCG1 expression at the post-transcriptional level [143-147]. Based on the reverse correlation between cholesterol content and RIP140 mRNA level shown above, we suspected a potential role for miR-33 in RIP140 expression. Interestingly, miR-33 was predicted to recognize a conserved 3′-UTR of RIP140 mRNA (Fig. 3A). We then compared RIP140 mRNA and mature miR-33 levels in Raw264.7 macrophages treated with or without simvastatin. It appeared that simvastatin not only reproducibly reduced RIP140 mRNA level but also increased miR-33 level (Fig. 3B). We further compared miR-33 levels in primary peritoneal macrophages from ND- and HFD-fed animals, and found that peritoneal macrophages from HFD-fed mice expressed a much lower level of mature miR-33 as compared to the ND group (Fig. 3C). To obtain direct evidence for a functional role of miR-33, we used Raw264.7 cell to assess the effects of gain- and loss-of-function of miR-33 on RIP140 expression. Figs. 3D and E show that RIP140 mRNA and protein levels were both reduced in Raw264.7 cells transfected with miR-33 mimic even without depleting cholesterol (by simvastatin treatment), and simvastatin-triggered reduction in RIP140 was abolished by a miR-33 inhibitor (Anti-miR-33).

To further confirm the effect and target of miR-33 on RIP140 mRNA, we generated luciferase reporter constructs containing either the wild type, or miR-33 target mutated, 3′-UTR of RIP140 mRNA (Fig. 4A) to assess the effects in 293T cells. In the presence of miR-33 mimic, the wild type, but not the mutated, reporter activity was significantly lowered as compared to the control reporter activity (Fig. 4B). Further, miR-33 mimic repressed the reporter activity in a dose dependent manner (Fig. 4C). These results confirm that miR-33 indeed acts by targeting the conserved 3′-UTR of RIP140 mRNA to suppress its expression. To further evaluate if this conserved miR-33 target sequence in the 3′-UTR of RIP140 was important for simvastatin-triggered reduction in RIP140 expression, we used this reporter system to assess the effect of simvastatin. Indeed, simvastatin inhibited only the wild type, but not the mutated or control reporter (Fig. 4D). Together, these experiments identify RIP140 as a target of miR-33, and delineate the

mechanism of cholesterol action in elevating RIP140 expression, which is mediated by down-regulating miR-33 that targets the 3′-UTR of RIP140 mRNA.

MicroRNA-33 decreases RIP140 expression to down-regulate inflammatory cytokines production

Simvastatin has been shown to possess anti-inflammatory activities by blocking NF-κB activity thereby reducing TNFα and IL-1β expression [151]. Since RIP140 could function as coactivator for NF-κB to activate TNFα and IL-1β expression, we hypothesized that reducing cholesterol content, such as by simvastatin treatment, may modulate NF-κB activity by, at least partially, controlling the level of RIP140. We used an NF-κB reporter in 293T cells to assess the effects of reducing cholesterol content (by simvastatin treatment) and expressing an RIP140 expression vector containing either the wild type or miR-33 target mutated 3′-UTR. As shown in Fig. 5A, co-transfection with either the wild type, or 3′-UTR mutated, RIP140 vector with NF-κB increased the NF-κB reporter activity in cells without simvastatin (Ctrl), supporting that RIP140 can co-activate NF-κB activity. However, simvastatin treatment significantly inhibited the NF-κB reporter activity in cells co-transfected with the wild type, but not the miR-33 target mutated, RIP140 vector. This result indicates that reducing cholesterol content by simvastatin treatment can repress NF-κB activity by reducing its co-activator RIP140 via elevating miR-33 that targets RIP140's 3'-UTR, and suggests that miR-33 can be anti-inflammatory and reduce inflammatory cytokines production in macrophages. Indeed, transfection of Raw264.7 macrophages with miR-33 not only reduced RIP140 mRNA level but also suppressed LPS-stimulated production of TNFα and IL-1β mRNA (Fig. 5B). Consistently, the secreted levels of TNFα and IL-1β in the cell culture media were also decreased (Fig. 5C). These experiments support our hypothesis that miR-33 can be anti-inflammatory in macrophages by inhibiting RIP140 expression. These results delineate a new mechanism by which simvastatin can exert an anti-inflammatory effect,

and identify miR-33 as a new microRNA involved in the regulation of macrophage inflammatory response.

RIP140 upregulates inflammatory cytokines production and increases the potential of acute septic shock

To provide a direct gain-of-function evidence for RIP140's role in TNFα and IL-1β expression, we over-expressed RIP140 in Raw264.7 macrophages and determined the mRNA levels of TNFα and IL-1β. Fig. 6A shows that over-expressing RIP140 in Raw264.7 macrophages significantly elevated both TNFα and IL-1β mRNA levels, with or without LPS stimulation. In contrast, silencing RIP140 in macrophages reduced the basal and LPS-stimulated levels of TNFα and IL-1β (Fig. 6B). These results further support that RIP140 can positively regulate proinflammatory cytokine production, and suggest that HFD might affect inflammatory potential, at least partially, through increasing RIP140 expression in macrophages.

To address this mechanism in the context of whole animals, we compared the immune responses of mice fed with either ND or HFD, using acute septic shock as the indicator. Mice fed with ND or HFD for 2 weeks were challenged with LPS and D-galactosamine and their survival rates within 18 hrs were monitored. It appeared that the HFD-fed mice had a higher mortality rate in response to LPS challenge, and they also died earlier, as compared to the ND-fed mice (Fig. 6C). In this septic shock model, robust elevation in circulating TNFα and IL-1β is responsible for multiple organ failure, tissue damage and death, and macrophages are the central players in the production and secretion of these cytokines [127, 152]. Accordingly, we predicted that HFD would elevate TNFα and IL-1β levels in macrophages and enhance their inflammatory potential. As expected, the basal and LPS-stimulated mRNA levels of TNFα and IL-1β in peritoneal macrophages of HFD-fed mice indeed were much higher as compared to that of ND-fed mice (Fig. 6D). The results are consistent with a contributory role for RIP140 in the response of HFD-animals to septic shock. Together with data shown in Fig.1, the results support that HFD

elevates RIP140 expression in peritoneal macrophages, which activates TNFα and IL-1β expression and enhances macrophages' inflammatory potential, thereby contributing to increased susceptibility to septic shock in certain conditions such as obesity.

Discussion

RIP140 is known to be involved in diet-induced diabetes and can be an important player in TLR-mediated inflammatory response. Because of its significantly altered subcellular distribution following a HFD, at least in adipocytes, it has also been proposed as a disease marker for the progression of metabolic diseases [85]. However, whether and how its expression level may alter in response to diet/nutritional factors or as a result of disease progression, remains elusive. Here, we identify intracellular cholesterol accumulation as an important trigger to elevate RIP140 expression in macrophages through decreasing a specific microRNA that negatively regulates RIP140 expression post-transcriptionally. Because RIP140 can function as a co-activator for NF-κB, its increased expression in macrophages would enhance their inflammatory responses. Interestingly, the key to this regulatory mechanism relies, at least partially, on the expression of a recently discovered microRNA, miR-33, derived from an intron of *SREBP-2* and reported to regulate several important genes in homeostatic control of cholesterol [143-147]. This current study further extends the finding to provide a potential mechanistic explanation for certain clinically important inflammatory diseases such as acute septic shock that can be more severe under the obese condition. Finally, this study also demonstrates miR-33 as an anti-inflammatory miRNA in macrophages.

ABCA1- and ABCG1-knockout mice aberrantly accumulated cholesterol and exhibited a higher inflammatory potential, i.e. they had increased inflammatory cytokines [132, 133]. It would be interesting to examine RIP140 expression in peritoneal macrophages from ABCA1- or ABCG1-knockout mice, which may provide a potentially new mechanism different from TLR activation. It is quite likely that macrophages utilize multiple

mechanisms/pathways to elicit inflammatory responses. Five groups recently reported miR-33 and proposed the therapeutic potential of anti-miR-33 in enhancing HDL level [143-147]. Based upon data presented in this current study, we propose that miR-33 may also be a potential anti-inflammatory therapeutic.

The mouse miR-33 is produced from an intron of *SREBP-2*. Human expresses miR-33a and miR-33b from introns of *SREBP-2* and *SREBP-1*, respectively. Cholesterol-depletion caused by HMG-CoA reductase inhibitor such as simvastatin results in the induction of miR-33 expression along with SREBP-2 expression [144]. SREBP-2 elevation can trigger reactions replenishing depleted intracellular cholesterol pool. Increased miR-33 in a cholesterol depleted state not only blocks cholesterol efflux by targeting ABCA1 and ABCG1 to facilitate the accumulation of intracellular cholesterol but also reduces RIP140 level in order to prevent potential inflammation caused by over-accumulation of cholesterol. In contrast, when macrophages engulf a massive amount of modified LDL, accumulation of cholesterol signals cells to reduce the expression of miR-33 along with SREBP-2. As a result, ABCA1 and ABCG1 are elevated to promote cholesterol efflux and RIP140 is also increased to promote inflammatory responses. The enhancement in macrophages' inflammatory response may be needed to react to tissue damage in the pathophysiological condition caused by hypercholesterolemia. Under other pathophysiological conditions, macrophages may infiltrate into damaged tissues and increase their intracellular cholesterol contents by taking up damaged or apoptotic cells via phagocytosis. This newly uncovered mechanism could also be in operation to modulate macrophages' inflammatory potential in these circumstances. This would allow fine-tuning the functions of macrophages in response to changes in the cholesterol status, and may also be involved in other metabolic disorders.

This study shows miR-33 as a novel anti-inflammatory microRNA by targeting the 3'-UTR of RIP140 mRNA. We previously reported another microRNA, miR-346, that could enhance RIP140 translation by associating with its 5′-UTR [96]. We also demonstrated that coregulators could modulate transcription factors' activity via competitive interaction and the level of their expression can be critical to specific gene regulation

[153, 154]. In future studies, it would be interesting and important to dissect the relationship of these microRNAs and the expression level of RIP140 in particular physiological conditions or during disease progression. It would also be interesting to explore the therapeutic potential of specific microRNAs to target RIP140.

Finally, simvastatin is the most potent cholesterol-lowering statin. We show its anti-inflammatory and RIP140-suppressing properties in macrophages in this current study, which is partially attributed to a cholesterol-dependent mechanism [134, 135]. However, the effects of simvastatin on RIP140 expression in other metabolic tissues remain to be examined. It is also important to investigate the effects of simvastatin on the expression of RIP140 in other types of cells Further, HFD could potentially affect not only cholesterol levels but also fat contents; therefore the effects observed in this HFD mouse model may also be contributed by alteration in fat content.

Figures

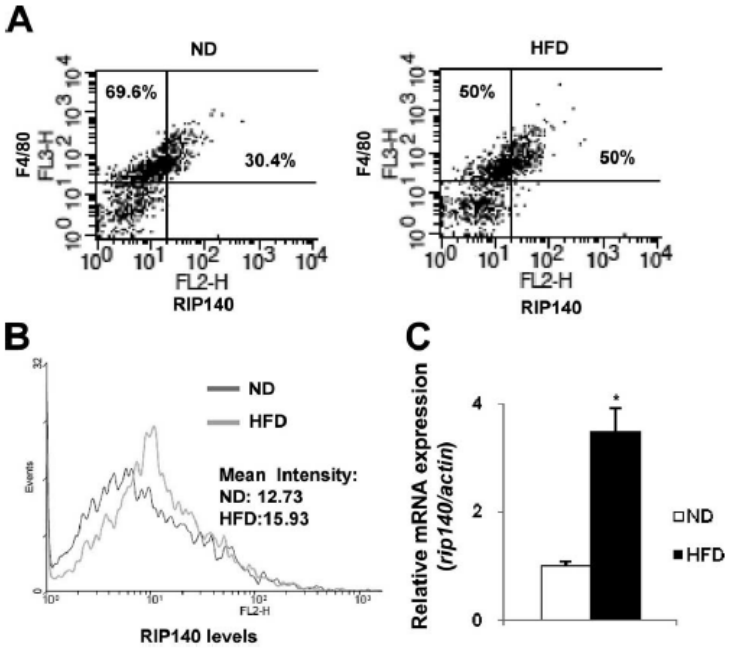

Figure 6-1 The effect of high-fat diet on RIP140 expression in peritoneal macrophages. *A)* Primary peritoneal macrophages were obtained from C56BL/6J mice fed with wither a normal diet (ND) or a high-fat diet (HFD) for 2 weeks. RIP140 and F4/80 expression profiles were determined by flow cytometry. Y-axis shows the staining intensity of macrophage marker F4/80. X-axis shows the staining intensity of RIP140. *B)* Histogram showing RIP140 expression from F4/80-positive peritoneal macrophages. Geological means for ND and HFD were indicated. *C)* Real-time analysis of RIP140 mRNA levels in peritoneal macrophages from animals fed the indicated diets. All values represent means ± SD., n=3; *: $P < 0.05$ compared to normal diet.

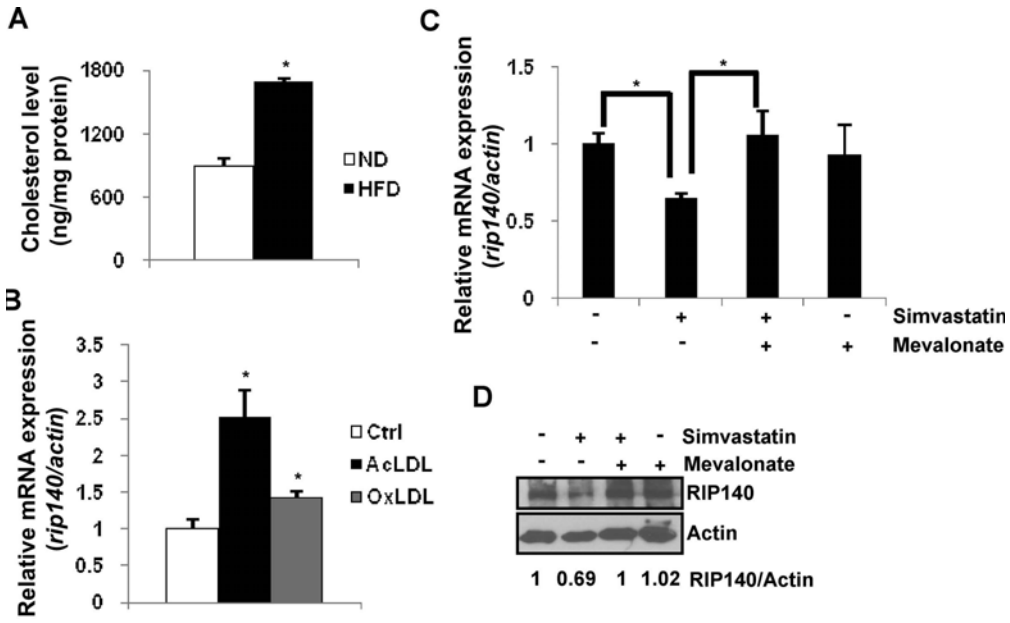

Figure 6-2. The effect of intracellular cholesterol level on RIP140 expression. *A)* Intracellular cholesterol contents of primary peritoneal macrophages from ND or HFD. The value represent means ± SD., n=3; *: $P < 0.05$ compared to normal diet. *B)* Raw264.7 murine macrophages were treated with vehicle, acetylated LDL (AcLDL) or oxidized LDL (OxLDL) in the media for 8 h. mRNA levels of RIP140 were determined by semi-quantitative real-time PCR. The values represent means ± SD., n=3; *: $P < 0.05$ compared to normal diet. *C)* mRNA and *D)* protein levels of RIP140 from Raw264.7 murine macrophages treated, as indicated, for 24 h. Quantified results are shown under the image. mRNA levels were determined by semi-quantitative real-time PCR and data show means ± SD., n=3; *: $P < 0.05$.

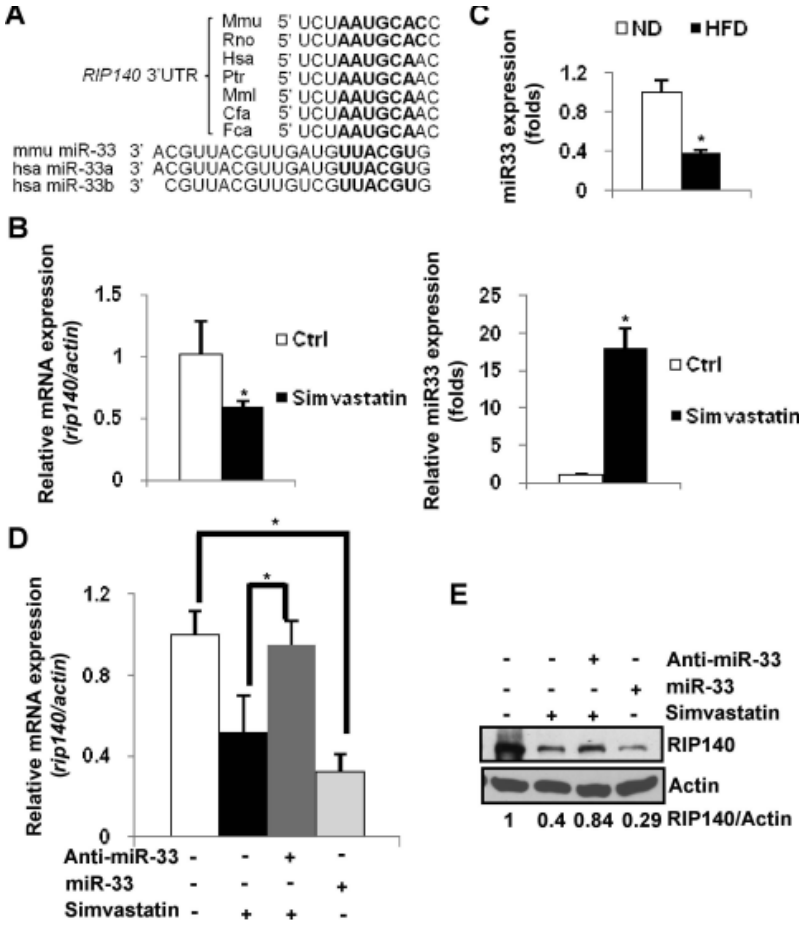

Figure 6-3. Simvastatin reduces RIP140 expression, mediated by miR-33. *A)* The predicted target site of miR-33 located in a conserved 3'-UTR of RIP140 mRNA, conducted by TargetScan. *B)* Left: RIP140 mRNA level. Right: mature miR-33 level. Samples were from Raw264.7 macrophages under control or simvastatin treatment for 24 h. *C)* Real-time analysis of mature miR-33 levels in peritoneal macrophages from mice fed with either ND or HFD for 2 weeks. *D)* RIP140 mRNA levels from Raw264.7 macrophages treated with control vehicle or simvastatin in the presence of miR-33 or miR-33 inhibitor. Anti-miR-33: miR-33 inhibitor. *E)* RIP140 protein levels from Raw264.7 macrophages treated with control vehicle or simvastatin in the presence of miR-33 or miR-33 inhibitor (Anti-miR-33). Quantified data are shown under the image. All values show means ± SD., n=3; *: $P < 0.05$.

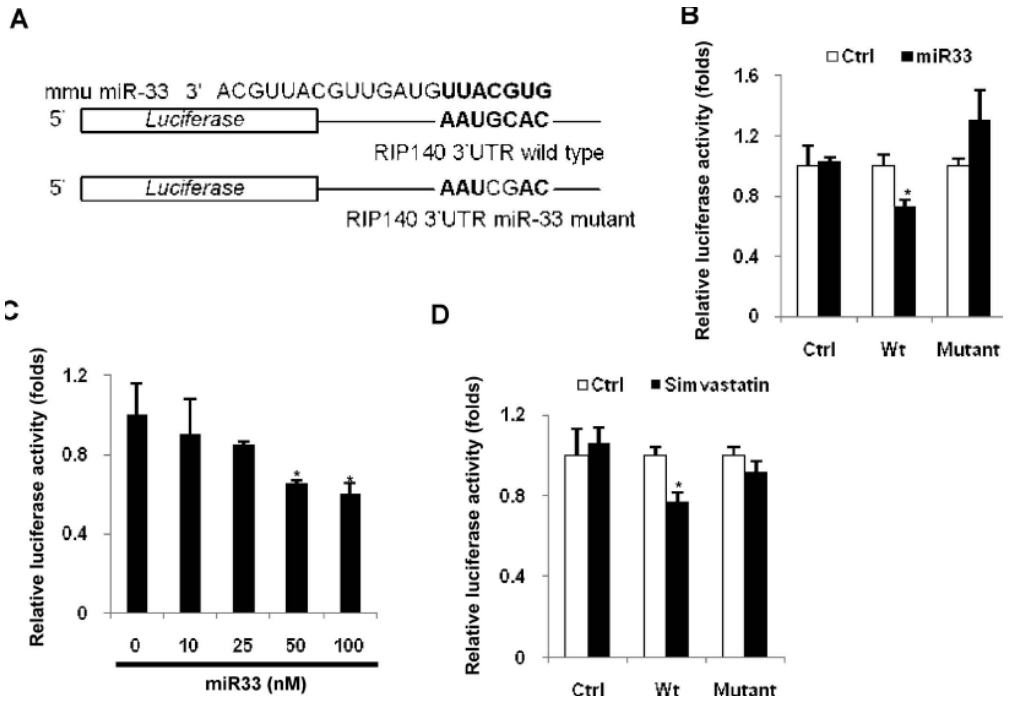

Figure 6-4. miR-33 targets a conserved 3'-UTR of RIP140 mRNA to repress RIP140. *A)* The schematic diagram showing reporter constructs containing the wild type or mutated 3'-UTR of RIP140 mRNA. *B)* miR-33 represses the luciferase activity of the wild type reporter but not the mutant reporter in 293T cells. *C)* Dose-dependent repressive effects of miR-33 mimic on the wild type reporter in 293T cells. All values show means ± SD., n=3; *: $P < 0.05$ compared to 0 nM. *D)* Simvastatin suppresses the luciferase activity of the wild type reporter but not the mutant reporter in BV2 cells. Ctrl: Control vector; Wt: wild type 3'-UTR reporter; Mutant: 3'-UTR reporter with mutations in the miR-33 target site. All values show means ± SD., n=3; *: $P < 0.05$ compared to control treatment.

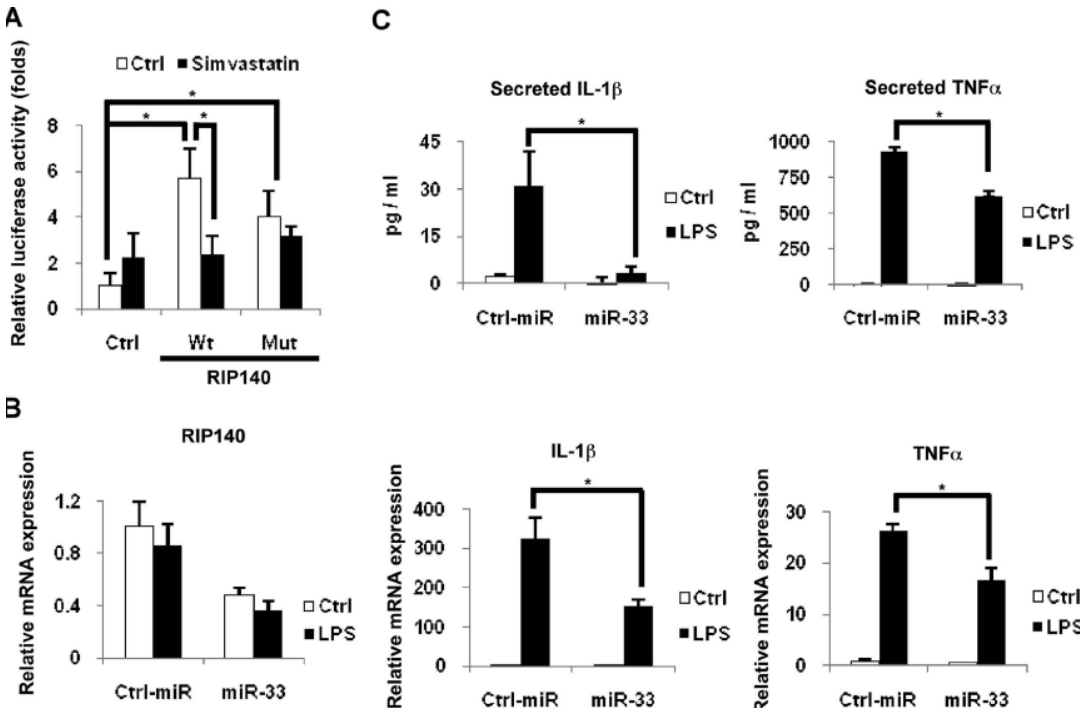

Figure 6-5 miR-33 modulates inflammatory cytokine production by controlling RIP140 expression. *A)* Simvastatin suppresses the effect of RIP140 on promoting NF-κB-driven reporter activity in 293T cells. After transfection with plasmids for 12 h, 293T cells were treated with vehicle (Ctrl) or simvastatin for another 24 h and, followed by assays of luciferase activity. *B)* Real-time analysis of mRNA levels of IL-1β and TNFα expression in Raw264.7 murine macrophages transfected with the control miR or miR-33 in the absence or presence of LPS for 4 h. All values show means ± SD., n=3; *: $P < 0.05$ C) miR-33 reduces IL-1β and TNFα contents in the culture supernatant of Raw264.7 macrophages in the absence or presence of LPS. Cytokine production was determined by ELISA. All values show ± SD., n=3; *: $P < 0.05$.

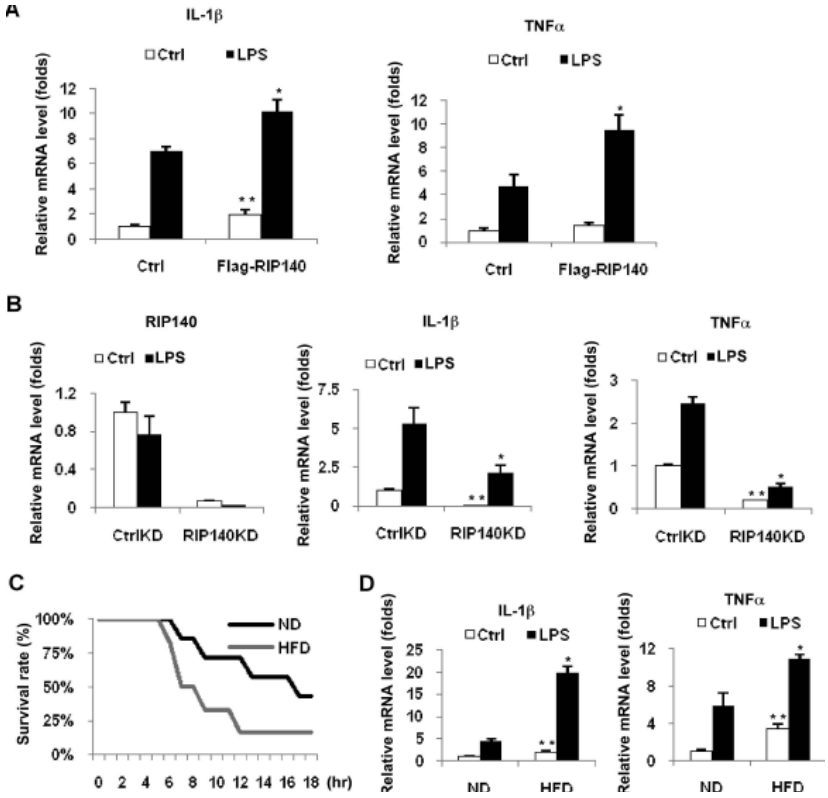

Figure 6-6. Expression of RIP140 in macrophages modulates inflammatory cytokines production and acute septic shock. *A)* Overexpression of RIP140 in Raw264.7 cells upregulated basal and LPS-induced levels of IL-1β and TNFα. *B)* Silencing RIP140 in Raw264.7 macrophages reduced the levels of IL-1β and TNFα. mRNA, determined by real-time qPCR. All values show means ± SD., n=3; *: $P < 0.05$ compared to LPS treatment in the control vector or control siRNA group. **: $P < 0.05$ compared to the control treatment in the control vector or control siRNA group. *C)* HFD reduced the animal survival rate in the acute septic shock model. The difference was significant between ND and HFD in Kaplan-Meier analysis. *D)* Real-time analysis of mRNA levels of proinflammatory cytokines including IL-1β and TNFα, in the absence or presence of LPS, in peritoneal macrophages. Ctrl: control treatment. All values show means ± SD., n=3-4; *: $P < 0.05$ compared to LPS treatment in the ND group. **: $P < 0.05$ compared to the control treatment in the ND group.

Preface

This chapter has been published:

Ping-Chih Ho, Yao-Chen Tsui, Xudong Feng, David R. Greaves, and Li-Na Wei (2012) NF-κB-mediated degradation of the co-activator RIP140 regulates inflammatory response and contributes to endotoxin tolerance. Published by Nature Immunology (In press)

CHAPTER VII

NF-κB-mediated degradation of the co-activator RIP140 regulates inflammatory response and contributes to endotoxin tolerance

Introduction

Pattern recognition receptors (PRRs), including Toll-like receptors (TLRs), are responsible for sensing microbial infection, tissue damage, and initiation of innate immune responses. Upon exposure to TLR ligands in immune cells, TLRs trigger inflammatory signaling to activate NF-κB and MAPK pathways and promote proinflammatory cytokine production such as tumor necrosis factor (TNF) and interleukin-1β (IL-1β) [38, 39]. These proinflammatory cytokines not only induce inflammation but also modulate the adaptive immune response. Recently, chronic inflammation and aberrant production of proinflammatory cytokines have been demonstrated to play critical roles in many diseases, especially metabolic diseases such as Type II diabetes mellitus (T2DM) and atherosclerosis [150, 155, 156]. Therefore, tight control of proinflammatory cytokine production and resolution of inflammation after infection and/or tissue damage are important for maintaining tissue homeostasis. Diminished proinflammatory signaling, non-permissive histone modifications, chromatin remodeling and microRNA production induced by inflammatory stimuli have all been shown to resolve inflammation by impairing proinflammatory cytokine production via inhibiting NF-κB and MAP kinase (MAPK) activities [39, 157-160].

Endotoxin tolerance (ET) provides a protective mechanism to reduce over production of proinflammatory cytokines in response to infection. Defects in the establishment of ET lead to a higher incidence of septic shock and mortality in individuals with infection. However, individuals with ET become immunocompromised [43, 46]. Therefore, understanding the mechanisms controlling ET is important to the design of interventions to fine tune immune responses. Besides monocytes, macrophages are the major cell type involved in ET in animals, and LPS, a TLR4 ligand, is most commonly used to induce ET *in vivo* and *in vitro* [160, 161]. Although suppression of TLR-mediated inflammatory signaling pathways by negative regulators has been proposed as a mechanism for the establishment of ET, this mechanism cannot fully explain why and how certain genes are efficiently silenced whereas some other genes using the same signaling pathways can still be activated in tolerated macrophages [159]. A growing number of studies have

demonstrated that changes on chromatin, including loss of RelA binding, histone modification and chromatin remodeling, provide the major regulatory mechanisms for the suppression of specific genes in ET [159-162]. But how these changes on specific chromatin targets are controlled is largely unclear.

Receptor-interacting protein 140 (RIP140) can act as co-repressor or a co-activator for various transcriptional factors and nuclear receptors, and it is mainly expressed in metabolic organs and tissues, including adipose tissue, liver, and muscle [2, 66, 82]. RIP140-null mice resist diet-induced T2DM, and RIP140 regulates lipid and glucose metabolism in metabolic tissues through its nuclear and cytoplasmic functions [5, 10, 82, 84, 85, 163]. Proteomic analyses have identified various post-translational modifications of RIP140 that modulate its function and sub-cellular distribution, such as serine and threonine phosphorylation, lysine acetylation, sumoylation, and lysine and arginine methylation [4, 18, 19, 21]. But tyrosine phosphorylation has not been detected on RIP140 in earlier studies. Recently, RIP140 was found to function in macrophages as a co-activator for NF-κB by recruiting CREB-binding protein (CBP) to modulate TLR-induced (at least TLR2, TLR3, and TLR4) production of proinflammatory cytokines such as TNF, IL-1β, and IL-6 [11]. Additionally, modulation of RIP140 expression by microRNA-33 affected inflammatory potential of macrophages in response to intracellular cholesterol levels [10]. These studies reveal a role for RIP140 in proinflammatory cytokine production, and suggest that it is important to regulate RIP140 expression to modulate inflammatory potential in macrophages.

Ubiquitin contains five lysine residues (K6, K11, K29, K48, and K63) that are involved in monoubiquitination and polyubiquitination. Specifically, K48-linked ubiquitination targets proteins to proteasome-mediated degradation [164]. Ubiquitination and proteasome-mediated protein degradation are involved in both positive and negative regulation of TLR signal transduction. To this end, IκB degradation is best characterized, which controls NF-κB activity by regulating subcellular localization of NF-kB [38, 39]. Additionally, SOCS1 (suppressor of cytokine-signaling-1)-Rbx1 (ring-box protein 1) is known to interact with RelA and promote RelA degradation in nuclei [165, 166]. But it is

largely unknown how regulation on specific chromatin targets to negatively regulate the inflammatory response is achieved.

We report here that RIP140 degradation, triggered by exposure of macrophages to TLR ligands, as a novel mechanism for negatively regulating specific genomic targets in the inflammatory response to promote ET. LPS stimulates the interaction of RIP140 with RelA, which leads to the recruitment of SOCS1-Rbx1 E3 ligase. In addition, LPS activates Syk-mediated phosphorylation of RIP140 on Tyr364, Tyr418 and Tyr436, facilitating its ubiquitination. Together these trigger efficient RIP140 protein degradation to dampen inflammation and induce ET. Prevention of RIP140 degradation by pre-treatment of macrophages with IFNγ or over-expression of a non-degradable RIP140 effectively diminished LPS-induced ET *in vitro* and *in vivo*. These results not only uncover a novel regulatory mechanism of inflammatory response by RIP140, but also show that RelA acts as an adaptor for E3 ligase to dynamically control its specific co-activator to fine-tune its own transcriptional activity for specific chromatin targets.

Materials and Methods

Cell culture, transfection and mice. Raw264.7 macrophage cell line was purchased from American Type Culture Collection and maintained in DMEM medium with 10% FBS and 1% antibiotics. Lipofectamine 2000 (Invitrogen) and lipofectamine LTX (Invitrogen) were used for plasmid transfection. siRNAs were purchased from Qiagen and transfected by Hiperfect (Qiagen). All male C56BL/6J mice were obtained from Jackson labtorary and maintained in the animal facility of Univerisity of Minnesota and were used at 6-12 weeks of age. Animal studies were performed with approval of University of Minnesota Institutional Animal Care and Use Committee. Peritoneal macrophages were elicited by 4% thioglycolate and isolated as previous report [10]. For the derivation of transgenic mice that overexpress shRNA to target RIP140 in macrophage lineage, the shRNA for RIP140 was mimicked as endogenous microRNA following reported method [167]. The expression of this shRNA was driven by hCD68 promoter [168] and the expression DNA fragment was cloned into pWhere vector. Transgenic DNA fragment was excised by PacI and then injected into C57BL/6 mouse

oocytes (Mouse genetics laboratory, University of Minnesota). Transgenic founder mice were genotyped by PCR using following primer set: Forward: 5'-GAGTTCTCAGACGCTGGAAAGCC-3' and Reverse" 5'-GTCCAATTATGTCACACCACAGAAG-3'.F1-F4 progeny were used for this study.

Reagents. LPS and IFNγ were purchased from Sigma-Aldrich and Invitrogen, respectively. Recombinant mouse IL-4 was purchased from eBioscience. TNFα was from Cell Signaling. Mouse TNFα ELISA kit and mouse IL-1β ELISA kit were from BD Biosciences and Ray Biotech, respectively. siRNAs and Hiperfect were from Qiagene. Antibodies for actin, HA-tag, RelA (p65) and Syk were from Santa Cruz. Anti-RIP140 antibody was purchased from Abcam. Anti-SOCS1, anti-Rbx1 and anti-K48 conjugated ubiquitin antibodies were from Millipore. Protein G agarose-conjugated with anti-phospho-tyrosine antibody was ordered from Cell signaling. Anti-Syk antibody purchased from BioLegend and anti-RIP140 antibody were used for proximal ligation assay. MG132 was from Sigma-Aldrich and genistein was ordered from EMD chemicals.

Flow cytometry analysis. Mice were injected with 3ml 4% thioglycolate intraperitoneally. After two days, mice were injected intraperitoneally with low dose of LPS to achieve endotoxin tolerance (0.1 μg/25 g body weight) [10]. After 24 h, mice were sacrificed and primary peritoneal macrophages were isolated and plated in DMEM with 0.1% fatty acid-free BSA for 1 h and then adherent cells were collected for flow cytometry analysis of RIP140 and F4/80. Flow cytometry analysis was performed as previous report [10].

***In vivo* ubiquitination assay.** For *in vivo* ubiqtuination assay, 2 μg Flag-RIP140 and 0.2 μg HA-ubiquitin plasmids were transfected into 293T cell with or with 1 μg HA-SOCS1 or HA-Rbx1. After 24 h, the media were changed to normal culture medium with 5 μg/ml MG132 for another 6 h. Cells were collected and lysed with RIPA buffer. Immunoprecipitated complexes were subjected into SDS-PAGE and probed with anti-HA antibody.

Immunofluorescence analysis and proximal ligation assay. Immunofluorescence analysis was conducted as previous report [85]. For proximal ligation assay to detect the interaction of RIP140 with Syk, anti-RIP140 antibody (ab-42126, Abcam) and anti-Syk antibody (626201, Biolegend) were used with Duolink PLA assay kit (Olink Bioscience). Images were acquired by FluoView 1000 IX2 confocal microscope (Olympus).

Syk kinase assay. For *in vitro* Syk kinase assay, wild type and mutant forms of Flag-RIP140 were purified from transfected 293T cell lysates by immunoprecipitation. Immunoprecipitates were incubated with 10 ng active Syk (Cell Signaling) in Syk kinase assay buffer (50 mM Tris-HCl pH 7.5, 2.5 mM β-glycerophosphate, 1mM EGTA, 0.4 mM EDTA, 5 mM $MgCl_2$, 0.05 mM DTT and 200 μM ATP) at 25^{o}C for 1h. After reaction, immunoprecipitates were subjected into SDS-PAGE and then immunoblotted with anti-phospho-tyrosine.

Chromatin-immunoprecipitation assays. Chromatin immunoprecipitation was conducted as the instruction of EZ ChIP kit (Millipore) with modifications. Briefly, 1 x 10^7 cells were treated with 10 ng/ml LPS for 2 h and then fixed by formaldehyde at room temperature for 10 min. Cells were then collected and lysed in SDS lysis buffer. Equal amount of cell lysates were used for chromatin immunoprecipitation by anti-p65 (Abcam), anti-acetylated-histone H4 (Millipore) and control IgG (Santa Cruz). DNA was purified by DNA purification column as manufacturer's instruction (Qiagen). Relative occupancy was determined by quantitative PCR for sample from specific antibody versus control IgG.

Lentivirus production, concentration and transduction. Production and concentration of lentivirus were performed as described previously [163]. Briefly, 293T cells were transfected with expression vectors (hCD68 promoter-driven expression of wild type or mutant forms of RIP140) and packing system (System Biosciences). Lentivirus-containing media were collected at 48 and 96 h after transfection. Virus was concentrated by lenti-X concentrator (Clontech). For transduction, $1x10^6$ peritoneal macrophages in 1 ml medium with polybrene (10 μg/ml) were incubated with lentivirus (MOI:50). Cells

were spun down at 1,000 X g for 1 h at 25^{o}C and then plated in culture plates. After 16 h, the medium was changed to normal culture medium.

ET, acute septic shock animal model and macrophage reconstitution. For ET animal model, 6~8-week-old male C56BL/6J mice were injected peritoneally with 0.1 μg LPS/25 g body weight. After 16 h, mice were injected with LPS (100 μg/ 25 g body weight) and D-galactosamine (0.5 mg/ g body weight) to induce acute septic shock. Survival was monitored every hour for the next eight hour. For macrophage reconstitution, 8~10-week-old male C56BL/6J mice were injected peritoneally with 200 μl clondronate-containing liposome (Encapsula Nano Sciences) to deplete their macrophages. After 2 day, 5 x 10^6 primary macrophages were injected peritoneally. 6 h later, mice were injected with LPS (500 μg/ 25 g body weight) and serum were collected 1 h after LPS injection. Reconstituted peritoneal macrophages were collected from 8~10-week-old male C56BL/6J mice and then transduced by lentivirus to over-express wild type RIP140 or tyrosine mutant RIP140 (Y3F). Transduction was performed twice in 5 day culture. On day 5 of culture, primary macrophages were treated with or without LPS (100 ng/ml). After 24 h, cells were collected and injected peritoneally into macrophage-depleted mice.

Statistical analysis. Results are presented in means ± SD. Statistical analysis was examined by Student's *t* test and *P* value < 0.05 is statistically significant.

Results

TLR ligands decreases RIP140 protein levels in macrophages. To determine whether RIP140 expression can be modulated by LPS exposure in the establishment of ET, we pre-injected mice with saline (control vehicle) or a low dose of LPS, challenged animals with a lethal dose of LPS and D-galatosamine 16 h later, and then monitored the animals' survival (Supplementary Fig. 1). As predicted, exposure to a low dose of LPS prior to the lethal dose of LPS substantially increased the survival [48](Fig. 1a). We monitored the intensity of RIP140 in F4/80^{+}-peritoneal macrophages, and found RIP140 protein in LPS-

tolerated mice decreased ~ 40% as compared to the saline group (Fig. 1b). We reasoned that since RIP140 modulates proinflammatory cytokine production by acting as an NF-κB co-activator [10, 11], down-regulation of RIP140 level in macrophages may dampen inflammatory responses and improve the survival in acute sepsis. To test this theory we made a transgenic mouse model with macrophage-specific silencing of RIP140, because RIP140 whole body knockout mice exhibited altered lipid and glucose metabolism which made the use of this mouse line in a septic shock model intractable. The human CD68 promoter was used for macrophage-specific expression of RIP140-specific siRNA[168] (Supplementary Fig. 2a). Macrophages from these transgenic knock-down mice (KD) expressed lower mRNA levels of RIP140 (by ~20%) (Supplementary Fig. 2b). As predicted, RIP140 KD mice had a higher survival (Fig. 1c) and lower circulating TNF and IL-1β as compared to the wild type (WT) mice (Fig. 1d). These results show that down-regulation of RIP140 in macrophages can be protective against septic shock.

Macrophage polarization, including classical (M1) and alternative (M2) activation plays a critical role in various diseases [40, 44]. Since LPS is a stimulus for M1 activation, we asked whether RIP140 was differentially affected in M1 versus M2 activation in macrophages. In agreement with the *in vivo* data, M1 stimulus (IFNγ+LPS), but not M2 stimulus (IL4), reduced RIP140 protein in both primary (Fig. 1e) and Raw264.7 (RAW) macrophages (Supplementary Fig. 3) without significantly affecting RIP140 mRNA levels. Furthermore, LPS exposure decreased RIP140 protein levels in a dose- and time-dependent manner (Supplementary Fig. 4). To differentiate various TLRs and adaptors' signaling pathways, we examined the effects of Pam3CSK4 (TLR2 ligand) and poly (I:C) (TLR3 ligand) on RIP140 protein. Stimuli for TLR2, TLR3 or TLR4 could all reduce RIP140 (Fig. 1f). Altogether, these results reveal that RIP140 protein is down-regulated in macrophages after exposure to ligands for TLR2, TLR3 or TLR4, and suggest that reduction of RIP140 may provide a regulatory mechanism to reduce inflammatory response and the establishment of ET.

LPS triggers RIP140 degradation by SOCS1-Rbx1 E3 ligase complex. To determine whether protein degradation contributes to LPS-triggered reduction in RIP140 protein

levels, we treated RAW cells with LPS in the absence or presence of proteasome inhibitor, MG132. MG132 effectively increased ubiquitination on RIP140 under LPS treatment (Fig. 2a), suggesting that proteasome-mediated degradation of ubiquitinated RIP140 contributes to LPS-triggered reduction in RIP140 protein in tolerated macrophages. LPS also promoted RIP140 degradation when examined using a pulse-chase experiment (Supplementary Fig. 5). In a bacterial two-hybrid screening, we identified ring-box protein 1 (Rbx1) as an RIP140-interacting protein (data not shown). Because Rbx1 is a component of SCF (Skp, culin, F-box-containing) E3 ligase complex that transfers the polyubiquitin chain to lysine residues of target proteins [165], we then examined whether Rbx1 contributes to LPS-triggered ubiquitination of RIP140. Indeed knocking down Rbx1 blocked LPS-induced degradation of RIP140 in both primary macrophages (Fig. 2b) and RAW cells (Supplementary Fig. 6a). SOCS1, another component of SCF E3 ligase, can associate with Rbx1 and is responsible for target recognition, and SOCS1 also negatively regulates inflammation and contributes to the establishment of ET [169-171]. We therefore examined whether SOCS1 was involved in LPS-triggered degradation of RIP140. As expected LPS induced the expression of SOCS1 protein; and silencing SOCS1 also reduced LPS-triggered RIP140 degradation in primary macrophages (Fig. 2c) and RAW cells (Supplementary Fig. 6b). To determine if RIP140 could be a direct target of SOCS1-Rbx1 E3 ligase, we performed *in vivo* ubiquitination assay in 293T cells by ectopically co-expressing Flag-tagged RIP140 and hemagglutinin (HA)-tagged Rbx1 or SOCS1, in the presence of the wild type, or its mutant form, of ubiquitin. Indeed, both SOCS1 and Rbx1 promoted RIP140 ubiquitination in the presence of the wild type ubiquitin, but not the lysine-to-arginine (K48) mutated ubiquitin (Fig 2d and 2e). These experiments also confirm that RIP140 can associate with Rbx1 and SOCS1. Because SOCS1 recognizes tyrosine-phosphorylated substrates through its SH_2 domain [165, 166, 171], we then determined whether SOCS1's SH_2 domain was required for RIP140 degradation by using an SH_2-mutated SOCS1 (SOCS1-ΔSH) that failed to recognize its specific targets. Unlike the wild type SOCS1 that effectively stimulated RIP140 ubiquitination, SOCS1-ΔSH failed

to do so (Fig. 2f). These results demonstrate that LPS triggers RIP140 degradation by promoting SOCS1-Rbx1 E3 ligase-mediated ubiquitination of RIP140.

RelA is an adaptor for SOCS1 to associate with RIP140. Although we demonstrated that SOCS1-Rbx1 can associate with RIP140 *in vivo*, we failed to detect direct interaction of RIP140 with SOCS1 *in vitro* (data not shown). Since RelA has been shown as a target for nuclear SOCS1-Rbx1 E3 ligase and RIP140 interacts with RelA to coactivate its transcriptional activity [11, 165, 166], we then asked whether RIP140 associates with SOCS1 in a RelA-dependent manner in co-immunoprecipitation assays. We found that, in 293T cells with ectopic expression of Flag-tagged RIP140 with or without HA-tagged SOCS1, RIP140 failed to associate with SOCS1 in RelA-silenced cells (Fig. 3a). Further, RIP140 could no longer be degraded in RelA-silenced primary macrophages (Fig. 3b) or RAW cells (Supplementary Fig. 6c), under LPS stimulation. These results suggest that the association of RIP140 with RelA provides a regulatory step for recruiting SOCS1 to RIP140. Because RelA interacts with the amino-terminus of RIP140 [11], we tested whether over-expressing a Flag-tagged amino-terminus of RIP140 (Flag-RD1) could reduce the association of RIP140 with RelA and LPS-triggered RIP140 degradation. Indeed, over-expressing Flag-RD1 reduced LPS-triggered association of RIP140 with RelA in RAW cells, down-regulated target genes' expression (such as TNF and IL-1β) (Fig. 3c), and dampened LPS-triggered RIP140 degradation (Fig. 3d). Taken together, our results show that RelA acts as an adaptor for SOCS1-Rbx1 E3 ligase to control RIP140's degradation.

In addition to ligands for TLRs, TNF can also activate signaling cascade to promote NF-κB mediated proinflammatory cytokine production [155, 161], but it promotes ET through distinct mechanisms from that of LPS-induced ET [161]. TNF failed to enhance RIP140-RelA complex formation above the basal level (Fig. 3e); and more importantly, after 24 h treatment, TNF still failed to decrease RIP140 protein levels in both primary macrophages (Fig. 3f) and RAW cells (Supplementary Fig. 7). These results further support our hypothesis that LPS-stimulated interaction of RIP140 with RelA results in the

recruitment of SOCS1-Rbx1 E3 ligase in a TLR-specific manner, which is required for RIP140's degradation.

RIP140 degradation requires phosphorylation on RIP140. Tyrosine phosphorylation has a critical role in regulating proteasome-mediated protein degradation via various mechanisms [158, 164]. Analysis of LPS-induced tyrosine phosphorylation on RIP140 revealed that RIP140 was phosphorylated within 1 h after LPS challenge, immediately before RIP140 degradation could be detected (Fig. 4a and Supplementary Fig. 4b). Syk, a non-receptor tyrosine kinase, showed a similar activation kinetic after LPS challenge (Fig. 4b). Syk also plays an important role in resolving inflammation, and Syk-null mice are susceptible to LPS-induced sepsis [172, 173]. We found that treating LPS-exposed RAW cells with the Syk inhibitor helped to sustain their RIP140 protein levels (Fig. 4c), and knocking down Syk prevented LPS-triggered RIP140 degradation in both primary macrophages and RAW cells (Fig. 4d). Additionally, we found that Syk was accumulated in the nuclei under LPS treatment (Supplementary Fig. 8a). Using a proximal ligation assay, we detected increased interaction of RIP140 with Syk in the nuclei of LPS-challenged RAW macrophages (Supplementary Fig. 8b). These results suggest that Syk may phosphoryate RIP140 to regulate its stability.

An *in vitro* kinase assay showed that Syk phosphorylated RIP140 on its tyrosine residues, and was blocked by the Syk inhibitor (Fig. 4e). Using group-based prediction system (GPS), we identified three highly conserved tyrosine residues on RIP140, which were predicted as Syk target sites (Fig. 5a). Using the same *in vitro* kinase assay, we demonstrated that mutations on all three tyrosine residues (Y3F: Y364F, Y418F and Y436F) effectively blocked Syk-mediated tyrosine phosphorylation on RIP140 (Fig. 5b). RIP140 with mutations on these three tyrosine residues (Y3F) exhibited drastically reduced tyrosine phosphorylation (Fig. 5c and Supplementary Fig. 9) and became resistant to degradation in macrophages following LPS challenge (Fig. 5e). Both wild type and Y3F mutated RIP140's still interacted with Syk in primary macrophages following LPS challenge (Fig. 5d). Although the Y3F mutated RIP140 exhibited a greater stability, it was possible that these mutations abolished the interaction of RIP140 with

RelA, thereby reducing the association of RIP140 with SOCS1-Rbx1 E3 ligase. It appeared that the Y3F mutant could still interact with RelA under the basal condition, and this interaction was also enhanced by LPS treatment (Supplementary Fig. 10). Further, this Y3F mutant remained associated with SOCS1 (Supplementary Fig. 11a). *In vitro* phosphorylated wild type Flag-RIP140 failed to associate with SOCS1 in a direct protein interaction assay (Supplementary Fig. 11b). These data support our conclusion that RelA acts as an adaptor to facilitate the association of RIP140 with SOCS1, and validate that Syk-mediated phosphorylation at three conserved tyrosine residues of RIP140 is critical for the conjugation of polyubiquitin chain on RIP140. But this is not required for SOCS1 to recognize RIP140 or the interaction of RIP140 with RelA.

Attenuation of ET by preventing RIP140's degradation. Exposure to LPS induced RIP140 degradation and reduced production of inflammatory cytokines in macrophages, suggesting that RIP140 degradation may resolve inflammation and promote the establishment of ET. IFN-γ activates macrophages to amplify the inflammatory response, and one of its important functions is to reduce ET and restore pro-inflammatory cytokine production [160, 174]. Pre-treatment of macrophage with IFN-γ has been shown to overcome LPS-induced ET [160]. Therefore we asked whether pre-treatment with IFN-γ could block RIP140 degradation, and if RIP140 was required for IFN-γ-restored inflammatory cytokine production, especially TNF and IL-1β, in tolerated macrophages. Indeed, pre-treatment with IFN-γ effectively suppressed LPS-triggered RIP140 degradation in primary (Fig. 6a) and RAW (Supplementary Fig. 12) macrophages, and IFNγ failed to restore TNF and IL-1β production when RIP140 was silenced (Supplementary Fig. 13). We also confirmed the requirement for RIP140 in IFN-γ's effect to prevent ET, in experiments using primary peritoneal macrophages from wild type or macrophage-specific RIP140-silenced (KD) mice (Supplementary Fig. 14). IFN-γ effectively prevented ET in macrophages from the WT but not RIP140-silenced mice (Fig. 6b). To further investigate the role of RIP140 degradation in the establishment of ET, we introduced a control (Ctrl), wild type RIP140 (WT) or Y3F mutated RIP140 (Y3F) into RAW cells, induced their tolerance with LPS and then monitored production of

proinflammatory cytokines under the second LPS stimulation. The Y3F mutant, but not the control or wild type RIP140, were resistant to tolerance induction with LPS, based on criteria like mRNA expression and protein production of TNF after the second LPS challenge (Fig. 6c). The effect on IL-1β mRNA expression was in agreement with this notion (Supplementary Fig. 15). Since altered signaling cascades in LPS-stimulated IKK and MAPK activations are also important characteristics of ET, we thus investigated whether the Y3F mutant prevented ET by augmenting these signaling pathways. This proved to be not the case because we did not observe any significant changes in these signaling cascades in RAW cells transfected with the wild type (WT) or Y3F mutant of RIP140, as compared to the control vector (Supplementary Fig. 16). These results show that expressing the non-degradable RIP140 (Y3F) attenuates ET, which occurs in a MAPK and IKK signaling-independent manner.

To further validate the effect of expressing the non-degradable RIP140 (Y3F) on ET *in vivo*, we introduced the wild type (WT) or Y3F mutant (Y3F) RIP140 into primary macrophages by lentiviral infection, and challenged them with LPS for 24 h. These macrophages were collected and injected into macrophage-depleted mice to achieve macrophage reconstitution (Supplementary Fig. 17). After macrophage reconstitution, mice were then challenged with LPS for 1 h and serum TNFα levels were determined by ELISA assays. As expected, mice reconstituted with WT RIP140 macrophages failed to promote TNF production. However, mice reconstituted with Y3F mutant RIP140 macrophages still produced a higher amounts of serum TNFα in response to the second LPS challenge (Fig. 6d). Overall, our results demonstrate that RIP140 degradation is essential for the establishment of ET, at least based upon the criteria of TNF and IL-1β production. Moreover, prevention of RIP140 degradation, such as by pre-treatment with IFN-γ, can attenuate ET.

Non-degradable RIP140 reduces tolerance of specific genes. Genes expression from either LPS-tolerated or non-tolerated macrophages demonstrates TLR-induced histone modifications and chromatin remodeling in a gene-specific manner [45, 159]. Microarray analysis has shown that most differentially expressed genes in RIP140-null macrophages

were proinflammatory genes [11]. We therefore compared the genes differentially expressed in RIP140-null macrophages to the tolerated and non-tolerated genes categorized in previous publications [11, 159], and found that nine of the tolerated genes but only one of the non-tolerated gene were RIP140 target genes (Supplementary Fig. 18). We examined whether over-expression of the non-degradable RIP140 (Y3F) in macrophages prevented ET for RIP140's target genes. Ectopic expression of the Y3F mutant, but not the control vector or wild type RIP140, reduced tolerization of RIP140's target genes (including *Ptgs2*, *Traf1*, *Socs3* and *Il6,* in addition to *Tnfα* and *Il1b*). However, the Y3F mutated RIP140 failed to reduce tolerization of genes that are not the targets of RIP140, such as *Ccl22*, *cd40* and *Nos2* in both primary macrophages (Fig. 7a) and RAW cells (Supplementary Fig. 19). These results clearly show that RIP140 degradation contributes to the establishment of ET in a gene-specific manner.

Most tolerated genes, such as TNF and IL-1β, are characterized by their non-permissive histone modifications and lower NF-κB binding on their promoters under LPS challenge[45, 159-162, 175]. However, the underlying mechanism for these changes was unclear. Thus, we asked whether degradation of RIP140 is involved in changing these specific chromatin targets, by expressing the control vector, wild type RIP140 or Y3F mutant in RAW cells and inducing tolerance with LPS challenge. After stimulation with the second dose of LPS in macrophages, RelA and RIP140 binding on TNF, IL-1β, Ccl5 and Nos2 promoters were monitored by chromatin immunoprecipitation (ChIP). In response to LPS treatment, RIP140 binding on its targets (TNF and IL-1β) was enhanced, which did not happen on the non-RIP140 targets (Ccl5 and Nos2). RelA binding on promoters of TNF and IL-1β was also increased in the Y3F-transfected macrophages but not the other groups (Fig. 7b). We also monitored active histone modification, including acetylated histone H4 (AcH4), acetylated histone H3 (AcH3) and phosphor-S10 histone H3 (p-S10 H3) on RelA binding regions of TNF and IL-1β promoters. In addition to phosphor-S10 on histone H3, H3 and H4 acetylation was also increased in the Y3F-transfected macrophages, but not in the other groups in the tolerated state (Fig. 7c). Taken together, these results support the view that LPS-stimulated degradation of RIP140

contributes to the loss of RelA binding and active histone modifications on the promoters of pro inflammatory cytokine genes in tolerated macrophages.

Discussion

RIP140 promotes proinflammatory cytokine production by serving as a co-activator for NF-κB in macrophages exposed to TLR ligands. In this study, we show that exposure to TLR ligands triggers RIP140 degradation, leading to resolution of the inflammatory response and contributing to ET in a gene-specific manner. Syk-mediated tyrosine phosphorylation and RelA-dependent SOCS1-Rbx1 E3 ligase recruitment are two prerequisites for LPS-triggered RIP140 degradation (Supplementary Fig. 20). To our knowledge, this unexpected finding is the first example of negative regulation of a TLR-mediated inflammatory response through targeting a specific NF-κB co-activator. This study also reveals that NF-kB, specifically the RelA subunit, can modulate its own transcriptional activity by recruiting the SCF (Skp, culin, F-box-containing) E3 ligase complex to target its associated co-activator.

Most studies of negative regulation of inflammation focus on TLR-mediated signal transduction and suggest that these regulations are involved in the establishment of ET [43, 45, 46]. However, alterations on chromatin, including histone modifications and chromatin remodeling, have been shown to be able to render complete and gene-specific tolerance with a reduced signaling cascade [39, 45, 175]. Although several potential negative regulatory mechanisms in the nucleus have been proposed, the link between these mechanisms and the specific changes on chromatin targets under ET induction was unclear. Among these nuclear regulatory events, it has been shown that the SOCS1-Rbx1 E3 ligase, an SCF E3 ligase, can degrade RelA to terminate NF-κB's transcriptional activity [165, 166, 176] and SOCS1 recognizes its substrate via its SH2 domain which interacts with phospho-tyrosine residues on substrate protein [171]. We found Syk phosphorylates RIP140 on three tyrosine residues but failed to detect direct interaction of RIP140 with SOCS1, even for the RIP140 that had been phosphorylated by Syk. We did

confirm that SH2 domain of SOCS1 to be essential for ubiquitination of RIP140. Since RelA association with SOCS1-Rbx1 E3 ligase requires the SOCS1 SH2 domain [165, 176], and RelA directly interacts with RIP140, we conclude that RelA acts as an adaptor for SOCS1-Rbx1 E3 ligase to recruit RIP140 into the E3 complex. Consistent with this notion, SOCS1 knockout mice have a higher inflammatory response and reduced survival under septic shock, and SOCS1-deficient macrophages exhibit less ET [169, 170], which also supports our findings that SOCS1-mediated degradation of RIP140 resolves inflammation and promotes the establishment of ET. This study also reveals a previously unrecognized mechanism exerted by RelA itself to down-regulate its co-activator. This is the first case of regulation of a co-activator's stability by an SCF E3 ligase via interaction with RelA.

Syk-null mice also have reduced survival and more severe inflammatory responses under LPS challenge, which suggests that Syk is involved in resolution of inflammation [172]. A recent study reported that CD11b reduced TLR-triggered inflammatory response via Syk-mediated phosphorylation of MyD88 and TRIF [173]. Our results presented here further support the role of Syk in negative regulation of inflammatory response in macrophages. Syk interacts with RIP140 in the nuclei and then phosphorylates RIP140 on three conserved tyrosine residues. The Y3F mutant RIP140 resists LPS-stimulated protein degradation, which may be due to inefficient ubiquitination on RIP140, because phosphorylation of these three tyrosine residues appears to be independent of RelA binding to RIP140 and the association of RIP140 with SOCS1. To this end, recent reports have shown that tyrosine phosphorylation of a target protein can promote ubiquitination without affecting E3 ligase binding [177, 178]. On the basis of results presented here, we propose that phosphorylation of the three tyrosine residues may change RIP140's conformation and lead to exposure of specific lysine residues to E3 ligase. It remains to be determined which lysine residues on RIP140 are directly involved in ubiquitin conjugation and subsequent degradation.

This study demonstrates that RIP140 degradation contributes to ET in a gene-specific manner, which suggests that NF-κB interacts with RIP140 to activate only specific genes.

Syk-mediated phosphorylation of RIP140 was ruled out as a regulator of the interaction of RIP140 with RelA. Because RelA possesses various post-translational modifications, depending on the stimuli [179], we postulate that specific modifications of RelA may regulate its interaction with RIP140, and may further determine its specific target genes. Therefore, it would be of interest to investigate the regulation of RelA-RIP140 interaction in the future. RIP140 acts, mainly, as a co-repressor for most transcription factors and nuclear receptors by recruiting HDAC and CtBP [7, 180], but it functions as a co-activator for NF-κB by recruiting CBP [11]. It is possible that RIP140 may be modified by RelA-associated kinases or other enzyme machineries after interaction with RelA, which then leads to preferential recruitment of CBP. Recent studies have suggested that acetylation of histone H3 and H4 is important for NF-κB binding on chromatin [179]. It would be important to investigate if the non-degradable RIP140 can facilitate RelA binding in the tolerated state by enhancing the acetyaltion status of histones around the RelA-binding region and how RIP140 may modulate chromatin configuration on these proinflammatory cytokine genes. Future analyses are needed to further elucidate the differences in these RIP140 protein complexes; these differences may be part of a novel mechanism for modulating RIP140's biological activities.

It is generally believed that in metabolic tissues, RIP140 antagonizes the action of PGC-1 [66]. A previous study showed that a high-fat diet (HFD) increases RIP140 expression in macrophages, which enhances their proinflammatory potential [10]. PGC-1β can promote M2 activation of macrophages [168] and RIP140 is important for proinflammatory cytokine production characteristic of M1 activation. It is very interesting that in this current study we find that degradation of RIP140 is essential to the establishment of ET, and that failure to degrade RIP140 attenuates ET induction *in vitro* and *in vivo*. It would be important to evaluate whether the stability of RIP140, or its protein level, is related to individuals' sensitivity to septic shock in clinical conditions.

Figure

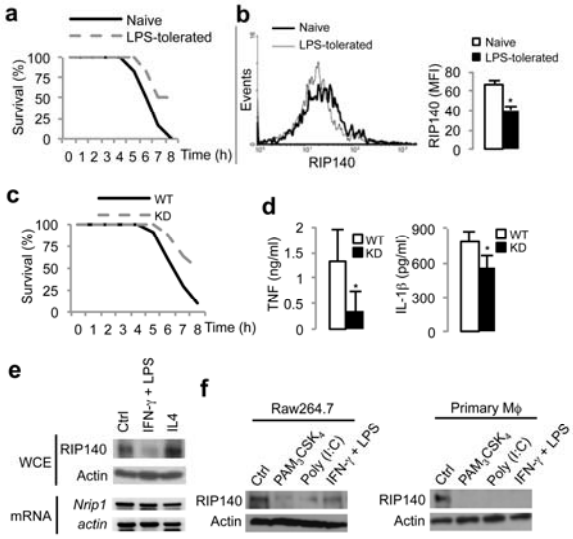

Figure 7-1. Exposure to TLR ligands reduces RIP140 levels in macrophage *in vitro* and *in vivo*. (a) Survival of mice, monitored every hour after challenging with a lethal dose of LPS with D-galactosamine. (n=10 per group). Exposure to a low dose of LPS prior to the lethal dose of LPS substantially increased the survival. (b) Left: histogram of RIP140 expression in F4/80 positive population from isolated peritoneal macrophages. Right: Mean fluorescence intensity of RIP140. Results are presented in mean ± SD., n=3; *: $P < 0.05$. (c) Survival of wild type mice (Wt) and macrophage-specific RIP140 knockdown mice (KD), monitored every hour after challenging with a lethal dose of LPS with D-galactosamine. (n=8 per group). (d) Serum TNFα and IL-1β from WT and KD mice after stimulation of LPS for 2 h. Results are presented in mean ± SD., n=4; *: $P < 0.05$ as compared to wild type group. (e) Immunoblot and semi-quantitative PCR analyses of RIP140 protein and mRNA levels in primary peritoneal macrophages after stimulating with the vehicle (Ctrl), M1 stimulus (LPS plus IFN-γ) or M2 stimulus (IL-4) for 24 h. (f) Expression of RIP140 in Raw264.7 and primary peritoneal macrophages after treatments - vehicle (Ctrl), Pam_3CSK_4, poly (I:C) or LPS with IFN-γ, for 24 h.

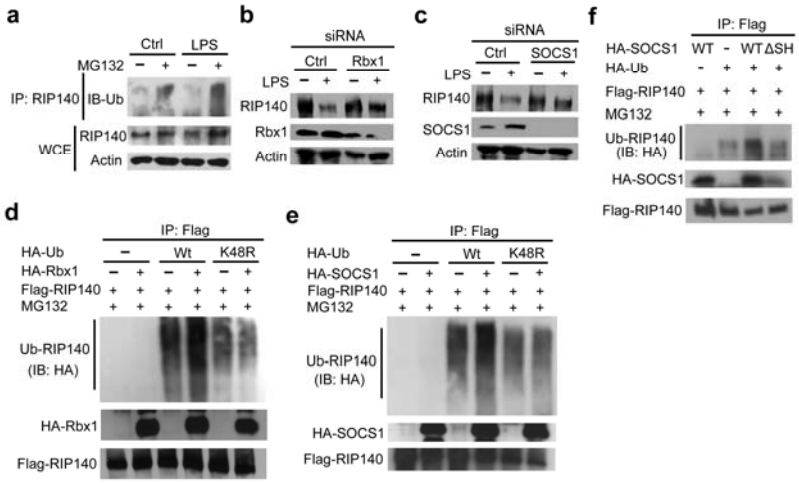

Figure 7-2. LPS promotes RIP140 degradation through SOCS1-Rbx1 E3 ligase-mediated K48 polyubiquitination. (a) Immunoblot analysis of RIP140 and polyubiquitinated RIP140 in Raw264.7 macrophages stimulated for 6 h with indicated treatments. (b) Immunoblot analysis of RIP140, Rbx1 and actin in primary peritoneal macrophages stimulated for 24 h with a control treatment or LPS after transfection with control or Rbx1 siRNAs. (c) Immunoblot analysis of RIP140, SOCS1 and actin in primary peritoneal macrophages stimulated for 24 h with a control treatment or LPS after trasfection with control or SOCS1 siRNAs. (d, e, f) *In vitro* ubiqtuination analysis of RIP140 in 293T cells. 293T cells were transfected with expression plasmids as indicated and treated with 10 μM MG132 for 6 h before lysis. (d) Cell lysates were immunopreciptated with anti-Flag-agarose beads and immunoprecipitates were immunoblotted with anti-Flag to detect Flag-RIP140 or anti-HA to detect polyubiquitinated RIP140 and HA-Rbx1. (e) Cell lysates were immunopreciptated with anti-Flag-agarose beads and immunoprecipitates were immunoblotted with anti-Flag to detect Flag-RIP140 or anti-HA to detect polyubiquitinated RIP140 and HA-SOCS1. (f) 293T cells were transfected with Flag-tagged RIP140 and HA-tagged Ub in conjunction with HA-tagged SOCS1 wild type (Wt) or HA-tagged SOCS1-ΔSH (ΔSH). Cells were treated with 10 μM MG132 for 6 h before lysis. Cell lysates were immunopreciptated with anti-Flag-agarose beads and immunoprecipitates were immunoblotted with anti-Flag to detect Flag-RIP140 or anti-HA to detect polyubiquitinated RIP140 and HA-SOCS1. All immunoblots were performed at least twice.

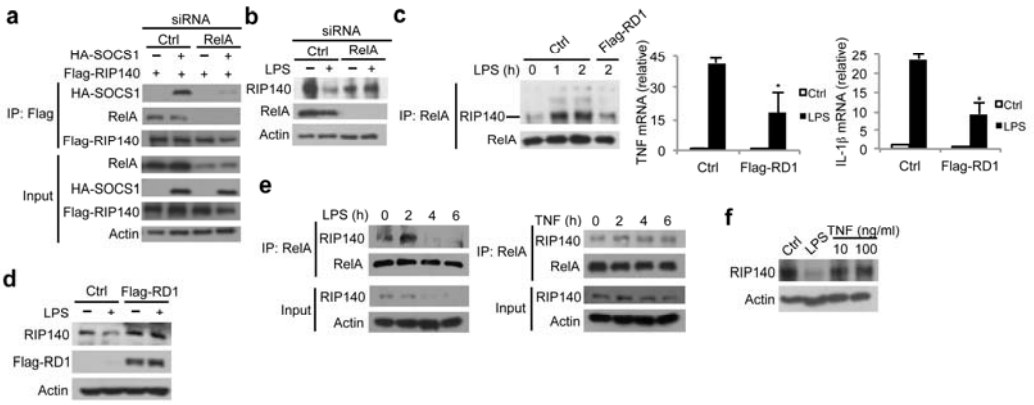

Figure 7-3. RelA acts as adaptor for SCF ubiquitin ligase complex to trigger RIP140 degradation. (a) RelA is required for the interaction of RIP140 with SOCS1-Rbx1 E3 ligase complex, determined by immunoprecipitation and immunoblot analyses. (b) Immunoblot analysis of RIP140, RelA and actin in primary peritoneal macrophages stimulated for 24 h with a control treatment or LPS after trasfection with control or RelA siRNA. (c) Over-expression of Flag-tagged RIP140 amino terminus (RD1) reduced the interaction of RIP140 with RelA. Raw264.7 macrophages were transfected with control plasmid (Ctrl) or Flag-tagged RD1 (RD1) and then stimulated with LPS for various durations. Cell lysates were collected and the interaction of RIP140 with RelA was determined by immunoprecipitation of RelA and then probed with RIP140. Right: the effect of RD1 on the basal and LPS-stimulated expression of TNF and IL-1β was determined by quantitative PCR. Results are presented in mean ± SD., n=3; *: $P < 0.05$ as compared to control treatment. (d) Raw264.7 macrophages were transfected with the indicated plasmid and then stimulated with, or without, LPS for 2 h. The expressions of RIP140 and indicated proteins were determined by immunoblot analysis. (e) Raw264.7 macrophages were treated with 10 μg/ml LPS (left panel) or 10 ng/ml TNF (right panel) for various durations and the interaction of RelA with RIP140 was determined by immunoprecipitation and immunblot. (f) The expression of RIP140 in primary peritoneal macrophages after 24 h treatments as indicated was determined by immunoblot analysis. All immunoblots were performed at least twice.

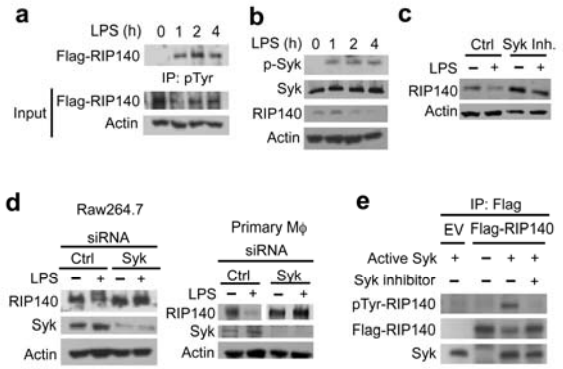

Figure 7-4. Syk activity is required for LPS-induced RIP140 degradation. (a) Raw264.7 macrophages were transfected with Flag-tagged wild type RIP140 and then treated with LPS (10 ng/ml) in the presence of MG132 for indicated duration. Cell lysates were immunoprecipitated with anti-phospho-tyrosine antibody-conjugated agarose. Phospho-RIP140 levels were determined by immunoblot of anti-flag. 10% input of cell lysate was used for immunblot. (b) Raw264.7 macrophages were treated with LPS (10 ng/ml) for indicated duration. Whole cell lysates were collected and indicated proteins were examined by immunoblot. (c) Raw264.7 cells were pre-treated with a control vehicle or Syk inhibitor (Syk In.: Bay 61-3606) for 30 min and then cells were treated with LPS for 24 h. Cell lysates were collected and indicated proteins were determined by immunoblot analysis. (d) Immunoblot analysis of RIP140 expression in Raw264.7 macrophages and primary peritoneal macrophages transfected with control or Syk siRNAs after LPS treatment for 24 h. (e) Syk directly phosphorylates RIP140 in an *in vitro* kinase assay as described in method.

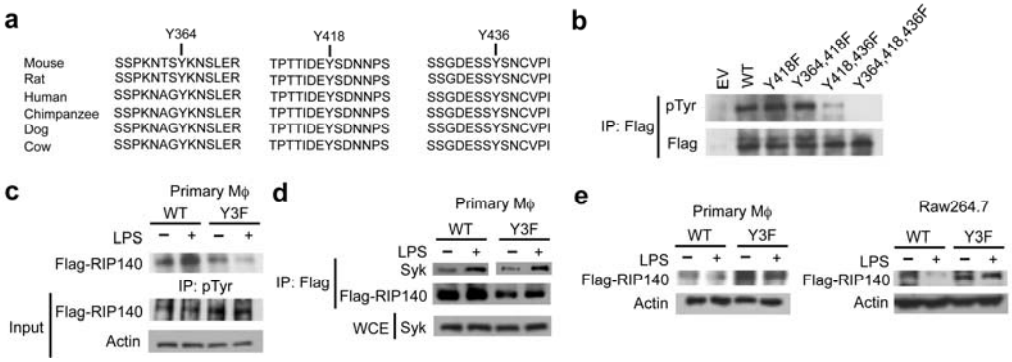

Figure 7-5. LPS-induced RIP140 degradation depends on Syk-mediated tyrosine phosphorylation on RIP140. (a) Schematic diagrams show the conserved amino acid sequences of RIP140 around the Syk target sites. (b) *In vitro* kinase assays of tyrosine phosphorylation on RIP140 with indicated mutations. (c) LPS-triggered tyrosine phosphorylation of WT RIP140 or tyrosine mutant RIP140 (Y3F) *in vivo*. Primary peritoneal macrophages were transfected with Wt RIP140 or tyrosine mutant RIP140 (Y3F) and then treated with or without LPS for 1 h. (d) The interaction of Flag-RIP140 with Syk in primary peritoneal macrophages challenged with LPS for 1 h. (e) Protein stability of WT RIP140 or tyrosine mutant RIP140 (Y3F) was determined by immunoblot analysis. Cells were treated with or without LPS for 24 h. All immunoblots were performed at least twice.

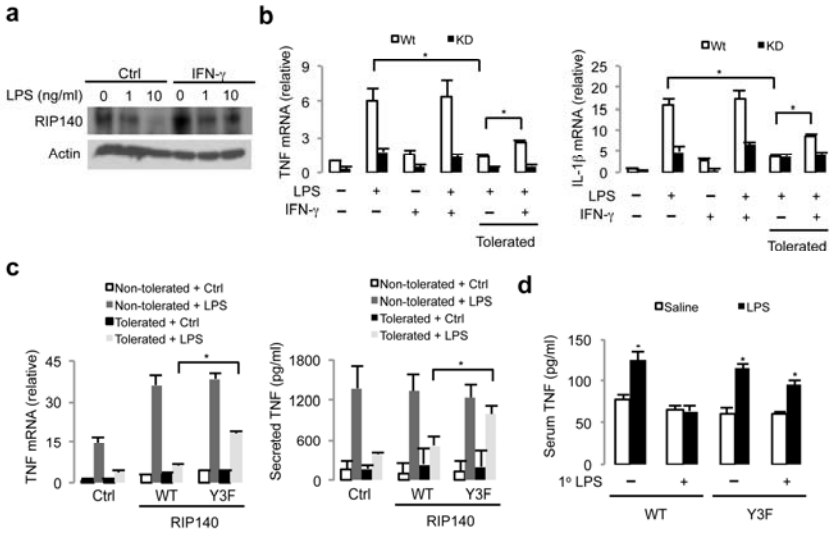

Figure 7-6. Degradation of RIP140 is involved in the establishment of ET. (a) Pre-treatment of IFN-γ in primary peritoneal macrophages prevents LPS-facilitated degradation of RIP140. Cells were pre-treated with or without IFN-γ for 16 h and then challenged with LPS for another 6 h. (b) The mRNA levels of TNF (upper panel) and IL-1β (lower panel) from primary peritoneal macrophages treated according to the experimental design. (c) Raw264.7 macrophages were transfected with the control vector (Ctrl), Flag-tagged WT RIP140 or tyrosine mutant RIP140 (Y3F). Cells were treated with or without LPS for 16 h to become non-tolerated or tolerated states, respective. After 24 h, cells were then challenged with LPS. Upper: mRNA levels of TNF were determined by quantitative PCR. Lower: the levels of secreted TNF from culture supernatants were determined by ELISA. (d) Serum TNF production from macrophage reconstituted mice after stimulation of LPS for 1 h. Results are presented in mean ± SD., n=4; *: $P < 0.05$ as compared to saline group.

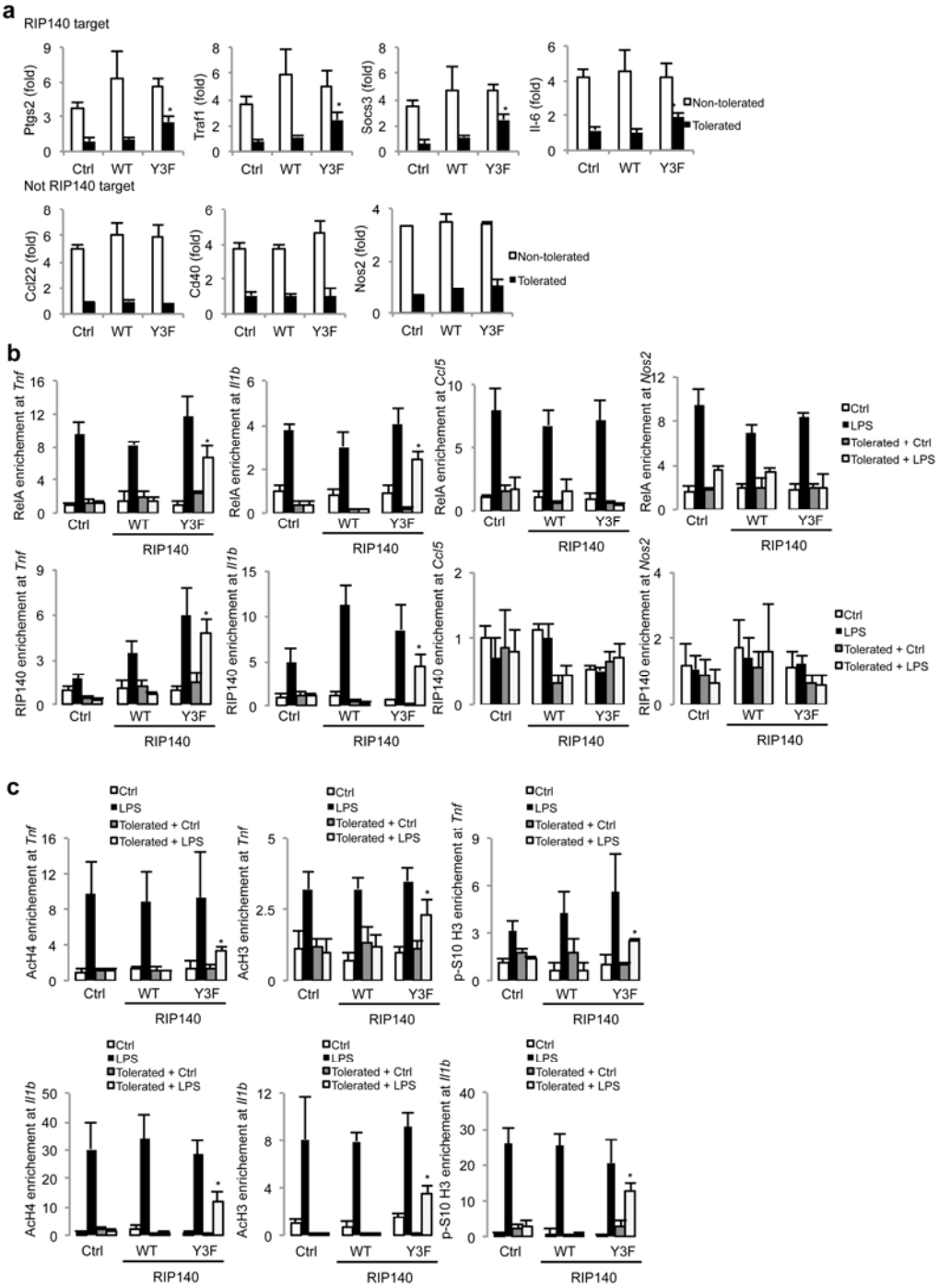
a
RIP140 target
Ptgs2 (fold)
Traf1 (fold)
Socs3 (fold)
Il-6 (fold)
Non-tolerated
Tolerated
Ctrl WT Y3F
Not RIP140 target
Ccl22 (fold)
Cd40 (fold)
Nos2 (fold)
b
RelA enrichement at Tnf
RelA enrichement at Il1b
RelA enrichement at Ccl5
RelA enrichement at Nos2
RIP140 enrichement at Tnf
RIP140 enrichement at Il1b
RIP140 enrichement at Ccl5
RIP140 enrichement at Nos2
Ctrl
LPS
Tolerated + Ctrl
Tolerated + LPS
RIP140
c
AcH4 enrichement at Tnf
AcH3 enrichement at Tnf
p-S10 H3 enrichement at Tnf
AcH4 enrichement at Il1b
AcH3 enrichement at Il1b
p-S10 H3 enrichement at Il1b

Figure 7-7. Prevention of RIP140 degradation retains RelA binding and increases active histone modification on tolerated genes' promoters. (a) Real-time PCR analysis of mRNA of indicated genes in non-tolerated or tolerated primary peritoneal macrophages transfected with the control vector (Ctrl), wild type RIP140 (WT) or non-degradable RIP140 (Y3F). Cells were induced into non-tolerated or tolerated status and then re-challenged with 10 ng/ml LPS for another 2 h or 6 h. Relative folds of mRNA levels after the second stimulation with LPS were determined. Results are presented in mean ± SD., n=3; *: $P < 0.05$ as compared to the non-tolerated+LPS group. (b,c) Raw264.7 macrophages transfected with the control vector (Ctrl), wild type RIP140 (WT) or non-degradable RIP140 (Y3F) were induced into non-tolerated or tolerated status. Cells were then re-challenged with 10 ng/ml LPS for another 2 h. Chromatin IP (ChIP) was performed for indicated antibodies. (b) Relative occupancy of RelA (p65) (upper panel) and RIP140 (lower panel) on *Tnf*, *Il1b*, *Ccl22* and *Nos2* promoters were determined by real-time PCR analyses. (c) Relative occupancy of acetylated histone H4 (AcH4), acetylated histone H3 (AcH3) and phosphor-S10 histone H3 (p-S10 H3) on *Tnf* and *Il1b* promoters were determined by real-time PCR analyses. Results are presented in mean ± SD., n=3; *: $P < 0.05$ as compared to the control treatment of tolerated macrophages.

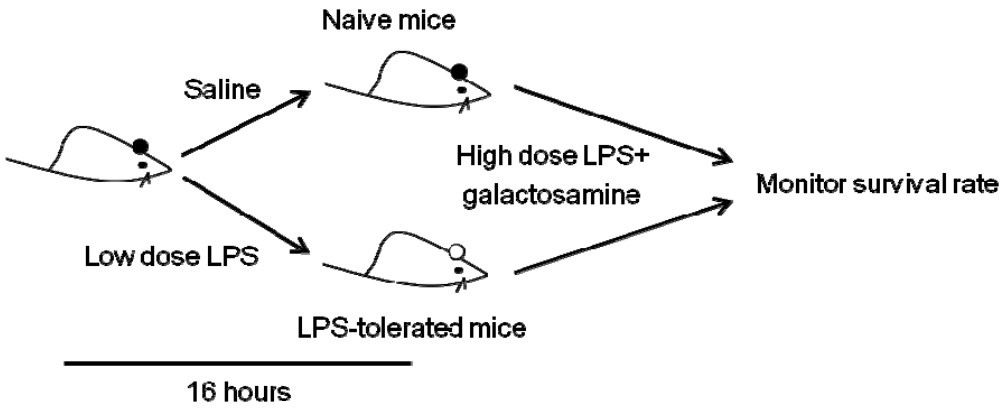

Supplementary Figure 7-1. Endotoxin tolerance *in vivo* model. A schematic diagram for the experimental design: mice were injected peritoneally with saline or LPS (0.1 μg/25 g body weight) for 16 h, followed by a lethal dose of LPS with D-galatosamine.

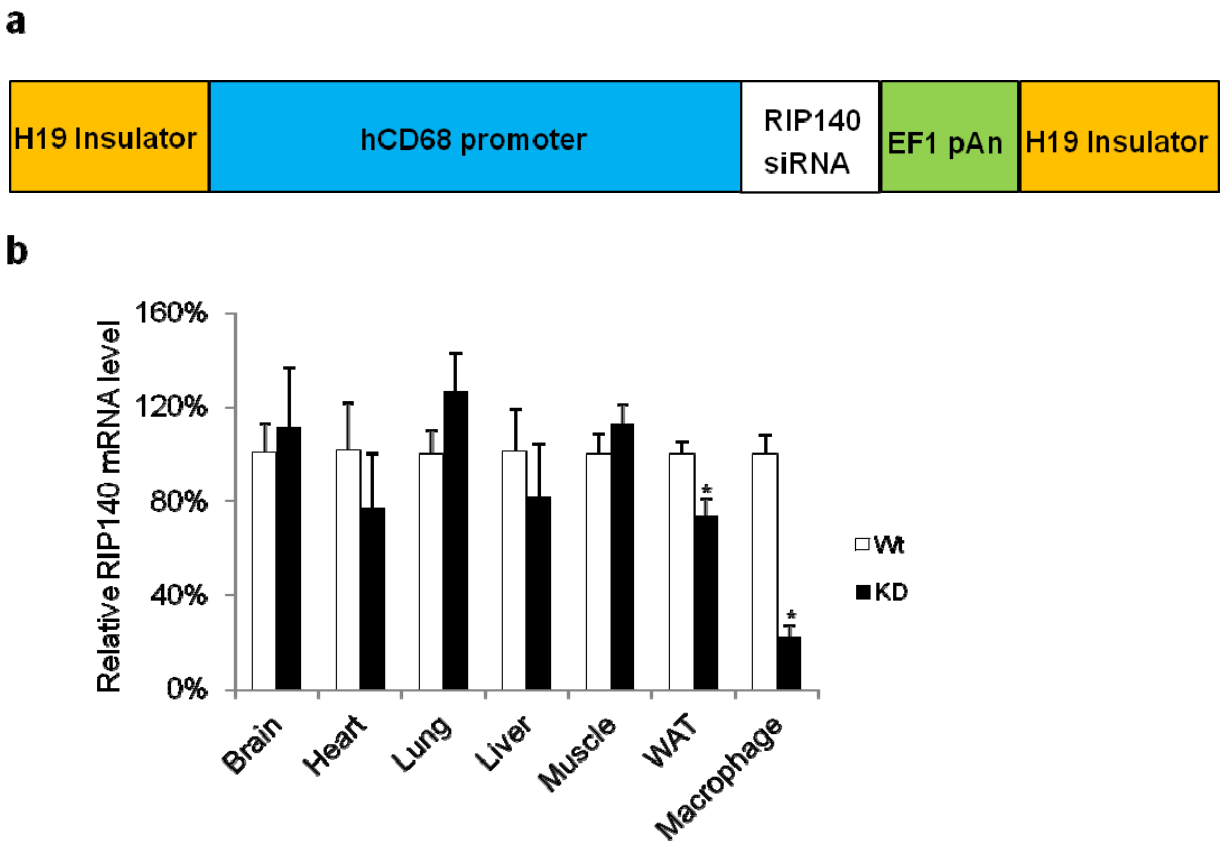

Supplementary Figure 7-2. Macrophage-specific knocking down of RIP140. (a) Illustration of transgenic vector. RIP140 siRNA was mimicked as endogenous miRNA and the expression was driven by human CD68 promoter. (b) The mRNA levels of RIP140 of indicated organs, tissues or primary peritoneal macrophages were measured by quantitative PCR. The expression level of RIP140 of indicated group from wild type mice was calculated as 100%. Result present in mean ± SD., n=3; *: $P < 0.05$.

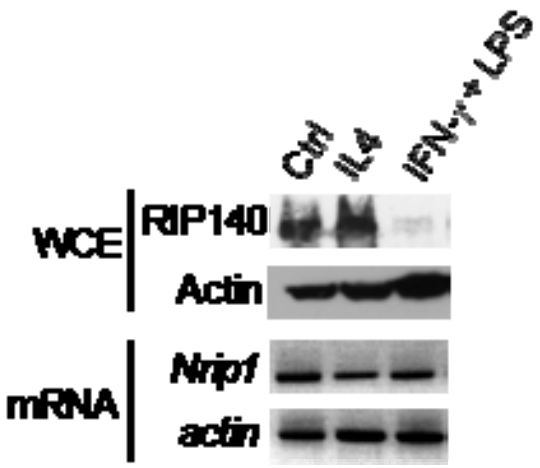

Supplementary Figure 7-3. M1, but not M2, stimulus reduces RIP140 level. Immunoblot and semi-quantitative PCR analyses of RIP140 protein and mRNA levels in Raw264.7 macrophages after stimulating with the vehicle (Ctrl), M1 stimulus (LPS plus IFN-γ) or M2 stimulus (IL-4) for 24 h.

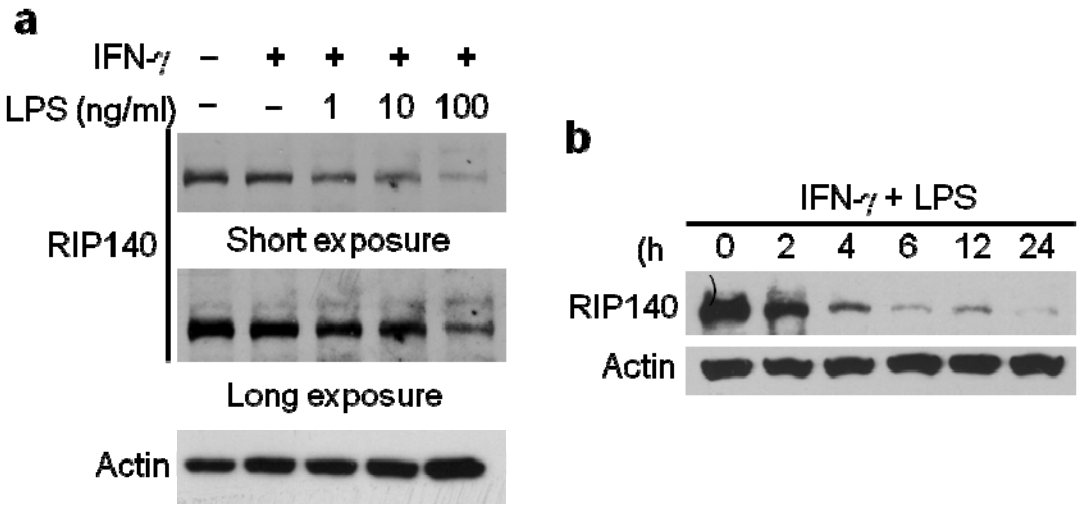

Supplementary Figure 7-4. LPS down-regulates RIP140 expression in a dose- and time-dependent manner. (a) Raw264.7 macrophages were treated with indicated treatments for 24 h. RIP140 and actin levels were analyzed by immunoblot. (b) Raw264.7 macrophages were co-treated with LPS plus IFN=γ for indicated duration. Cells were collected and the expression levels of indicated proteins were examined by immunoblot.

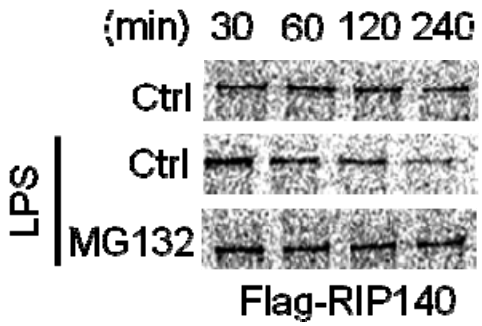

Supplementary Figure 7-5. LPS promotes proteasome-mediated RIP140 degradation in macrophages. Raw264.7 macrophages were transfected with Flag-tagged wild type RIP140. Cells were then cultured in the media containing ^{35}S-labeled methionine and cysteine. After 16 h, cells were washed by normal culture media and then treated control vehicle or LPS in the absence or presence of MG132 (5 μg/ml) for indicated duration. 300 μg cell lysate of each sample was used for immunoprecipitation of anti-Flag. Immunoprecipitates were then subjected into SDS-PAGE and Flag-RIP140 levels were determined.

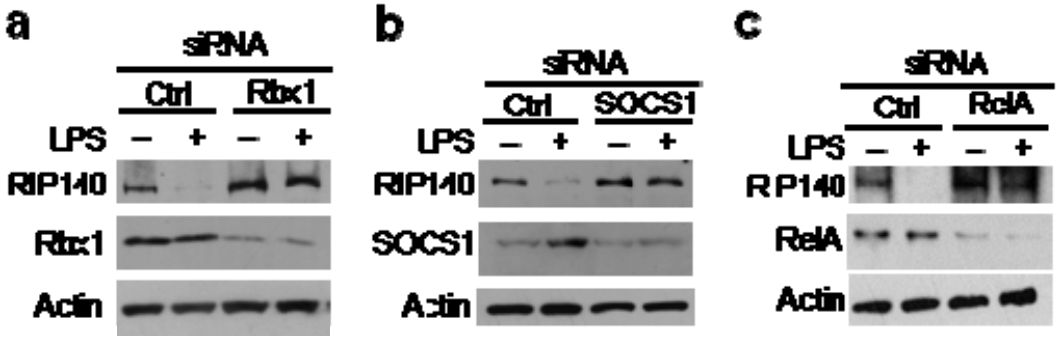

Supplementary Figure 7-6. Targeting SOCS1, Rbx1 or Syk diminished LPS-triggered reduction of RIP140 in Raw264.7 macrophages. Raw264.7 cells were transfected with control siRNA or indicated siRNA for 48 h. Cells were then treated with or without 100 ng/ml LPS for 24 h and whole cell lysates were collected for immunoblots of indicated proteins. Silencing of (a) SOCS1, (b) Rbx1 or (c) Syk blocked LPS-mediated reduction of RIP140.

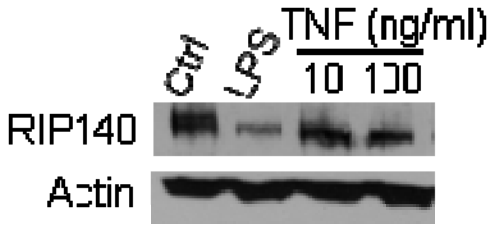

Supplementary Figure 7-7. TNF fail to reduce RIP140 protein level in Raw264.7 macrophages. The expression of RIP140 in Raw264.7 macrophages after 24 h treatments as indicated was determined by immunoblot analyses of RIP140 and actin.

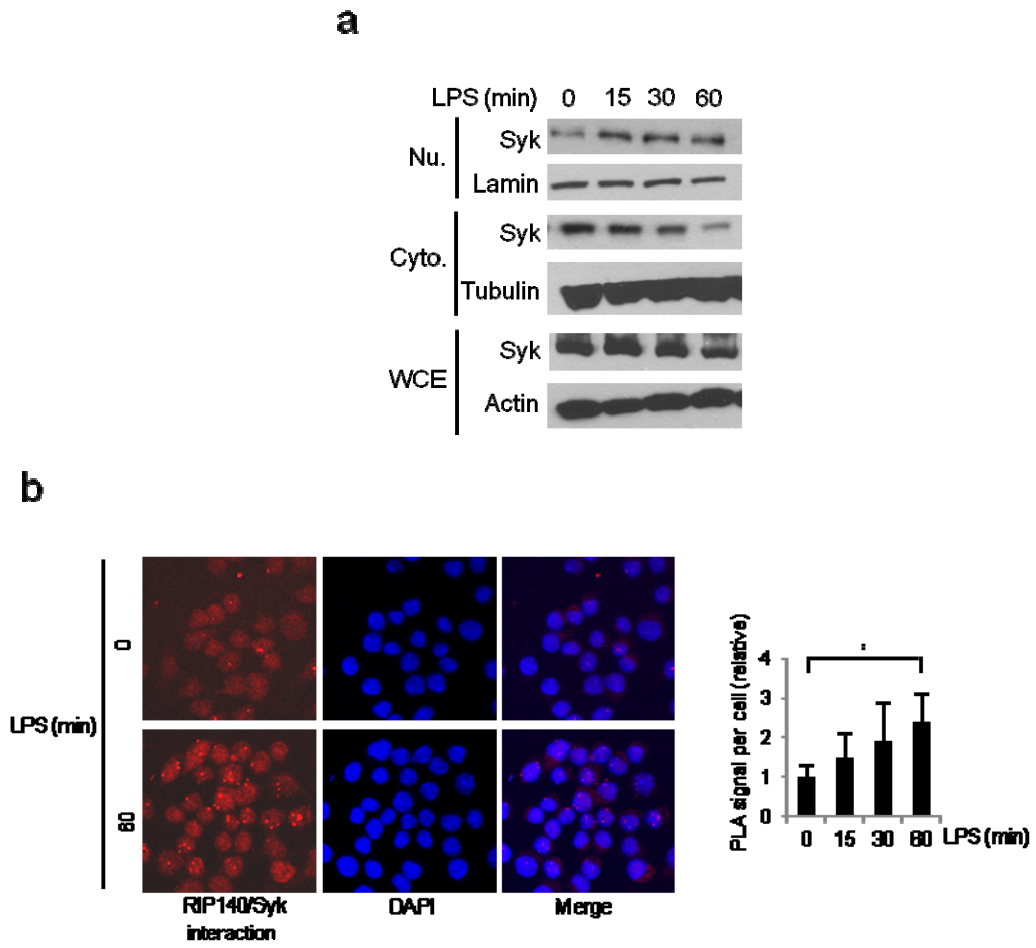

Supplementary Figure 7-8. LPS facilitates nuclear accumulation of Syk and the interaction of RIP140 with Syk in Raw264.7 macrophages. (a) Raw264.7 macrophages were treated with 100 ng/ml LPS for different duration. Whole cell extract (WCE), nuclear (Nu.) and cytoplasmic (Cyto.) fractions were collected and subjected into SDS-PAGEs for immunoblotting of indicated proteins. Actin, lamin and tubulin were used for loading controls. (b) LPS-facilitated interaction of RIP140 with Syk in the nuclei was determined by proximal ligation assay. DAPI shows nuclear staining. Right: a quantitative result for interaction signal intensity. Results are presented in mean ± SD. ; *: $P < 0.05$.

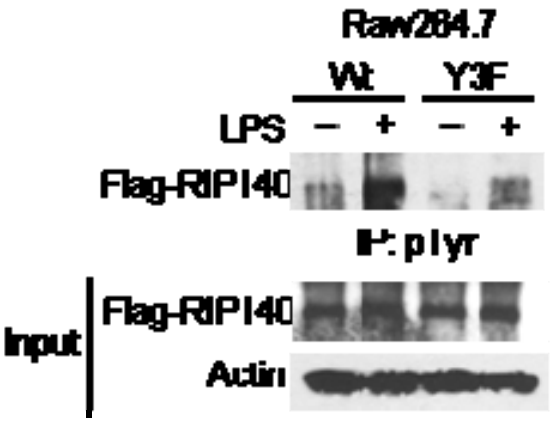

Supplementary Figure 7-9. LPS facilitates tyrosine phosphorylation of RIP140 on Y364,418,436 in Raw264.7 macrophages. Raw264.7 macrophages were transfected with wild type RIP140 (Wt) or tyrosine mutant RIP140 (Y3F) and then treated with or without LPS for 1 h.

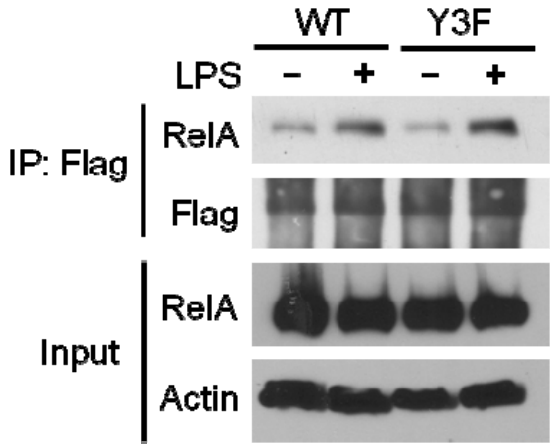

Supplementary Figure 7-10. LPS-stimulated interaction of RIP140 with RelA does not require tyrosine phosphorylation on Y364,418,436 of RIP140. Raw264.7 macrophages were transfected with Flag-tagged wild type RIP140 (Wt) or tyrosine mutant form of RIP140 (Y3F). Cells were then treated with or without LPS for 2 h. Cell lysates were for co-immunoprecipitation of Flag-RIP140. RelA and Flag-RIP140 levels in immunoprecipitates were determined by immunoblot. The levels of RelA and actin in inputs were determined by immunblot.

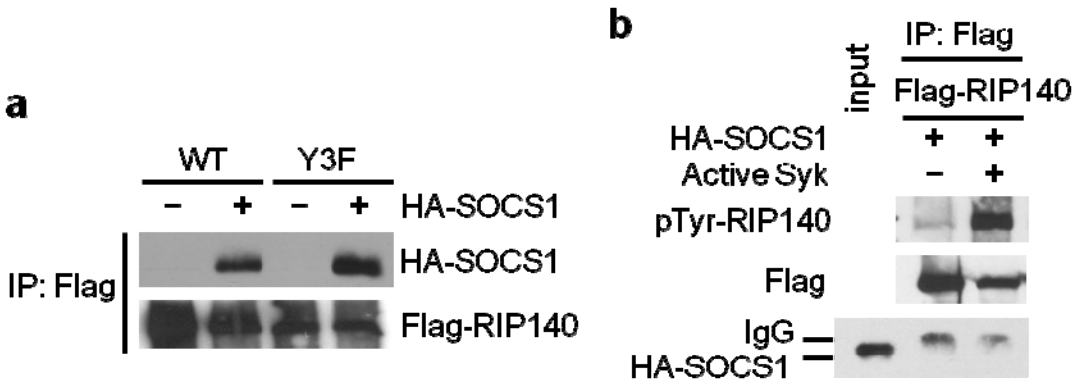

Supplementary Figure 7-11. SOCS1 associates with RIP140 does not require Syk-mediated tyrosine phosphorylations on RIP140. (a) 293T cells were transfected with Flag-tagged wild type (Wt) or tyrosine mutant form (Y3F) of RIP140 with control vector or HA-tagged SOCS1. After lysis, cell lysates were immunopreciptated with anti-Flag-agarose beads and immunoprecipitates were immunoblotted with anti-Flag to detect Flag-RIP140 or anti-HA to detect HA-SOCS1. (b) Cell lysates from 293T cell over-expressed Falg-tagged wild type RIP140 were immunoprecipitated by anti-Flag agarose. Immunoprecipitates were incubated with or without active Syk in kinase reaction buffer for 1 h. After washing, reacted immunoprecipitates were then incubated with in vitro translated HA-SOCS1 for 16 h to examine direct interaction. Afetr washing, the precipitates were subjected into SDS-PAGE and immunblots of anti-phospho-tyrosine, andti-Flag and anti-HA were performed to examine the levels of phosphor-Flag-RIP140, Flag-RIP140 and HA-SOCS1 in these reacted immunoprecipitates.

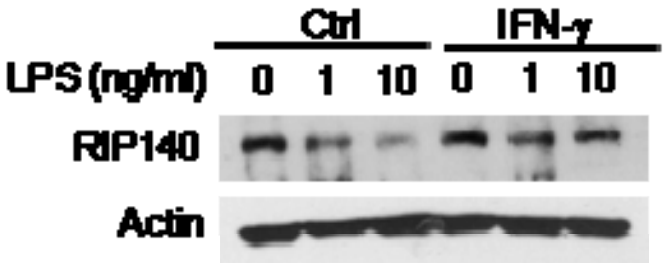

Supplementary Figure 7-12. IFN-γ prevent LPS-induced RIP140 degradation in Raw264.7 macrophages. Pre-treatment of IFN-γ in primary peritoneal macrophages prevents LPS-facilitated degradation of RIP140. Cells were pre-treated with or without IFN-γ for 16 h and then challenged with LPS for another 6 h.

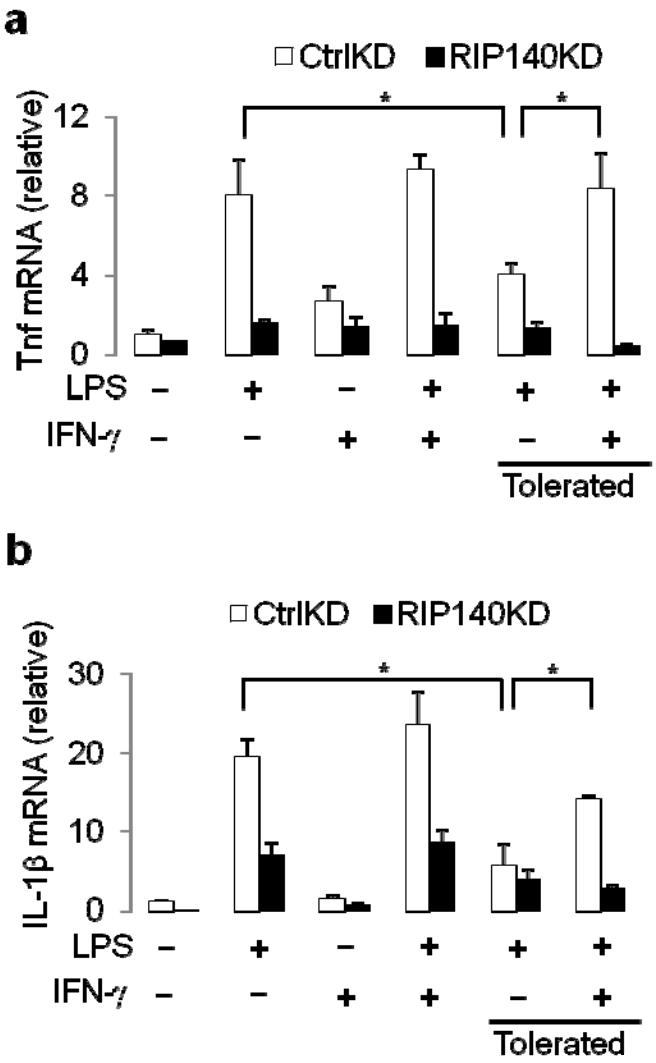

Supplementary Figure 7-13. IFN-γ fails to prevent endotoxin tolerance in RIP140-silencing macrophages. Raw264.7 macrophages were treated with or without IFNγ for 16 h, followed by control treatment or LPS challenge. After 24 h, cells were then re-challenged with LPS for another 2 h. The mRNA levels of (a) TNFα and (b) IL-1β from Raw264.7 macrophages were measured by quantitative PCR. Result present in mean ± SD., n=3; *: $P < 0.05$.

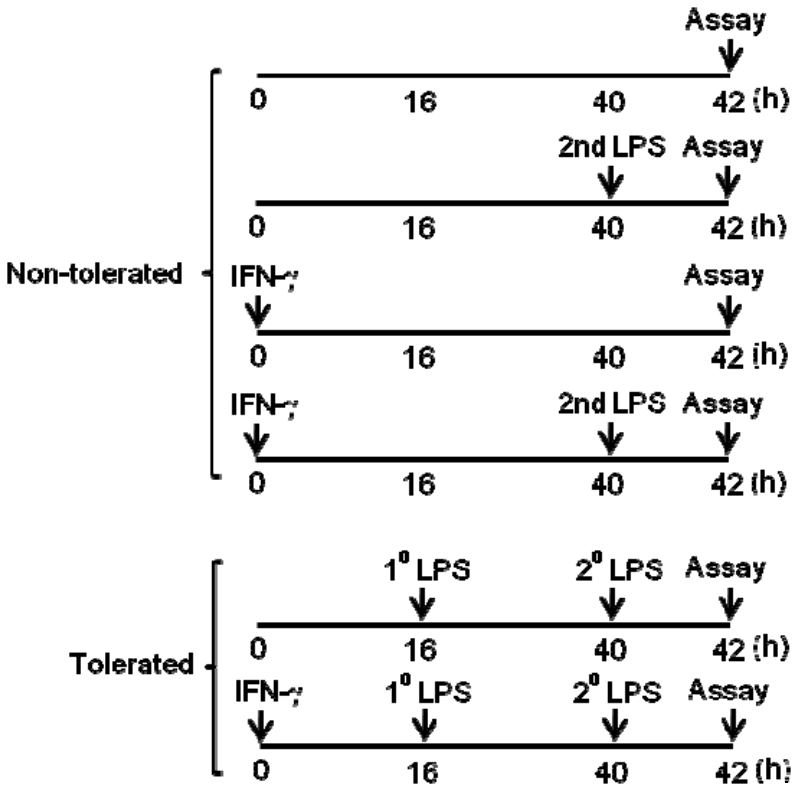

Supplementary Figure 7-14. Experimental design for IFN-γ effect on endotoxin tolerance. A schematic diagram for experimental design: macrophages were treated with or without IFNγ for 16 h, followed by control treatment or LPS challenge. After 24 h, cells were then re-challenged with LPS.

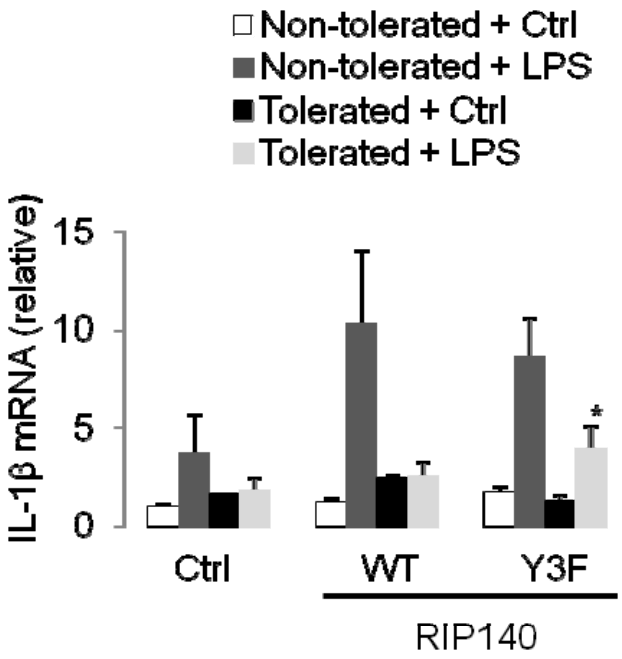

Supplementary Figure 7-15. Degradation of RIP140 involves in the establishment of endotoxin tolerance on IL-1β production. Raw264.7 macrophages were transfected with control vector (Ctrl), Flag-tagged wild type RIP140 (Wt) or tyrosine mutant RIP140 (Y3F). Cells were treated with or without LPS for 16 h to become non-tolerated or tolerated states, respective. After 24 h, cells were then challenged with LPS for another 2 h. mRNA levels of IL-1β were determined by quantitative PCR. Result present in mean ± SD., n=3; *: $P < 0.05$ as compared to control treatment of tolerated group.

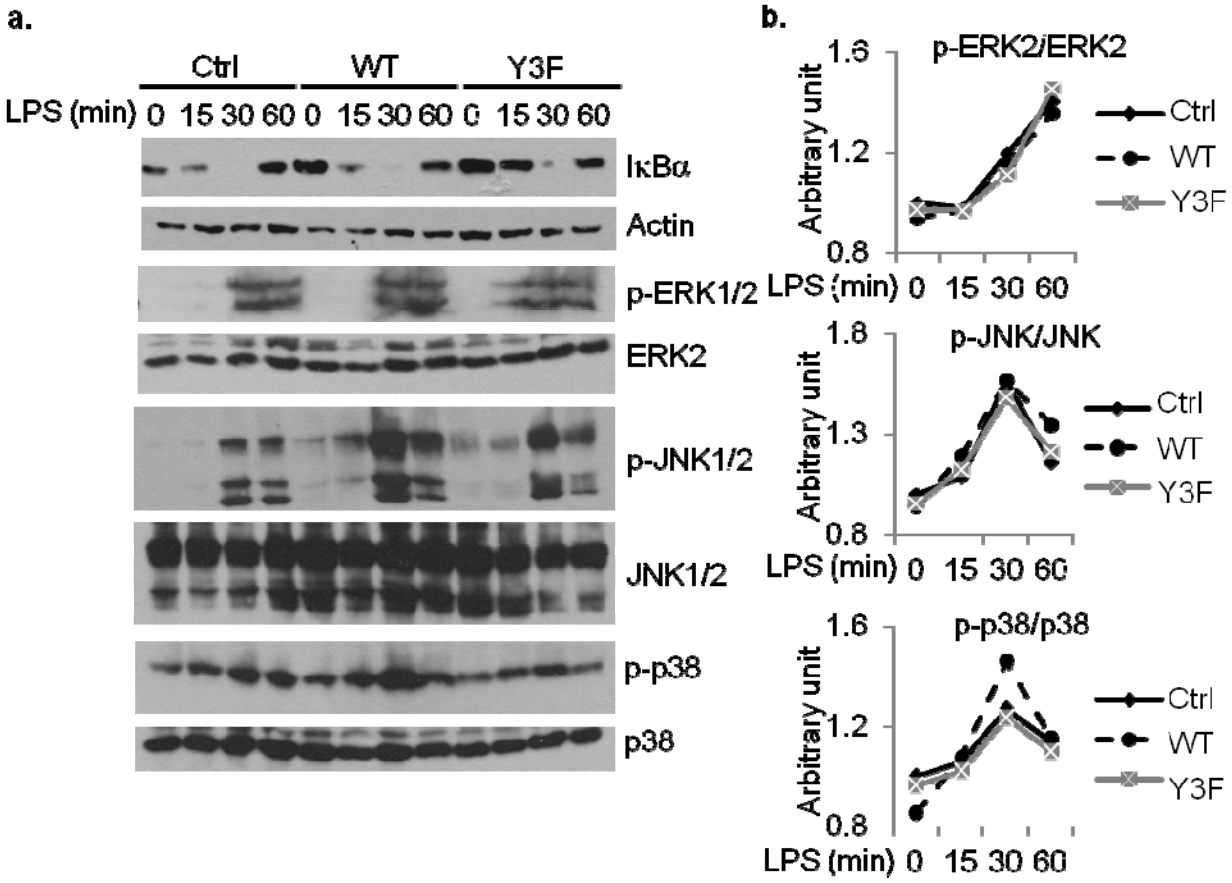

Supplementary Figure 7-16. RIP140 does not affect proinflammaotry signaling in endotoxin tolerance state in macrophages. Raw264.7 macrophages were transfected with control vector (Ctrl), Flag-tagged wild type RIP140 (Wt) or tyrosine mutant RIP140 (Y3F). Cells were treated with or without LPS for 16 h to become tolerated states. After 24 h, cells were then challenged with LPS for various durations. Indicated protein levels were determined by immunoblot analyses of whole cell lysates.

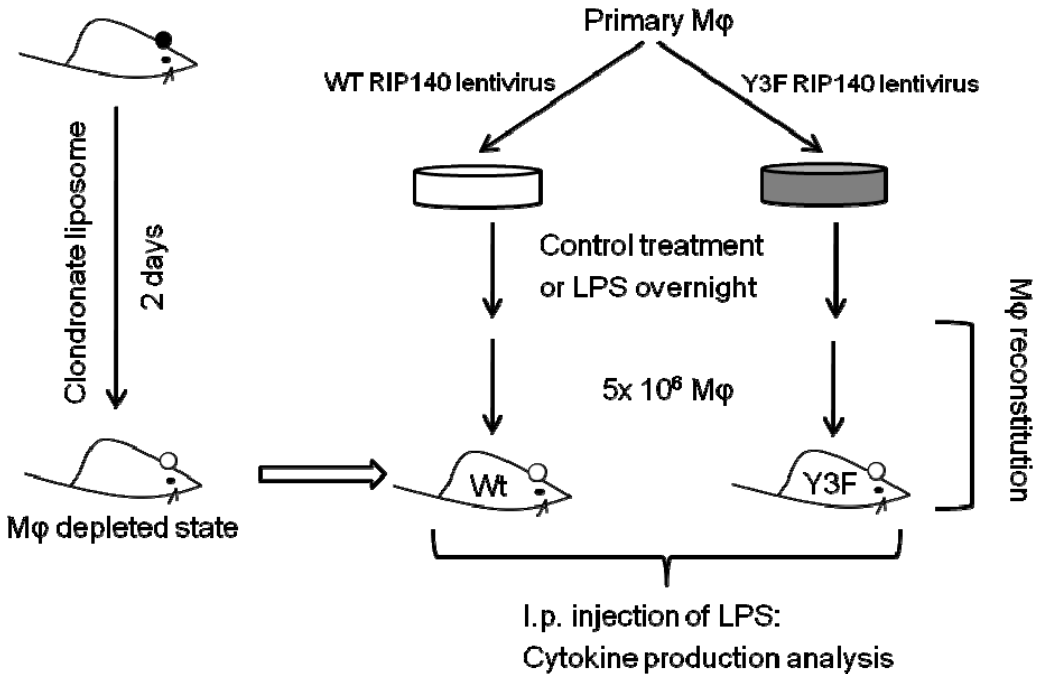

Supplementary Figure 7-17. Non-degradable RIP140 prevents endotoxin tolerance in macrophage reconstitution model. A schematic diagram for macrophage reconstitution experiment. Macrophage depletion was achieved by injecting animals with clondronate liposome. Primary peritoneal macrophages were isolated from normal mice and transduced by lentivirus containing the indicated form of RIP140. These macrophages were induced into a non-tolerated or tolerated state *in vitro*, and injected into the macrophage-depleted mice.

Tolerated genes regulated by RIP140

Symbol	Gene name
IL1B	Interleukin 1 beta
TNF	Tumor necrosis factor
IL6	Interleukin 6
TNFSF4	Tumor necrosis factor (ligand) superfamily 4
TRAF1	TNF receptor associated factor 1
SOCS3	Suppressor of cytokine signaling 3
PTGS2	Prostaglandin-endoperoxide synthase 2
COL18A1	Collagen, type XVIII, alpha 1
SELP	Selectin, platelet

Non-tolerated genes regulated by RIP140

Symbol	Gene name
THBS1	Thrombospondin 1

Supplementary Figure 7-18. Most proinflammatory genes affected by RIP140 are tolerated genes. This table is an organized list for comparison of genes affected by RIP140 with tolerated and non-tolerated genes categorized by Medzhitov's group. Nine genes affected by RIP140 are tolerated genes and only one gene, *Thbs1*, affected by RIP140 is non-tolerated.

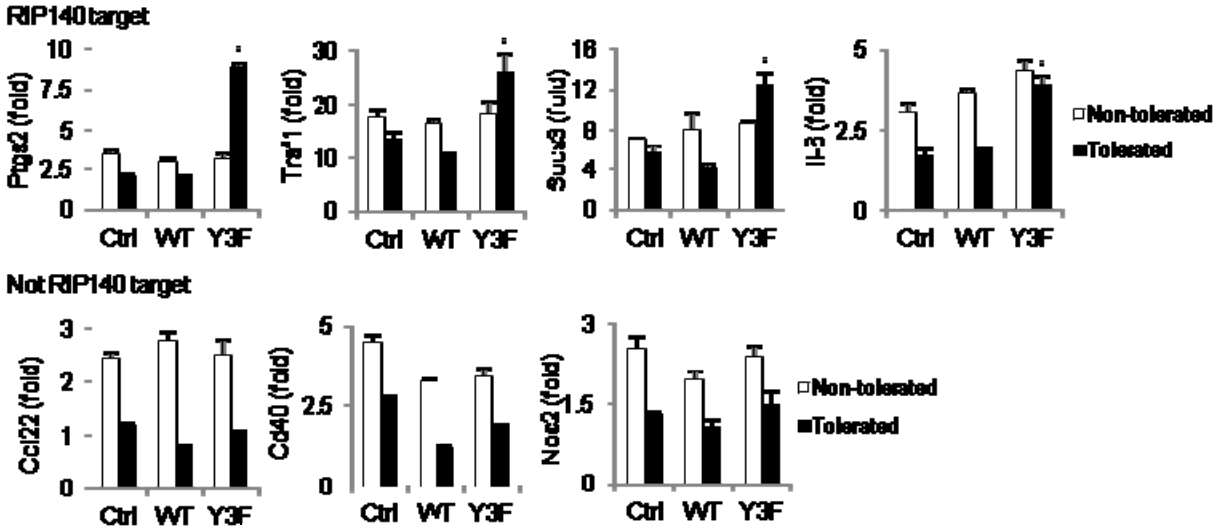

Supplementary Figure 7-19. RIP140 degradation contribute to endotoxin tolerance in Raw264.7 macrophages. Real-time PCR analysis of mRNA of indicated genes in non-tolerated or tolerated Raw264.7 macrophages transfected with the control vector (Ctrl), wild type RIP140 (Wt) or non-degradable RIP140 (Y3F). Relative folds of mRNA levels after the second stimulation with LPS were determined. Results are presented in mean ± SD., n=3; *: $P < 0.05$ as compared to the non-tolerated+LPS group.

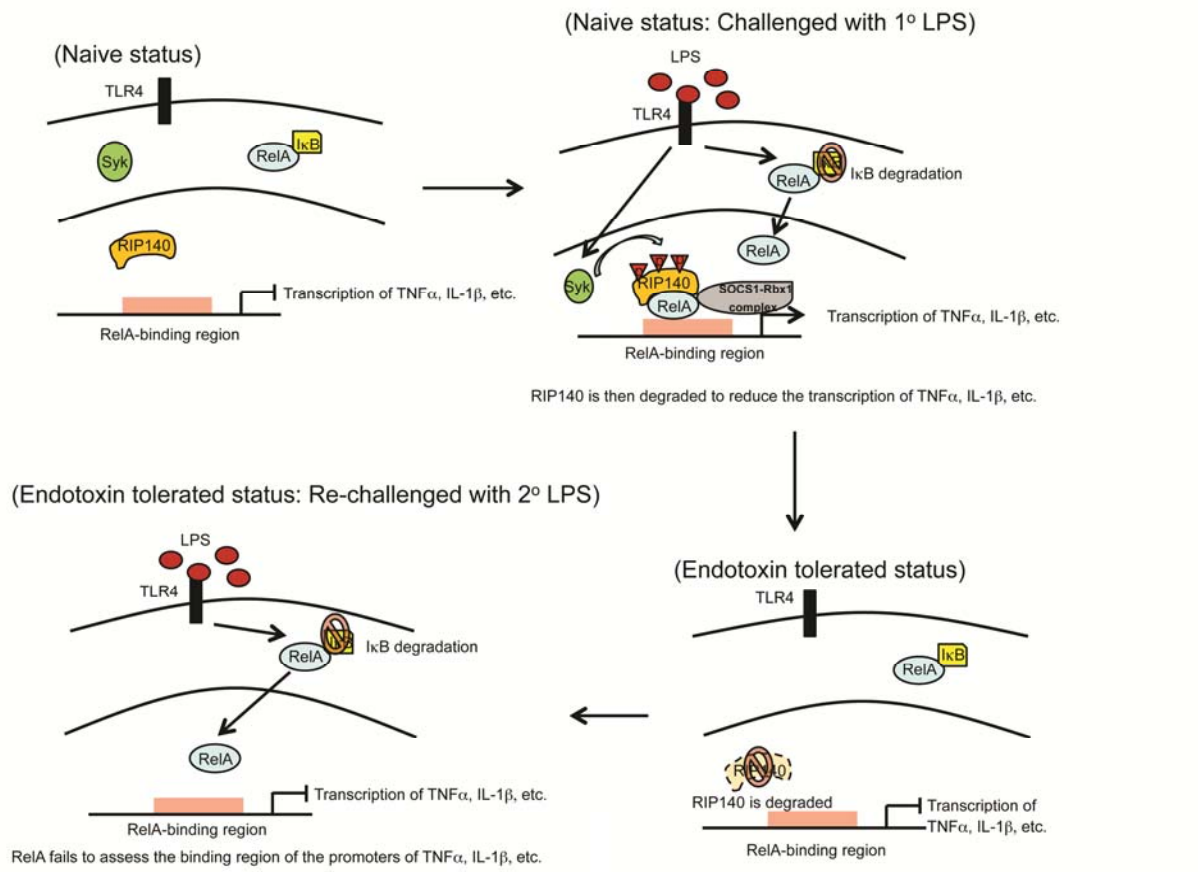

Supplementary Figure 7-20. A model for RIP140 degradation during the establishment of ET. Following the exposure of macrophages to LPS, RelA translocates into the nucleus and interacts with RIP140 to activate transcription of TNFα and IL-1β, and Syk phosphorylates RIP140 on Tyr364/418/436. The interaction of RelA with RIP140 further recruits SOCS1-Rbx1 E3 ligase to RelA-RIP140 complex on specific chromatin targets. In cooperation with Syk-mediated phosphorylation, SOCS1-Rbx1 E3 ligase promotes RIP140 polyubiquitination and subsequent degradation, which in turn reduces proinflammatory cytokine production and promotes the establishment of ET on specific genes. When these macrophages are challenged with the second LPS, although RelA still translocates into the nucleus, it fails to activate promoters of TNFα and IL-1β because of the lack of specific coactivator RIP140 for these genes.

CHAPTER VIII

Conclusion and Future Studies

The abundant expression of RIP140 in adipocytes and macrophages indicates that RIP140 must regulate essential functions in these cells. Using whole-body RIP140-null mice, the importance of RIP140 in regulating lipid and glucose metabolism in adipose tissue and the inflammatory response in macrophages has been identified [5, 11, 84]. Activity of RIP140 in the nuclei is considered the major driver for these phenotypes. Based on proteomic analysis, many PTMs of RIP140 have been identified. These PTMs have been shown to affect RIP140's activity and cellular distribution in a transrepressive reporter assay and an overexpression system in COS-1 cells [4, 14-18, 20]. However, the involvement of RIP140 PTMs in T2DM and the role of cytoplasmic RIP140 in T2DM remain unknown. Moreover, the regulation of RIP140's expression and stability also remain largely unknown. The mRNA of both human and mouse RIP140 contains long 5'- and 3'-UTRs and RIP140's amino acid sequence is highly conserved among species. These results and observations led us to following hypotheses: 1) cytoplasmic RIP140 may contribute to parts of the phenotype exhibited by RIP140-null mice, especially in lipid and glucose metabolism in adipocytes, 2) PTMs of RIP140 may regulate endogenous RIP140's stability and its ability to interact with partners, 3) RIP140's PTMs may play a role in sensing nutrient status to regulate RIP140's activity, and 4) the long UTR of RIP140's mRNA may be involved in modulating RIP140's expression.

In the study described here, we demonstrate that feeding mice a HFD can promote the accumulation of cytoplasmic RIP140 in adipocytes by activating nuclear PKCε [10, 85, 181]. Further analyses demonstrated that two stimuli can elevate nuclear PKCε activity: the extrinsic pathway which is activated by ET-1, and the intrinsic pathway, which is stimulated by intracellular lipid content [10, 181]. More importantly, we showed that cytoplasmic RIP140 can dampen the trafficking of GLUT4 vesicles and adiponectin vesicles by interacting with AS160 and also boost lipolysis by interacting with perilipin A on the surface of lipid droplets [85, 123]. These findings demonstrate that cytoplasmic RIP140 is not only an early marker for pre-diabetes under HFD feeding, but also a contributor to adipocyte dysfunctions, including lower glucose uptake, lower secreted adiponectin, and increased lipolysis. This study reveals that cytoplasmic RIP140 can be a therapeutic target for treating adipocyte dysfunctions and other metabolic disorders. Of

note, we also found evidence that administering ET_A antagonist to mice can block HFD-induced cytoplasmic RIP140 accumulation and its associated metabolic dysfunctions [181]. In addition to exploring RIP140's role in adipocytes, we explored the role and regulation of RIP140 in macrophages. We showed that cholesterol content within macrophages can modulate the stability of RIP140 mRNA in an miR-33-dependent manner. This finding indicates that HFD feeding reduces miR-33 expression in macrophages and elevates the inflammatory potential of macrophages by increasing RIP140 expression [10]. With further investigation, we demonstrated that TLR ligands can promote RIP140 degradation in macrophages by enhancing Syk-mediated tyrosine phosphorylation on RIP140 and E3 ligase recruitment in a RelA-dependent manner. This represents a new negative feedback mechanism for resolving inflammation and promoting the establishment of endotoxin tolerance in specific genes (Ho, Tsui, Feng et al., 2012). The failure of RIP140 to be degraded in response to TLRs ligands may cause a high incidence of septic shock and mortality in mice. These findings demonstrate that the expression and stability of RIP140 in macrophages are important for modulating macrophage inflammatory potential and may be involved in modulating systemic immune response by sensing nutrient status. Taken together, our results address the major parts of our hypotheses listed above and offer new perspectives on RIP140's pathophysiological functions and the importance of regulating RIP140's expression.

Using ultracentrifuge in combination with immunofluorescence analysis and immunoblotting, we confirmed that cytoplasmic RIP140 can be detected in cytosolic fraction, lipid droplets, and endoplasmic reticulum (ER) [10]. We also confirmed the interacting proteins of cytoplasmic RIP140 in the cytosolic fraction and lipid droplets but we do not know the functional role of cytoplasmic RIP140 in the ER fraction. Based on multiple functions of the ER, the functions of cytoplasmic RIP140 in the ER could link to the known functions of RIP140 in lipid and glucose metabolism and mitochondrial activity. Although we showed that cytoplasmic RIP140 contributes to adipocte dysfunctions by interacting with various proteins, we do not know the regulatory mechanisms that modulate RIP140's specificity for different interacting partners. We hypothesize that the extensive PTMs on RIP140 may play a regulatory role in modulating

RIP140's specificity with regard to its interacting proteins and cytoplasmic localization. It would be informative to enrich RIP140 in specific locations and then perform proteomic analysis. The comparison of the PTM patterns of RIP140 in different locations may reveal new mechanisms for regulating the distribution of RIP140 and help us design therapies for modulating specific functions of RIP140. It would also be interesting to isolate cytoplasmic RIP140 and analyze its interacting proteins by mass spectrometry. These analyses would allow us to determine the full spectrum of cytoplasmic RIP140's activities.

Chronic low grade inflammation mediated by macrophages is key factor in many metabolic disorders [23, 39]. In our study, we confirmed the role of RIP140 in the production of pro-inflammatory cytokines in macrophages [10, 11]. This indicates that RIP140's functions in macrophages may contribute to some phenotypes shown by RIP140-null mice on diet-induced metabolic disorders [5, 84]. We further confirmed that 1) cholesterol content within macrophages can control RIP140 levels to modulate inflammatory potential, and 2) LPS, as well as other TLRs ligands, can induce RIP140 protein degradation to resolve inflammation and promote endotoxin tolerance in a gene-specific manner. In the production of pro-inflammatory cytokines, LPS can trigger the interaction of RIP140 with NF-κB, and RIP140 acts as a co-activator for NF-κB. However, we do not know the underlying mechanisms by which NF-κB recruits RIP140 and why RIP140 acts as a co-activator for NF-κB, instead of a co-repressor for other transcription factors. Although LPS triggers Syk-mediated phosphorylation of three tyrosine residues on RIP140, the phosphorylation status does not affect the RIP140 interaction with NF-κB or RIP140 co-activator activity. It will be important for future studies to examine the difference between PTM patterns of NF-κB-associated RIP140 and RIP140 that acts as co-repressor. Moreover, differences in the recruiting of co-regulator complexes by these RIP140s need to be examined.

Recently, the balance of M1 and M2 macrophages has been shown to be important for many diseases, including metabolic disorders and autoimmune diseases [40, 44, 155]. Several studies show that after M1 activation, endotoxin tolerated macrophages exhibit

some features of M2 activation. Importantly, these M2-skewed macrophages are important for tissue repair and can prevent further inflammation [40-42, 44]. Although current studies of RIP140 in macrophages mainly focus on its role in M1 activation, it is not clear if RIP140 has a regulatory role in M2 activation. Our study demonstrates that TLRs ligands can promote RIP140 degradation for resolving inflammation and promoting the establishment of endotoxin tolerance [182]. Although several studies demonstrate the M1/M2 switch in inflammation and the importance of the phenotype switch in tissue homeostasis and repair, the underlying mechanisms regulating this phenotype switch remain unknown. It would be interesting to determine if RIP140 degradation is involved in the M1/M2 switch in the future studies.

Bibliography

[1] Lee CH, Wei LN, J Biol Chem. 1999;274:31320-31326.

[2] Lee CH, Chinpaisal C, Wei LN, Mol Cell Biol. 1998;18:6745-6755.

[3] Cavailles V, Dauvois S, L'Horset F, Lopez G, Hoare S, Kushner PJ, Parker MG, EMBO J. 1995;14:3741-3751.

[4] Mostaqul Huq MD, Gupta P, Wei LN, Curr Med Chem. 2008;15:386-392.

[5] Christian M, Kiskinis E, Debevec D, Leonardsson G, White R, Parker MG, Mol Cell Biol. 2005;25:9383-9391.

[6] Fritah A, Steel JH, Nichol D, Parker N, Williams S, Price A, Strauss L, Ryder TA, Mobberley MA, Poutanen M, Parker M, White R, Cardiovasc Res. 2010;86:443-451.

[7] Vo N, Fjeld C, Goodman RH, Mol Cell Biol. 2001;21:6181-6188.

[8] Persaud SD, Huang WH, Park SW, Wei LN, Mol Endocrinol. 2011;25:1689-1698.

[9] Park SW, Huang WH, Persaud SD, Wei LN, Nucleic Acids Res. 2009;37:7085-7094.

[10] Ho PC, Chuang YS, Hung CH, Wei LN, Cell Signal. 2011;23:1396-1403.

[11] Zschiedrich I, Hardeland U, Krones-Herzig A, Berriel Diaz M, Vegiopoulos A, Muggenburg J, Sombroek D, Hofmann TG, Zawatzky R, Yu X, Gretz N, Christian M, White R, Parker MG, Herzig S, Blood. 2008;112:264-276.

[12] Ho PC, Chang KC, Chuang YS, Wei LN, FASEB J. 2011;25:1758-1766.

[13] Herzog B, Hallberg M, Seth A, Woods A, White R, Parker MG, Mol Endocrinol. 2007;21:2687-2697.

[14] Mostaqul Huq MD, Gupta P, Tsai NP, White R, Parker MG, Wei LN, EMBO J. 2006;25:5094-5104.

[15] Huq MD, Khan SA, Park SW, Wei LN, Proteomics. 2005;5:2157-2166.

[16] Huq MD, Tsai NP, Lin YP, Higgins L, Wei LN, Nat Chem Biol. 2007;3:161-165.

[17] Huq MD, Wei LN, Mol Cell Proteomics. 2005;4:975-983.

[18] Ho PC, Gupta P, Tsui YC, Ha SG, Huq M, Wei LN, Cell Signal. 2008;20:1911-1919.

[19] Gupta P, Ho PC, Huq MD, Khan AA, Tsai NP, Wei LN, PLoS ONE. 2008;3:e2658.

[20] Gupta P, Huq MD, Khan SA, Tsai NP, Wei LN, Mol Cell Proteomics. 2005;4:1776-1784.

[21] Huq MD, Ha SG, Barcelona H, Wei LN, J Proteome Res. 2009;8:1156-1167.

[22] Rytinki MM, Palvimo JJ, J Biol Chem. 2008;283:11586-11595.
[23] Guilherme A, Virbasius JV, Puri V, Czech MP, Nat Rev Mol Cell Biol. 2008;9:367-377.
[24] Zimmermann R, Lass A, Haemmerle G, Zechner R, Biochim Biophys Acta. 2009;1791:494-500.
[25] Dridi S, Taouis M, J Nutr Biochem. 2009;20:831-839.
[26] Lago F, Gomez R, Gomez-Reino JJ, Dieguez C, Gualillo O, Trends Biochem Sci. 2009;34:500-510.
[27] Antoniades C, Antonopoulos AS, Tousoulis D, Stefanadis C, Obes Rev. 2009;10:269-279.
[28] Shibata R, Ouchi N, Murohara T, Circ J. 2009;73:608-614.
[29] Kotani K, Peroni OD, Minokoshi Y, Boss O, Kahn BB, J Clin Invest. 2004;114:1666-1675.
[30] Unger RH, Scherer PE, Trends Endocrinol Metab. 2010;21:345-352.
[31] Erion DM, Shulman GI, Nat Med. 2010;16:400-402.
[32] Szczepaniak LS, Victor RG, Orci L, Unger RH, Circ Res. 2007;101:759-767.
[33] Leichman JG, Lavis VR, Aguilar D, Wilson CR, Taegtmeyer H, Clin Res Cardiol. 2006;95 Suppl 1:i134-141.
[34] Kim JY, van de Wall E, Laplante M, Azzara A, Trujillo ME, Hofmann SM, Schraw T, Durand JL, Li H, Li G, Jelicks LA, Mehler MF, Hui DY, Deshaies Y, Shulman GI, Schwartz GJ, Scherer PE, J Clin Invest. 2007;117:2621-2637.
[35] Wang MY, Grayburn P, Chen S, Ravazzola M, Orci L, Unger RH, Proc Natl Acad Sci U S A. 2008;105:6139-6144.
[36] Trinchieri G, Sher A, Nat Rev Immunol. 2007;7:179-190.
[37] Kawai T, Akira S, Nat Immunol. 2010;11:373-384.
[38] Takeuchi O, Akira S, Cell. 2010;140:805-820.
[39] O'Neill LA, Immunity. 2008;29:12-20.
[40] Gordon S, Nat Rev Immunol. 2003;3:23-35.
[41] Pena OM, Pistolic J, Raj D, Fjell CD, Hancock RE, J Immunol. 2011;186:7243-7254.

[42] Porta C, Rimoldi M, Raes G, Brys L, Ghezzi P, Di Liberto D, Dieli F, Ghisletti S, Natoli G, De Baetselier P, Mantovani A, Sica A, Proc Natl Acad Sci U S A. 2009;106:14978-14983.
[43] Biswas SK, Lopez-Collazo E, Trends Immunol. 2009;30:475-487.
[44] Mosser DM, Edwards JP, Nat Rev Immunol. 2008;8:958-969.
[45] Medzhitov R, Horng T, Nat Rev Immunol. 2009;9:692-703.
[46] Nathan C, Ding A, Cell. 2010;140:871-882.
[47] Cavaillon JM, Adib-Conquy M, Crit Care. 2006;10:233.
[48] Freudenberg MA, Galanos C, Infect Immun. 1988;56:1352-1357.
[49] Herman MA, Kahn BB, J Clin Invest. 2006;116:1767-1775.
[50] Doria A, Patti ME, Kahn CR, Cell Metab. 2008;8:186-200.
[51] Schenk S, Saberi M, Olefsky JM, J Clin Invest. 2008;118:2992-3002.
[52] Huang S, Czech MP, Cell Metab. 2007;5:237-252.
[53] Tilg H, Moschen AR, Trends Endocrinol Metab. 2008;19:371-379.
[54] Muoio DM, Newgard CB, Annu Rev Biochem. 2006;75:367-401.
[55] Wellen KE, Hotamisligil GS, J Clin Invest. 2005;115:1111-1119.
[56] Sakamoto K, Holman GD, Am J Physiol Endocrinol Metab. 2008;295:E29-37.
[57] Hou JC, Pessin JE, Curr Opin Cell Biol. 2007;19:466-473.
[58] Ng Y, Ramm G, Lopez JA, James DE, Cell Metab. 2008;7:348-356.
[59] Sano H, Kane S, Sano E, Miinea CP, Asara JM, Lane WS, Garner CW, Lienhard GE, J Biol Chem. 2003;278:14599-14602.
[60] Larance M, Ramm G, Stockli J, van Dam EM, Winata S, Wasinger V, Simpson F, Graham M, Junutula JR, Guilhaus M, James DE, J Biol Chem. 2005;280:37803-37813.
[61] Christian M, White R, Parker MG, Trends Endocrinol Metab. 2006;17:243-250.
[62] Wei LN, Curr Med Chem. 2004;11:1527-1532.
[63] Huq MD, Ha SG, Barcelona H, Wei LN, J Proteome Res. 2009.
[64] Yu C, Cresswell J, Loffler MG, Bogan JS, J Biol Chem. 2007;282:7710-7722.
[65] Romero R, Casanova B, Pulido N, Suarez AI, Rodriguez E, Rovira A, J Endocrinol. 2000;164:187-195.

[66] White R, Morganstein D, Christian M, Seth A, Herzog B, Parker MG, FEBS Lett. 2008;582:39-45.
[67] Powelka AM, Seth A, Virbasius JV, Kiskinis E, Nicoloro SM, Guilherme A, Tang X, Straubhaar J, Cherniack AD, Parker MG, Czech MP, J Clin Invest. 2006;116:125-136.
[68] Puri V, Virbasius JV, Guilherme A, Czech MP, Acta Physiol (Oxf). 2008;192:103-115.
[69] Seth A, Steel JH, Nichol D, Pocock V, Kumaran MK, Fritah A, Mobberley M, Ryder TA, Rowlerson A, Scott J, Poutanen M, White R, Parker M, Cell Metab. 2007;6:236-245.
[70] Ozcan U, Yilmaz E, Ozcan L, Furuhashi M, Vaillancourt E, Smith RO, Gorgun CZ, Hotamisligil GS, Science. 2006;313:1137-1140.
[71] Duffaut C, Galitzky J, Lafontan M, Bouloumie A, Biochem Biophys Res Commun. 2009;384:482-485.
[72] Samuel VT, Liu ZX, Wang A, Beddow SA, Geisler JG, Kahn M, Zhang XM, Monia BP, Bhanot S, Shulman GI, J Clin Invest. 2007;117:739-745.
[73] Laybutt DR, Schmitz-Peiffer C, Saha AK, Ruderman NB, Biden TJ, Kraegen EW, Am J Physiol. 1999;277:E1070-1076.
[74] Schmitz-Peiffer C, Laybutt DR, Burchfield JG, Gurisik E, Narasimhan S, Mitchell CJ, Pedersen DJ, Braun U, Cooney GJ, Leitges M, Biden TJ, Cell Metab. 2007;6:320-328.
[75] Schmitz-Peiffer C, Biden TJ, Diabetes. 2008;57:1774-1783.
[76] Farese RV, Jr., Walther TC, Cell. 2009;139:855-860.
[77] Shi H, Kokoeva MV, Inouye K, Tzameli I, Yin H, Flier JS, J Clin Invest. 2006;116:3015-3025.
[78] Gaidhu MP, Anthony NM, Patel P, Hawke TJ, Ceddia RB, Am J Physiol Cell Physiol. 2010;298:C961-971.
[79] Langin D, Cell Metab. 2010;11:242-243.
[80] Granneman JG, Moore HP, Trends Endocrinol Metab. 2008;19:3-9.
[81] Guo Y, Cordes KR, Farese RV, Jr., Walther TC, J Cell Sci. 2009;122:749-752.
[82] Fritah A, Christian M, Parker MG, Am J Physiol Endocrinol Metab. 2010;299:E335-340.

[83] White R, Leonardsson G, Rosewell I, Ann Jacobs M, Milligan S, Parker M, Nat Med. 2000;6:1368-1374.
[84] Leonardsson G, Steel JH, Christian M, Pocock V, Milligan S, Bell J, So PW, Medina-Gomez G, Vidal-Puig A, White R, Parker MG, Proc Natl Acad Sci U S A. 2004;101:8437-8442.
[85] Ho PC, Lin YW, Tsui YC, Gupta P, Wei LN, Cell Metab. 2009;10:516-523.
[86] Zinchuk V, Zinchuk O, Okada T, Acta Histochem Cytochem. 2007;40:101-111.
[87] Cho SY, Shin ES, Park PJ, Shin DW, Chang HK, Kim D, Lee HH, Lee JH, Kim SH, Song MJ, Chang IS, Lee OS, Lee TR, J Biol Chem. 2007;282:2456-2465.
[88] Sakane F, Imai S, Kai M, Yasuda S, Kanoh H, Curr Drug Targets. 2008;9:626-640.
[89] Takahashi H, Takeishi Y, Seidler T, Arimoto T, Akiyama H, Hozumi Y, Koyama Y, Shishido T, Tsunoda Y, Niizeki T, Nozaki N, Abe J, Hasenfuss G, Goto K, Kubota I, Circulation. 2005;111:1510-1516.
[90] Shen WJ, Patel S, Miyoshi H, Greenberg AS, Kraemer FB, J Lipid Res. 2009;50:2306-2313.
[91] Brasaemle DL, J Lipid Res. 2007;48:2547-2559.
[92] Choi CS, Savage DB, Abu-Elheiga L, Liu ZX, Kim S, Kulkarni A, Distefano A, Hwang YJ, Reznick RM, Codella R, Zhang D, Cline GW, Wakil SJ, Shulman GI, Proc Natl Acad Sci U S A. 2007;104:16480-16485.
[93] Zhang D, Christianson J, Liu ZX, Tian L, Choi CS, Neschen S, Dong J, Wood PA, Shulman GI, Cell Metab. 2010;11:402-411.
[94] Kadowaki T, Yamauchi T, Kubota N, Hara K, Ueki K, Tobe K, J Clin Invest. 2006;116:1784-1792.
[95] Folco EJ, Rocha VZ, Lopez-Ilasaca M, Libby P, J Biol Chem. 2009;284:25569-25575.
[96] Tsai NP, Lin YL, Wei LN, Biochem J. 2009;424:411-418.
[97] Bogan JS, Lodish HF, J Cell Biol. 1999;146:609-620.
[98] Tulipano G, Spano P, Cocchi D, Mol Cell Endocrinol. 2008;292:42-49.
[99] Rasouli N, Yao-Borengasser A, Varma V, Spencer HJ, McGehee RE, Jr., Peterson CA, Mehta JL, Kern PA, Arterioscler Thromb Vasc Biol. 2009;29:1328-1335.

[100] Bedi D, Clarke KJ, Dennis JC, Zhong Q, Brunson BL, Morrison EE, Judd RL, Biochem Biophys Res Commun. 2006;345:332-339.
[101] Wang Y, Lam KS, Yau MH, Xu A, Biochem J. 2008;409:623-633.
[102] Xie L, Boyle D, Sanford D, Scherer PE, Pessin JE, Mora S, J Biol Chem. 2006;281:7253-7259.
[103] Xie L, O'Reilly CP, Chapes SK, Mora S, Biochim Biophys Acta. 2008;1782:99-108.
[104] Clarke M, Ewart MA, Santy LC, Prekeris R, Gould GW, Biochem Biophys Res Commun. 2006;342:1361-1367.
[105] Stenmark H, Nat Rev Mol Cell Biol. 2009;10:513-525.
[106] Welsh GI, Leney SE, Lloyd-Lewis B, Wherlock M, Lindsay AJ, McCaffrey MW, Tavare JM, J Cell Sci. 2007;120:4197-4208.
[107] Potenza MA, Gagliardi S, Nacci C, Carratu MR, Montagnani M, Curr Med Chem. 2009;16:94-112.
[108] Rehsia NS, Dhalla NS, Heart Fail Rev. 2010;15:85-101.
[109] Schneider JG, Tilly N, Hierl T, Sommer U, Hamann A, Dugi K, Leidig-Bruckner G, Kasperk C, Am J Hypertens. 2002;15:967-972.
[110] Humbert M, Sitbon O, Simonneau G, N Engl J Med. 2004;351:1425-1436.
[111] Braunwald E, N Engl J Med. 2008;358:2148-2159.
[112] Archer SL, Weir EK, Wilkins MR, Circulation. 2010;121:2045-2066.
[113] Takahashi K, Ghatei MA, Lam HC, O'Halloran DJ, Bloom SR, Diabetologia. 1990;33:306-310.
[114] Chai SP, Chang YN, Fong JC, Biochim Biophys Acta. 2009;1790:213-218.
[115] Ishibashi KI, Imamura T, Sharma PM, Huang J, Ugi S, Olefsky JM, J Clin Invest. 2001;107:1193-1202.
[116] O'Carroll SJ, Mitchell MD, Faenza I, Cocco L, Gilmour RS, Cell Signal. 2009;21:926-935.
[117] Marasciulo FL, Montagnani M, Potenza MA, Curr Med Chem. 2006;13:1655-1665.
[118] Ellershaw DC, Gurney AM, Br J Pharmacol. 2001;134:621-631.
[119] Casserly B, Klinger JR, Drug Des Devel Ther. 2009;2:265-280.

[120] Shetty N, Derk CT, Inflamm Allergy Drug Targets. 2011;10:19-26.
[121] Ishibashi K, Imamura T, Sharma PM, Ugi S, Olefsky JM, Endocrinology. 2000;141:4623-4628.
[122] Ho PC, Chuang YS, Hung CH, Wei LN, Cell Signal. 2011.
[123] Ho PC, Wei LN, Cell Signal. 2012;24:71-76.
[124] Chawla A, Circ Res. 2010;106:1559-1569.
[125] Maxfield FR, Tabas I, Nature. 2005;438:612-621.
[126] Chen GY, Nunez G, Nat Rev Immunol. 2010;10:826-837.
[127] Russell JA, N Engl J Med. 2006;355:1699-1713.
[128] Vachharajani V, Vital S, J Intensive Care Med. 2006;21:287-295.
[129] Rivera CA, Gaskin L, Singer G, Houghton J, Allman M, BMC Physiol. 2010;10:20.
[130] Hotamisligil GS, Erbay E, Nat Rev Immunol. 2008;8:923-934.
[131] Naura AS, Hans CP, Zerfaoui M, Errami Y, Ju J, Kim H, Matrougui K, Kim JG, Boulares AH, Lab Invest. 2009;89:1243-1251.
[132] Yvan-Charvet L, Wang N, Tall AR, Arterioscler Thromb Vasc Biol. 2010;30:139-143.
[133] Yvan-Charvet L, Welch C, Pagler TA, Ranalletta M, Lamkanfi M, Han S, Ishibashi M, Li R, Wang N, Tall AR, Circulation. 2008;118:1837-1847.
[134] Schonbeck U, Libby P, Circulation. 2004;109:II18-26.
[135] Gao F, Linhartova L, Johnston AM, Thickett DR, Br J Anaesth. 2008;100:288-298.
[136] Gilroy DW, Lawrence T, Perretti M, Rossi AG, Nat Rev Drug Discov. 2004;3:401-416.
[137] Lefevre L, Gales A, Olagnier D, Bernad J, Perez L, Burcelin R, Valentin A, Auwerx J, Pipy B, Coste A, PLoS One. 2010;5:e12828.
[138] Strandberg L, Verdrengh M, Enge M, Andersson N, Amu S, Onnheim K, Benrick A, Brisslert M, Bylund J, Bokarewa M, Nilsson S, Jansson JO, PLoS One. 2009;4:e7605.
[139] O'Connell RM, Rao DS, Chaudhuri AA, Baltimore D, Nat Rev Immunol. 2010;10:111-122.
[140] O'Connell RM, Taganov KD, Boldin MP, Cheng G, Baltimore D, Proc Natl Acad Sci U S A. 2007;104:1604-1609.

[141] Tili E, Michaille JJ, Cimino A, Costinean S, Dumitru CD, Adair B, Fabbri M, Alder H, Liu CG, Calin GA, Croce CM, J Immunol. 2007;179:5082-5089.
[142] El Gazzar M, McCall CE, J Biol Chem. 2010;285:20940-20951.
[143] Najafi-Shoushtari SH, Kristo F, Li Y, Shioda T, Cohen DE, Gerszten RE, Naar AM, Science. 2010;328:1566-1569.
[144] Rayner KJ, Suarez Y, Davalos A, Parathath S, Fitzgerald ML, Tamehiro N, Fisher EA, Moore KJ, Fernandez-Hernando C, Science. 2010;328:1570-1573.
[145] Horie T, Ono K, Horiguchi M, Nishi H, Nakamura T, Nagao K, Kinoshita M, Kuwabara Y, Marusawa H, Iwanaga Y, Hasegawa K, Yokode M, Kimura T, Kita T, Proc Natl Acad Sci U S A. 2010;107:17321-17326.
[146] Marquart TJ, Allen RM, Ory DS, Baldan A, Proc Natl Acad Sci U S A. 2010;107:12228-12232.
[147] Gerin I, Clerbaux LA, Haumont O, Lanthier N, Das AK, Burant CF, Leclercq IA, MacDougald OA, Bommer GT, J Biol Chem. 2010;285:33652-33661.
[148] Park SW, Huq MD, Hu X, Wei LN, Mol Cell Proteomics. 2005;4:300-309.
[149] Chang M, Jin W, Sun SC, Nat Immunol. 2009;10:1089-1095.
[150] Tabas I, Nat Rev Immunol. 2010;10:36-46.
[151] Hernandez-Presa MA, Ortego M, Tunon J, Martin-Ventura JL, Mas S, Blanco-Colio LM, Aparicio C, Ortega L, Gomez-Gerique J, Vivanco F, Egido J, Cardiovasc Res. 2003;57:168-177.
[152] Redmond HP, Chavin KD, Bromberg JS, Daly JM, Ann Surg. 1991;214:502-508; discussion 508-509.
[153] Chen Y, Kerimo A, Khan S, Wei LN, Mol Endocrinol. 2002;16:2528-2537.
[154] Chen Y, Hu X, Wei LN, Mol Cell Endocrinol. 2004;226:43-50.
[155] Baker RG, Hayden MS, Ghosh S, Cell Metab. 2011;13:11-22.
[156] Wen H, Gris D, Lei Y, Jha S, Zhang L, Huang MT, Brickey WJ, Ting JP, Nat Immunol. 2011;12:408-415.
[157] Sheedy FJ, Palsson-McDermott E, Hennessy EJ, Martin C, O'Leary JJ, Ruan Q, Johnson DS, Chen Y, O'Neill LA, Nat Immunol. 2010;11:141-147.

[158] Mansell A, Smith R, Doyle SL, Gray P, Fenner JE, Crack PJ, Nicholson SE, Hilton DJ, O'Neill LA, Hertzog PJ, Nat Immunol. 2006;7:148-155.
[159] Foster SL, Hargreaves DC, Medzhitov R, Nature. 2007;447:972-978.
[160] Chen J, Ivashkiv LB, Proc Natl Acad Sci U S A. 2010;107:19438-19443.
[161] Park SH, Park-Min KH, Chen J, Hu X, Ivashkiv LB, Nat Immunol. 2011;12:607-615.
[162] Chan C, Li L, McCall CE, Yoza BK, J Immunol. 2005;175:461-468.
[163] Ho PC, Wei LN, Cell Signal. 2011.
[164] Clague MJ, Urbe S, Cell. 2010;143:682-685.
[165] Natoli G, Chiocca S, Sci Signal. 2008;1:pe1.
[166] Maine GN, Mao X, Komarck CM, Burstein E, EMBO J. 2007;26:436-447.
[167] Rao MK, Wilkinson MF, Nat Protoc. 2006;1:1494-1501.
[168] Vats D, Mukundan L, Odegaard JI, Zhang L, Smith KL, Morel CR, Wagner RA, Greaves DR, Murray PJ, Chawla A, Cell Metab. 2006;4:13-24.
[169] Kinjyo I, Hanada T, Inagaki-Ohara K, Mori H, Aki D, Ohishi M, Yoshida H, Kubo M, Yoshimura A, Immunity. 2002;17:583-591.
[170] Nakagawa R, Naka T, Tsutsui H, Fujimoto M, Kimura A, Abe T, Seki E, Sato S, Takeuchi O, Takeda K, Akira S, Yamanishi K, Kawase I, Nakanishi K, Kishimoto T, Immunity. 2002;17:677-687.
[171] Dimitriou ID, Clemenza L, Scotter AJ, Chen G, Guerra FM, Rottapel R, Immunol Rev. 2008;224:265-283.
[172] Hamerman JA, Tchao NK, Lowell CA, Lanier LL, Nat Immunol. 2005;6:579-586.
[173] Han C, Jin J, Xu S, Liu H, Li N, Cao X, Nat Immunol. 2010;11:734-742.
[174] Hu X, Chakravarty SD, Ivashkiv LB, Immunol Rev. 2008;226:41-56.
[175] Smale ST, Cell. 2010;140:833-844.
[176] Strebovsky J, Walker P, Lang R, Dalpke AH, FASEB J. 2011;25:863-874.
[177] Yoon CH, Miah MA, Kim KP, Bae YS, EMBO Rep. 2010;11:393-399.
[178] Yoo Y, Ho HJ, Wang C, Guan JL, Oncogene. 2010;29:263-272.
[179] Oeckinghaus A, Hayden MS, Ghosh S, Nat Immunol. 2011;12:695-708.

[180] Wei LN, Hu X, Chandra D, Seto E, Farooqui M, J Biol Chem. 2000;275:40782-40787.
[181] Ho PC, Tsui YC, Lin YW, Persaud SD, Wei LN, Mol Cell Endocrinol. 2012; 351: 176-183.
[182] Ho PC, Tsui YC, Feng X, Greaves DR, Wei LN, Nat Immunol. 2012.